The Messenger

No. 157 – September 2014

The second generation VLTI instrument MATISSE
Maintaining Paranal instrumentation
MUSE commissioning
ALESS: ALMA survey of submillimetre galaxies

Groundbreaking for the European Extremely Large Telescope (E-ELT)

On 19 June 2014 a groundbreaking ceremony took place to mark the next major milestone in the construction of the European Extremely Large Telescope (E-ELT). Part of the 3000-metre peak of Cerro Armazones, which was selected as the site of the 39-metre telescope in 2010, was blasted away as a step towards levelling the summit in preparation for the construction of the E-ELT telescope and dome[1].

The groundbreaking ceremony was held at the Paranal Observatory, 20 kilometres away from Cerro Armazones. It was attended by distinguished guests from both Chile and the ESO Member States, as well as representatives of the local communities, senior officials from the project and ESO staff (see Figure 1). The event was also streamed live online and a recording of the event is available for download[2]. The ESO Director General, Tim de Zeeuw, gave a speech as part of the ceremony and the text is presented below. The order to proceed with the blasting itself was given by the Chilean Vice Minister of National Assets, Jorge Maldonado.

During the groundbreaking ceremony the Chilean company ICAFAL Ingeniera y Construcćion S. A. blasted part of the top of Cerro Armazones and loosened about 5000 cubic metres of rock (see Figure 2). This is the first stage of the levelling process which will landscape the mountain, so that it can accommodate the dome. A total of 220 000 cubic metres will need to be removed to make room for the 150 by 300 metre E-ELT platform.

Figure 2. The moment of the explosion which loosened ~ 5000 cubic metres of the summit of Cerro Armazones, photographed from a few hundred metres distance.

The Cerro Armazones civil works started in March 2014 and are expected to take 16 months. In addition to the construction of the summit platform, the works include the laying and maintenance of a paved road and the construction of a service trench to the summit.

Links

[1] The E-ELT Construction Proposal: http://www.eso.org/public/products/books/book_0046/
[2] Release eso1419, with access to images and videos: http://www.eso.org/public/news/eso1419/

Figure 1. The line-up of invited guests and ESO staff at the E-ELT groundbreaking ceremony held at the Paranal Observatory on 19 June 2014.

Welcome Speech

Tim de Zeeuw, ESO Director General

Distinguished sub-secretary of Biennes Nacionales, intendente of Region II, ambassadors, other authorities, dear colleagues and friends,

It is a great pleasure to welcome all of you to the milestone event that marks the beginning of the construction of the world's largest optical telescope, the European Extremely Large Telescope, the E-ELT, on nearby Cerro Armazones, which will be part of the world-leading system of telescopes here on Paranal.

The E-ELT will have a main mirror of 39 metres diameter and will take ten years to build. It will dwarf any other optical telescope and will allow tremendous astronomical discoveries, not only in the deep Universe but also closer to home, for example, providing an unprecedented look into the properties of the supermassive black hole that lurks in the centre of our Milky Way. One of the most exciting programmes will be to study the atmospheres of Earth-like planets orbiting other stars, and to search for signs of biological activity. Finding evidence of life elsewhere in the Universe would be a transformational development in the history of our species. It is ironic that this could happen here in the Atacama Desert, one of the most beautiful but lifeless locations on our own planet.

The construction of the E-ELT is supported by all 14 Member States of ESO, who have committed significant additional funding to make the dream a reality. The Chilean government was similarly supportive by protecting the night skies, and by generously donating a significant tract of land to extend the Paranal property to include Cerro Armazones. The discussions started during the time of the worldwide site selection process, towards the end of President Bachelet's first term, and the resulting E-ELT Agreement between Chile and ESO was signed in October 2011. Gabriel Rodriguez of MinRel had a key role in making this happen. Former President Piñera personally handed me the deed to the extension area right here in October of last year, clearing the way for today's event, now again under the aegis of President Bachelet.

The Republic of Chile has also assisted with the connection of the Paranal/Armazones Observatory to the electrical grid, as part of the regulated national system. It will be built by SAESA. This fulfils a key undertaking contained in the 2011 E-ELT Agreement for which ESO and its Member States are enormously grateful. I was very pleased to sign the contract with SAESA today, and am very happy that the SAESA leadership and the national authorities involved on energy matters are here with us as well.

The construction of the E-ELT provides many opportunities for industries in the ESO Member States and in Chile. The construction of the new access road and the telescope platform on Armazones, which are the subject of our groundbreaking ceremony today, is carried out by ICAFAL, whose leadership is also present here.

Exactly 30 years ago today my wife Ewine and I both received our PhD degrees in astronomy at Leiden University, with ESO founding fathers Jan Oort and Adriaan Blaauw in the committee. At this time La Silla was ESO's flagship, the Very Large Telescope was in the planning stages, ALMA was not yet conceived, and no serious thought was given to 40-metre-class optical telescopes. I suspect there were few, if any, who foresaw the tremendous evolution ESO's programme would experience in the next thirty years. Ewine and I certainly did not expect that our 30th PhD anniversary would coincide with the key milestone for astronomy we pass today, hopefully leading to first light in exactly ten years from now!

It has taken 15 years to get to this point, thanks to the efforts of many, many people, inside and outside ESO. Particular credit is due to Roberto Gilmozzi, a former Paranal Director, for starting the precursor 100-metre diameter OWL project, to Riccardo Giacconi for allowing it, to Catherine Cesarsky who steered the process that resulted in the start of a full design study for what was, by then, the E-ELT, and to Jason Spyromilio who led the design effort. It is unfortunate that for a variety of reasons none of them could be here today, to join us on this festive occasion.

Finally, it is important to recognise that Chile does not just provide a privileged platform for astronomical observations. ESO's telescopes also provide training and employment for many Chileans: administrative staff, astronomers, engineers, technicians and telescope operators. Chilean universities host internationally recognised astronomers who collaborate actively with colleagues in the ESO Member States. Some are now developing engineering programmes to produce state-of-the-art astro-technology products, creating capabilities and know-how that will benefit many other aspects of Chilean society. ESO is proud to be associated with this impressive growth of capabilities, and looks forward to starting exchange programmes as part of the E-ELT Agreement to strengthen the already existing cooperation further.

The E-ELT will no doubt produce discoveries that we simply cannot imagine today, and it will surely inspire numerous people around the world to think about science, technology and our place in the Universe. It is exciting to take the first step towards this goal today, so that the strong team led by Roberto Tamai can transform what was once a dream into a reality!

Telescopes and Instrumentation

The final ALMA antenna, the 66th, being delivered to the Array Operations Site on Chajnantor on a transporter (image from June 2014). This was the 25th and last of the 12-metre European antennas built for ALMA. See Announcement eso14048 for details.

A. Marinkovic/X-Cam/ALMA (ESO/NAOJ/NRAO)

The Spectro-Polarimetric High-contrast Exoplanet REsearch instrument (SPHERE) is being commissioned and first light images were released in June 2014 (see Release eso1417). SPHERE is shown shortly after installation at the Nasmyth focus of VLT Unit Telescope 3 (Melipal).

ESO/J. Girard

An Overview of the MATISSE Instrument — Science, Concept and Current Status

Bruno Lopez[1]
Stéphane Lagarde[1]
Walter Jaffe[2]
Romain Petrov[1]
Markus Schöller[3]
Pierre Antonelli[1]
Udo Beckmann[4]
Philippe Berio[1]
Felix Bettonvil[5]
Andreas Glindemann[3]
Juan-Carlos Gonzalez[3]
Uwe Graser[6]
Karl-Heinz Hofmann[4]
Florentin Millour[1]
Sylvie Robbe-Dubois[1]
Lars Venema[5]
Sebastian Wolf[7]
Thomas Henning[6]
Thierry Lanz[1]
Gerd Weigelt[4]
Tibor Agocs[5]
Christophe Bailet[1]
Yves Bresson[1]
Paul Bristow[3]
Michel Dugué[1]
Matthias Heininger[4]
Gabby Kroes[5]
Werner Laun[6]
Michael Lehmitz[6]
Udo Neumann[6]
Jean-Charles Augereau[8]
Gerardo Avila[3]
Jan Behrend[4]
Gerard van Belle[9]
Jean-Philippe Berger[3]
Roy van Boekel[6]
Serge Bonhomme[1]
Pierre Bourget[3]
Roland Brast[3]
Olivier Chesneau[1†]
Jean-Michel Clausse[1]
Claus Connot[4]
Ralf Conzelmann[3]
Pierre Cruzalèbes[1]
Gergely Csepany[10]
William Danchi[11]
Marco Delbo[1]
Françoise Delplancke[3]
Carsten Dominik[12]
Albert van Duin[5]
Eddy Elswijk[5]
Yan Fantei[1]
Gerd Finger[3]
Armin Gabasch[3]
Jean Gay[1]
Paul Girard[1]
Vincent Girault[1]
Philippe Gitton[3]
Annelie Glazenborg[13]
Frédéric Gonté[3]
Florence Guitton[1]
Serge Guniat[3]
Menno De Haan[5]
Pierre Haguenauer[3]
Hiddo Hanenburg[5]
Michiel Hogerheijde[2]
Rik ter Horst[5]
Josef Hron[14]
Yves Hugues[1]
Christian Hummel[3]
Jan Idserda[5]
Derek Ives[3]
Gerd Jakob[3]
Attila Jasko[9]
Paul Jolley[3]
Sandor Kiraly[9]
Rainer Köhler[6]
Jan Kragt[4]
Tim Kroener[6]
Sjouke Kuindersma[5]
Lucas Labadie[15]
Christoph Leinert[6]
Rudolf Le Poole[2]
Jean-Louis Lizon[3]
Christian Lucuix[3]
Aurélie Marcotto[1]
Frantz Martinache[1]
Grégoire Martinot-Lagarde[1]
Richard Mathar[6]
Alexis Matter[8]
Nicolas Mauclert[1]
Leander Mehrgan[3]
Anthony Meilland[1]
Klaus Meisenheimer[6]
Jeffrey Meisner[2]
Marcus Mellein[6]
Serge Menardi[3]
Jean-Luc Menut[1]
Antoine Merand[3]
Sébastien Morel[3]
Lazlo Mosoni[10]
Ramon Navarro[5]
Edmund Nussbaum[4]
Sébastien Ottogalli[1]
Ralf Palsa[3]
Johana Panduro[6]
Eric Pantin[16]
Thierry Parra[1]
Isabelle Percheron[3]
Thanh Phan Duc[3]
Jörg-Uwe Pott[6]
Eszter Pozna[3]
Frank Przygodda[17]
Yves Rabbia[1]
Andrea Richichi[18]
Florence Rigal[5]
Ronald Roelfsema[5]
Gero Rupprecht[3]
Dieter Schertl[4]
Christian Schmidt[3]
Nicolas Schuhler[3]
Menno Schuil[5]
Alain Spang[1]
Jörg Stegmeier[3]
Lamine Thiam[1]
Niels Tromp[5]
Farrokh Vakili[1]
Martin Vannier[1]
Karl Wagner[6]
Julien Woillez[3]

[1] Laboratoire Lagrange, UMR7293, Université de Nice Sophia-Antipolis, CNRS, Observatoire de la Côte d'Azur, Nice, France
[2] Leiden Observatory, Leiden University, the Netherlands
[3] ESO
[4] Max-Planck Institute for Radio Astronomy, Bonn, Germany
[5] NOVA ASTRON, Dwingeloo, the Netherlands
[6] Max-Planck Institute for Astronomy, Heidelberg, Germany
[7] Institute of Theoretical Physics and Astrophysics, Kiel University, Germany
[8] Université de Grenoble Alpes, CNRS, IPAG, Grenoble, France
[9] Lowell Observatory, Flagstaff, USA
[10] MTA Research Centre for Astronomy and Earth Sciences, Konkoly Thege Miklos Astronomical Institute, Budapest, Hungary
[11] NASA/Goddard Space Flight Center, Greenbelt, USA
[12] Sterrenkundig Instituut "Anton Pannekoek", University of Amsterdam, the Netherlands
[13] Kernfysisch Versneller Institute, Groningen, the Netherlands
[14] Institut für Astrophysik, University of Vienna, Austria
[15] I. Physics Institute, University of Cologne, Germany
[16] Laboratoire AIM, CEA/DSM–CNRS–Université Paris Diderot, IRFU/Service d'Astrophysique, CEA-Saclay, Gif-sur-Yvette, France
[17] Deutsche Thomson OHG, Villingen-Schwenningen, Germany
[18] National Astronomical Research Institute of Thailand, Chiang Mai, Thailand

MATISSE, a second generation Very Large Telescope Interferometer (VLTI)

instrument, is a combined imager and spectrograph for interferometry in the 3–5 μm region (*L*- and *M*-bands) and the 8–13 μm window (*N*-band). MATISSE builds on the experience gained with the VLTI's first generation instruments. It employs multi-axial beam combination while also providing wavelength differential visibility and phase, and closure-phase aperture-synthesis imaging at a range of spectral resolutions. MATISSE is designed for a broad range of science goals, and its potential for studies of the discs around young stars and active galactic nuclei are highlighted. The instrument concept and operating modes are described; construction is in progress towards installation at the VLTI in 2016.

The Multi AperTure mid-Infrared SpectroScopic Experiment (MATISSE) is the mid-infrared spectrograph and imager under construction for the VLTI. This second generation interferometric instrument will significantly contribute to several fundamental research topics in astrophysics, focussing, for instance, on the inner regions of discs around young stars where planets form and evolve, the surface structure and mass loss of stars at different evolutionary stages and the environment of black holes in active galactic nuclei (AGN).

MATISSE offers unique interferometric capabilities. The first is the opening of the *L*- and *M*-bands (respectively 3.0–4.0 and 4.6–5.0 μm) to long-baseline infrared interferometry. The angular resolution in the *L*-band will be about 3 milliarcseconds (mas) and various spectral resolutions between $R \sim 30$ and $R \sim 5000$ will be available. The second unique capability will be mid-infrared imaging — closure-phase aperture-synthesis imaging — performed with up to four Unit Telescopes (UTs) or Auxiliary Telescopes (ATs).

The MATISSE spectral bands will link the near-infrared spectral domain, for which several interferometric instruments have been developed, with the millimetre domain, where the Atacama Large Millimeter/Submillimeter Array (ALMA) provides a similar angular resolution. MATISSE can be seen as a successor to MIDI (the MID-infrared Interferometric instrument) because it will reconstruct images in the mid-infrared. The extension of MATISSE down to the infrared *L*-band makes it also an extension of AMBER (the Astronomical Multi-BEam CombineR) and of the second generation instrument GRAVITY (Eisenhauer et al., 2011). MATISSE will also be complementary to METIS (the Mid-infrared E-ELT Imager and Spectrograph for the European Extremely Large Telescope): while MATISSE will provide an angular resolution higher by a factor ~ 4–5, METIS will yield a higher sensitivity, higher spectral resolution and a broader wavelength coverage.

We present some of the main science objectives that have driven the instrument design. We introduce the physical concept behind MATISSE, including a description of the signal on the detectors and an evaluation of the expected performance, and discuss the project status. The operations concept will be detailed in a future article, which will illustrate the observing templates that operate the instrument, the data reduction and image reconstruction software.

Scientific motivation

From the very beginning of the project, MATISSE was planned as an interferometric imager for a broad range of astrophysical targets. To achieve this goal, stringent requirements for the instrument were derived from the most challenging science cases (Lopez et al., 2013): protoplanetary discs around progenitors to Solar-type stars (T-Tauri stars) and the dusty tori around AGN. The expected and achieved instrument characteristics will also open up other fields: the study of the birth of massive stars; the structure, dynamics and chemistry of evolved stars; the early evolution of Solar System minor bodies; exo-zodiacal dust discs of stars; properties of hot Jupiters; and the study of the immediate vicinity of the Galactic Centre (Wolf et al., 2007). In the following, we present an overview of the key astrophysical questions for which significant progress can be expected from observations with MATISSE.

Circumstellar discs

In the specific case of circumstellar discs, MIDI and AMBER allowed observers, for the first time, to investigate the potential planet-forming regions around young stars in nearby star-forming regions. The large-scale characteristics of these discs on scales of about 100 astronomical units (au) could be compared to the structure of the inner, au-scale regions (e.g., Leinert et al. 2004; Schegerer et al., 2009; Menu et al., 2014). Differences found in the grain size and crystallinity for the dust phase provided valuable insights into the physics determining the disc mineralogy (van Boekel et al., 2004), while the temporal variability of the re-emission brightness on scales of a few au sheds light on processes in young eruptive stars (Mosoni et al., 2013). In the near-infrared, AMBER was able to resolve the sub-au-scale gas and dust regions of accretion discs and the launching areas of winds in the continuum and emission lines (e.g., Br γ). Furthermore, the high spectral resolution offered by AMBER enabled the study of the kinematic properties of inner discs and disc wind regions (e.g., Weigelt et al., 2011). Such studies are important to improve our understanding of the fundamental accretion–ejection process.

MATISSE will allow us to continue from there, but with even more ambitious goals. This enthusiasm is justified on account of the following examples of the discovery potential of the instrument:

1. Direct detection of asymmetric disc structures, which can be used as tracers for the mechanisms of planet formation.
2. The extension to the *L*- and *M*-bands will allow the different spatial regions of the targeted objects, as well as different physical processes, to be investigated. While the *N*-band (7.5–14.5 μm) observations are dominated by the thermal emission of warm and cool dust, the *L*/*M*-band flux is expected to consist of both emission and scattering of short-wavelength radiation.
3. MATISSE will offer various spectral resolutions in the range of ~ 30 to ~ 5000, providing the means to study spectral features of amorphous and crystalline dust and polycyclic aromatic hydrocarbons (PAHs), as well as the distribution and kinematics of the gas.
4. Repeated observations will allow investigation of the temporal changes suggested from planet formation and planet–disc interaction scenarios.

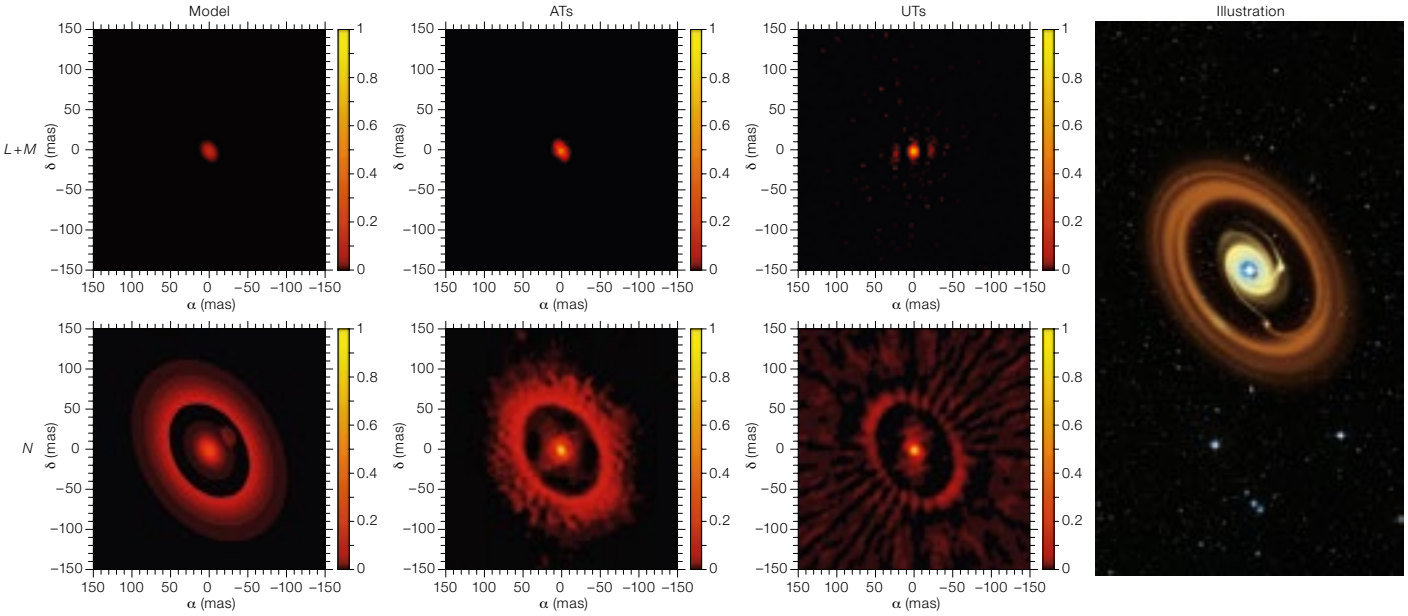

Figure 1. Illustration of the imaging capabilities of MATISSE in *L*-, *M*- and *N*-bands. A realistic scene representing the appearance of the young stellar object HD 100546 and its disc was simulated (leftmost column), fed into a MATISSE instrument simulator assuming three nights (for the ATs, second column) or one night (for the UTs, third column) of data collection. The reconstructed images were made using the MIRA software (Thiébaut & Giovannelli, 2010) and are shown in the second and third columns. The rightmost image, the genesis of the model, is based on Crida et al. (2008) and Crida (private communication).

Table 1. Selected spectral signatures accessible with MATISSE.

Feature	Wavelength (μm)
L- and *M*-bands (~ 2.8–5.0 μm)	
H_2O (ice)	3.14
H_2O (gas)	2.8–4.0
H lines (Br-α, Pf-β)	4.05, 4.65
PAHs	3.3, 3.4
Nano-diamonds	3.52
CO fundamental transitions	4.6–4.78
CO (ice)	4.6–4.7
N-band (~ 8.0–13.0 μm)	
Amorphous silicates	9.8
Crystalline silicates (olivines and pyroxenes)	9.7, 10.6, 11.3, 11.6
PAHs	8.6, 11.4, 12.2, 12.8
Fine structure lines (e.g., [S IV], [Ne III], [Ne II])	10.5, 10.9, 12.8

In combination with other high angular resolution instruments/observatories operating at complementary wavelength ranges (e.g., GRAVITY and ALMA), MATISSE will provide the means to study the planet-forming region in detail (see Figure 1). Specific key topics and questions that MATISSE can tackle include: the complexity of disc structures in the planet-forming zone of circumstellar discs at various stages of their evolution; the reasons for inner-disc clearing in transitional discs; constraints on properties, growth, and sedimentation of dust grains; tracers for giant protoplanets; the nature of outbursting young stellar objects; dust production as an outcome of planetesimal collisions and evaporation of exo-comets; and the launching region of winds and jets and the disc–outflow connection. Important spectral features of the gas and dust phase in these objects that will be accessible to MATISSE are listed in Table 1.

Active galactic nuclei

The other major observational topic for MATISSE concerns the study of AGN. The wavelength and baseline configurations provided by the VLTI allow observers to investigate the gas emission and dust emission in the temperature range 300–1500 K in the 0.1–5-parsec core region of the nearest AGNs. Astrophysical problems that can be addressed with observations in the mid-infrared spectral domain concern the morphology, chemistry and physical state of the circumnuclear dusty structures. Important questions that MATISSE will be able to advance, are, for example: the relative distribution of the warm and the hot dust and the origin of this dust; the mechanism that supports the thickness and determines the inner edge of the dusty torus; the effect of the torus on the energy balance of the accreting material and the AGN as a whole; the origin of the Type I/Type II dichotomy — as an inclination effect or fundamental morphological differences; and the relation between the dusty regions and the inner ionised broad line region (BLR).

The results achieved within studies of individual nearby bright AGNs with MIDI, AMBER and the Keck interferometer (Jaffe et al., 2004; Kishimoto et al., 2011; Meisenheimer et al., 2007; Petrov et al., 2012; Weigelt et al., 2012; Tristram et al. 2014; Lopez-Gonzaga et al., 2014) and the Large Programme survey of 25 Seyfert galaxies with MIDI (Burtscher & Tristram, 2013) have shown that warm (~ 300–1500 K) nuclear dust discs do indeed exist. However, in the *N*-band they appear smaller than expected (~ 1 pc), sometimes misaligned relative to the jets, and show indications of clumpiness. The spectrum of the silicate absorption does not resemble that in star-forming

regions. These results are interpreted as showing that the discs are comprised of dense clumps, optically thick even in the mid-infrared. Additional puzzling observations include the radio galaxy Centaurus A, which features a complicated mixture of thermal and synchrotron radiation and the quasar 3C273 (Petrov et al., 2012) with a BLR that extends beyond the inner edge of its dust torus.

MATISSE will allow us, for the first time, to reconstruct infrared aperture-synthesis images of the nearest AGN — NGC 1068, Circinus, and Centaurus A. Their mid-infrared dust emission in the circum-nuclear region was too complex for MIDI to disentangle and true mapping with closure phases is needed. MATISSE will allow the relative astrometry of features in these AGN to be probed over its broad wavelength range (3–13 μm).

However, to make full use of the potential of MATISSE and thus to fully achieve the above goals, improvements in the VLTI infrastructure are mandatory. In particular, these concern the decrease of the vibration level of the UTs, adaptive optics on the ATs, and, most important, the availability of a second generation fringe tracker (2GFT) for MATISSE. A 2GFT will improve the sensitivity, accuracy and spectroscopic capability of MATISSE and will thus have a direct impact on the scientific potential of the instrument, in the following ways:

– The sensitivity achievable with a 2GFT is required for the study of AGNs and the discs around young stars. For example, with a 2GFT, longer baselines can be used to establish the connections between the high surface brightness inner discs and the asymmetric larger components.
– Higher accuracy is important for closure-phase imaging in the *L*-, *M*- and *N*-bands, which provides constraints on the radial and vertical temperature gradient and opacity structure in discs of young stars.
– Medium and high spectral resolution interferometry will become feasible.

MATISSE concept

MATISSE uses an all-in-one multi-axial beam combination scheme. We concluded that this type of combination is the most suitable for an interferometric instrument with more than two apertures and operating in the mid-infrared. Initially, based on the efficiency of the two-telescope MIDI recombination scheme, a pairwise co-axial concept was considered. The advantage of this scheme is the simultaneous delivery of two interferometric signals per baseline, phase shifted by π. The correlated flux is then obtained by subtracting the two signals. In this way, the thermal background level and its associated temporal fluctuations are directly eliminated, but not the related thermal photon noise. However, in spite of good expected efficiency in terms of signal-to-noise ratio (SNR), this scheme displays a number of issues when extended from two to four telescopes: a possible weakness in the stability of the closure-phase measurements and a high instrumental complexity due to numerous opto-mechanical elements required in the cold environment. These issues led us to consider multi-axial global combination as the more robust and simpler scheme.

The multi-axial global beam combination scheme (see Figure 2) means that the four beams are combined simultaneously on the detector. The interferometric fringe pattern and the four individual photometric signals receive respectively 67 % and 33 % of the incoming flux. MATISSE will observe in three bands simultaneously: *L*, *M* and *N*. The signals are spectrally dispersed using grisms: spectral resolutions of 30 and 220 are provided in the *N*-band and four resolutions in the *L*- and *M*-bands of 30, 500, 1000 and 3500–5000. The spatial extent of the interferometric pattern is larger than the photometric signals in order to optimise the sampling of the six different spatial fringe periods. The beams are combined by the camera optics. At this plane, the beam configuration is non-redundant in order to produce different spatial fringe periods, and thus to avoid crosstalk between the fringe peaks in Fourier space. The separation B_{ij} between beams *i* and *j* in the output pupil is respectively equal to 3*D*, 9*D* and 6*D*, where *D* is the beam diameter.

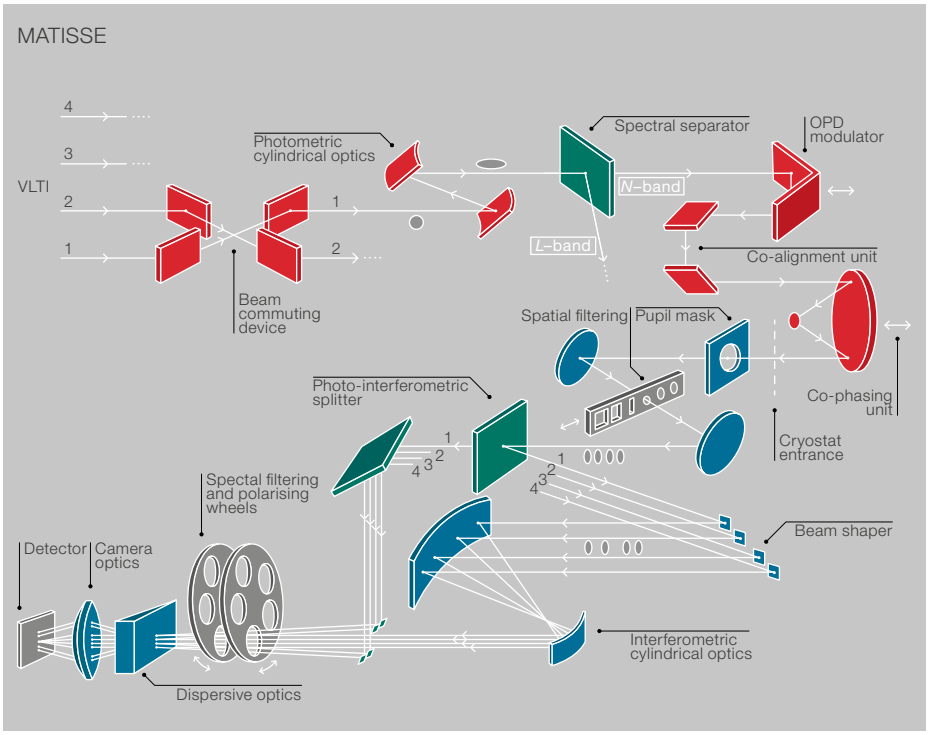

Figure 2. The schematic layout of the MATISSE instrument concept is shown. The red parts represent optical elements located on the warm optics table at ambient temperature. The blue parts represent optical elements of the cold optics bench located in the cryostats. Only one COB with its elements and detector is shown.

Since the thermal background at the longest wavelengths is variable, and much exceeds the target coherent flux, it is important to limit the cross-talk between the low frequency peak and the high frequency fringe peaks to a level below the thermal background photon noise limit. Two methods are used in MATISSE to ensure this result and estimate the coherent flux with high accuracy: spatial modulation, as in AMBER, and temporal modulation, as in MIDI, with both methods combined by varying the optical path difference (OPD) between the beams.

For each of the six baselines used and in each of the spectral channels, the observable quantities are the following:

1. photometry;
2. coherent flux of the source;
3. absolute visibility derived from the photometry and the coherent flux measurements;
4. wavelength-differential visibility (i.e., change of visibility with wavelength);
5. wavelength-differential phase; and
6. closure phase.

In order to measure the visibility, we need to extract the source photometry by separating the stellar flux from the sky background using sky chopping. The problem with chopping is that the observation of the sky and that of the target are not simultaneous. Therefore, thermal background fluctuations will be the most important contribution to the visibility error. Fortunately, chopping is unnecessary for measuring the coherent flux, the wavelength-differential and closure phases.

Operating modes

MATISSE has two standard operating modes. The HighSens mode does not provide photometry and all photons are collected in the interferometric fringe pattern beam. This maximises the sensitivity for the wavelength-differential and closure phases. In this mode it is possible to make photometric observations sequentially after the interferometric observations. In the SiPhot mode, two thirds of the flux goes into the interferometric channel and one third into the photometric channels. Chopping is used to measure the average source photometry and extract the visibility from the coherent flux. These two modes can also be mixed, that is the HighSens mode in *N*-band and the SiPhot in *L*-band.

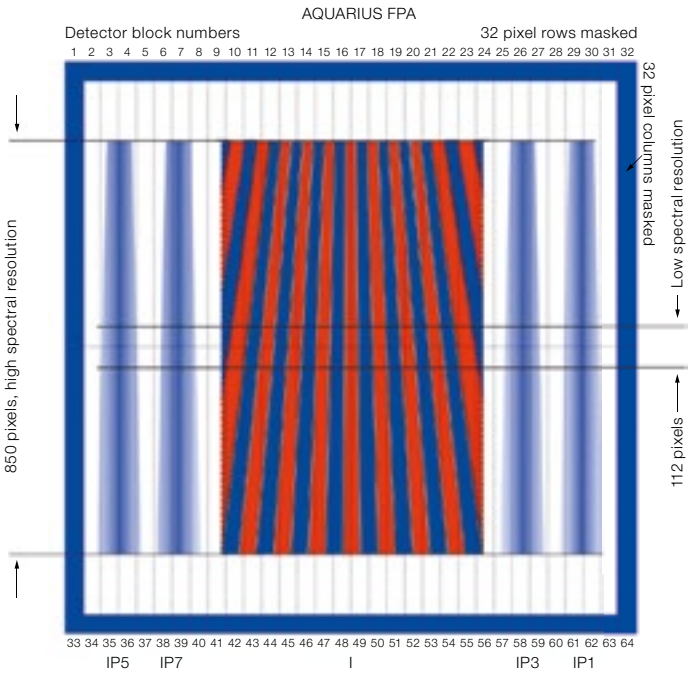

Figure 3. The layout of the interferometric pattern (central detector blocks, dispersion direction vertical) and the four photometric signals (outer detector blocks) on the AQUARIUS detector is shown for the SiPhot mode in *N*-band with medium spectral resolution dispersion.

In the SiPhot mode, the detector simultaneously collects the light of up to five instrument outputs: four photometric signals in addition to the interferometric pattern (see Figure 3). During observations with four telescopes, the interferogram contains the combined dispersed fringe pattern of six baselines, but because the beam combination is non-redundant, the information on the fringes corresponding to six different spatial periods can directly be recovered. In the spatial direction, minimum sampling of the interferometric signal requires 4 pixels per period of the narrowest fringes (24 for the widest) at the short end of the spectral bands covered by the instrument. The sampling of the interferometric beam is 72 pixel per λ/D in the spatial direction and 3 pixels per λ/D in the spectral direction, corresponding to an anamorphic factor of 24.

In the spatial direction, the interferometric field is about 468 pixels wide (corresponding to a field of 4λ/D) and the photometric field is about 78 pixels. The size in the spectral direction depends on the spectral resolution and varies from 100 pixels for *L*- and *M*-bands at low spectral resolution (150 pixels for the *N*-band at low resolution) to the full detector for medium and high spectral resolution (indicated on Figure 3).

Performance

Tables 2 and 3 give the limiting fluxes and specifications for MATISSE. The values take into account all characteristics of the VLTI (e.g., optical transmission, adaptive optics performance, tip-tilt, focal laboratory) and a full calibration procedure (Lagarde et al., 2012).

The expected ultimate performance requires some evolution of the VLTI infrastructure: external fringe tracking, collecting data such as OPD and tip-tilt residu-

Table 2. *L*- and *N*-band limiting fluxes.

	L-band sensitivity	*N*-band sensitivity
AT	Spec = 6.5 Jy (*L* = 4.1), Goal = 1.25 Jy	Spec = 45 Jy (*N* = –0.25), Goal = 10 Jy
UT	Spec = 0.65 Jy (*L* = 6.6), Goal = 0.12 5Jy	Spec = 3 Jy (*N* = 2.7), Goal = 0.75 Jy

		L-band	*N*-band
Visibility	AT	≤ 7.5 % (Goal: 2.5 %)	≤ 30 % (Goal: 10 %)
	UT	≤ 7.5 % (Goal: 2.5 %)	≤ 7.5 % (Goal: 2.5 %)
Closure phase	AT	≤ 80 mrad	≤ 80 mrad
	UT	≤ 40 mrad	≤ 40 mrad
Differential visibility	AT	≤ 3 % (Goal: 1 %)	≤ 30 % (Goal: 10 %)
	UT	≤ 1.5 % (Goal: 0.5 %)	≤ 5 % (Goal: 2 %)
Differential phase	AT	≤ 60 mrad	≤ 60 mrad

Table 3. *L*- and *N*-band specifications (and goals) for a 20 Jy unresolved source observed at low spectral resolution.

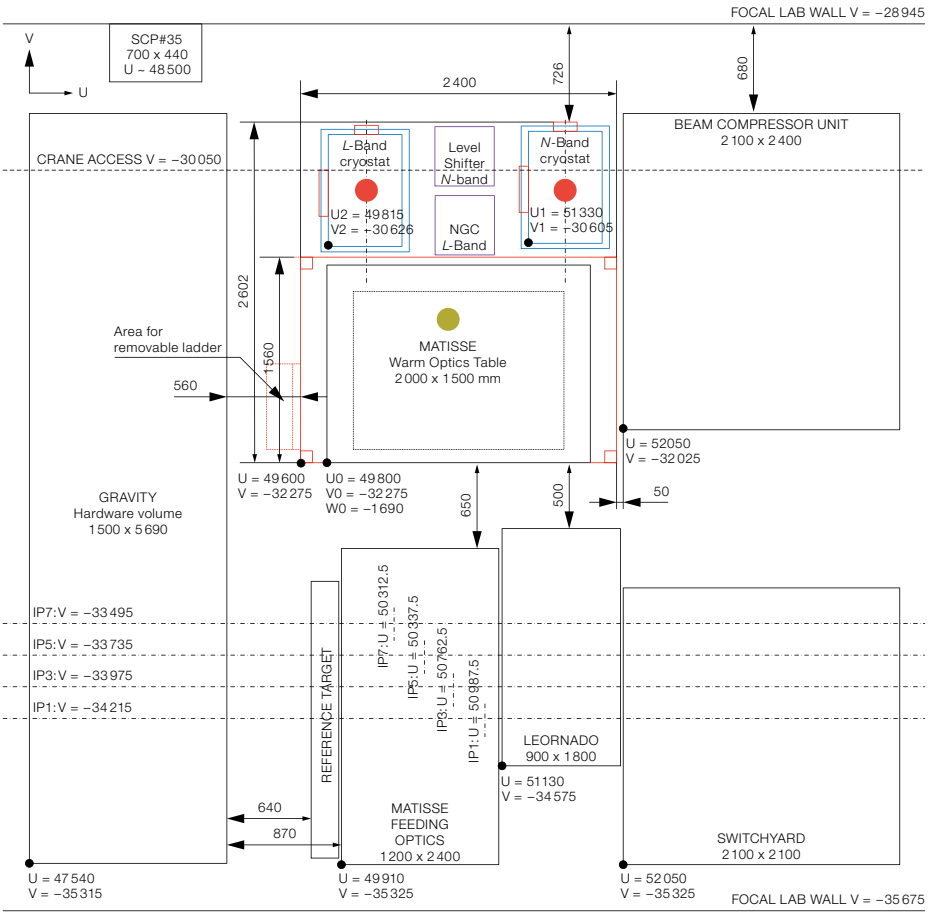

Figure 4. The future location of MATISSE in the VLTI laboratory is sketched. The warm optics table and the two cryostats are viewed from above. This location is currently used by MIDI. Sub-figure **(a)** shows the MATISSE warm optics bench with its optical components; **(b)** one of the two MATISSE cryostats, which holds the cold optics bench and the detector; and **(c)** shows one of the MATISSE cold optics benches.

als, and lateral pupil motion monitoring or even active correction.

Instrument design

MATISSE is composed of the Warm OPtics (WOP) and two Cold Optics Benches (COB). There are two mid-infrared detectors, each housed, with a COB, in its own cryostat; see Figure 2 where only a single COB is sketched. The locations of the different parts of the instrument inside the VLTI laboratory are illustrated in Figure 4.

The WOP rests on a 2 by 1.5 metre optical table and receives four beams — designated IP7/5/3/1 — through the feeding optics, coming from either the UTs or ATs. These four beams enter first into the beam commuting devices, which allow the commutation of beams IP7 and IP5 and beams IP3 and IP1. The beams are then individually anamorphosed with a ratio of 1:4 by the cylindrical optics. The beams are spectrally separated with individual dichroics in order to form the *L*- and *M*-band and the *N*-band beams. Before entering into the cryostats, each beam passes through two modules. The first one is a periscope that is used for the co-alignment of image and pupil. The second module is a delay line that delivers the pupil plane at the correct position into the COB and equalises the optical path differences between the beams and the differential optical path between the *L*- and *M*- and the *N*-bands.

The WOP also contains the OPD modulation function, which is part of the spectral separator. In addition, the WOP accommodates two internal optical sources in a tower, one visible light source for alignment purposes (a fibred laser diode) and one infrared source for calibration purposes (a ceramic with thermal insulation housing). These internal optical sources deliver four identical beams and are injected into the instrument through the SOurce Selector module (SOS).

The cold optics benches consist of several modules. The beam selector cartridge holds four shutters. The re-imager box supports the cold stop in the pupil plane, curved optics and the spatial filters in

the image plane with its pinhole and slit slider. The beam-shaper box contains the beam splitters with a slider, several folding mirrors, the anamorphic optics and the photometric re-injection mirrors. The wheel box includes the filter wheel, the polarising wheel and the dispersive wheel and the camera box carries the two camera lenses, a folding mirror and the detector mount (see Figure 2).

Light enters the entrance windows of the cryostats with an anamorphic factor of 4, passing the cold stops and the off-axis optics and spatial filtering module of the re-imager unit, until it reaches the beam splitter. The light is split into the interferometric channel and the photometric channels. The anamorphism of the interferometric channel is further increased by a factor of 6, to a total of 24 by the anamorphic optics. Finally, after passing the filter, polariser and dipersion wheels, the light will reach the detector via the camera (Figure 2).

MATISSE uses two different detectors. The MATISSE *L*- and *M*-band detector is a Teledyne HAWAII-2RG of 2048 × 2048 pixels, grouped in 32 blocks of 64 × 2048 pixels. The MATISSE *N*-band detector is a Raytheon AQUARIUS, which has a format of 1024 × 1024 pixels, grouped in 2 × 32 blocks of 32 × 512 pixels.

Genesis and future of the project

In 2002 the two-telescope VLTI instrument MIDI had first light. Already at that time, the idea of an upgrade to an interferometric imager was born. A first prototype was studied and built, leading to a first concept, called APreS-MIDI (Aperture SynthesiS with MIDI), which was presented at the ESO VLTI conference in 2005 (Richichi et al., 2008).

Following a recommendation by ESO, the MATISSE Consortium initiated a conceptual design study for a second generation VLTI instrument. The MATISSE Preliminary Design Review was held in December 2010 in Garching, and the Final Design Reviews occurred in September 2011 for cryogenics and optics and April 2012 for the whole instrument. Currently, we are building the instrument;

Figure 5. Some views from the laboratories: 5a: A view of some of the components of the cold optics bench, including the beam-shaper box presented in front of the COB backbone; 5b: A discussion concerning the cool-down procedure; 5c: Two of the three electronics cabinets; 5d: Both cryostats at MPIA; 5e: The *N*-band cryostat and cold optics delivered to Nice in July 2014 and now installed in front of the warm optics bench. This moment marks the beginning of the global integration of all the MATISSE subsystems.

preliminary acceptance in Europe is planned for November 2015 and the first light at Paranal is foreseen in 2016.

The project became possible thanks to the scientific research conducted in our laboratories and institutes in the field of interferometric concepts and observing methods and the experience acquired on AMBER and MIDI. The availability of several new key technological components, like large detectors, efficient cooling devices and state-of-the-art cryomechanisms have contributed to make MATISSE possible and enable a highly automated instrument. The numerous interactions between people and institutes from different countries as well as the engineering challenges have made our project a pleasant human adventure that has generated a lot of creativity.

As a general user instrument, the aim is that MATISSE observations should be conducted by many researchers from the international community. MATISSE will offer unique and fascinating observational capabilities: new spectral observing windows at the VLTI and closure-phase image reconstruction in the mid-infrared. The high-resolution observations of young circumstellar discs where planets form and evolve, of surface structures and mass-loss of stars in late evolutionary stages, and of the environments of black holes in AGN will contribute to answering several fundamental astrophysical questions and will surely lead to unexpected discoveries. We hope that all future observers will benefit from use of MATISSE.

Status of the project

The different MATISSE subsystems are being integrated and tested at the NOVA-ASTRON Institute in Dwingeloo, the Max-Planck Institute for Astronomy in Heidelberg (MPIA), the Max-Planck Institute for Radio Astronomy in Bonn (MPIfR), the detector department of ESO Garching and the Observatory of the Côte d'Azur (OCA) in Nice.

Figure 5 shows some views of the different subsystems integrated in our laboratories. Figure 6 shows images from the first laboratory fringes obtained in spring 2014. It shows the first infrared illumination and fringes on the AQUARIUS detector. A mid-infrared laser beam was feeding three of the four MATISSE beams.

The different subsystems integrated and tested in the different institutes of the Consortium are presently being sent to OCA for global integration and testing of the instrument. Following delivery of part of the electronics and the instrument software from MPIA to OCA in April 2014, the *N*-band cold optics, its cryostat and the AQUARIUS detector are being delivered in the period July–September 2014. The *L*- and *M*-band COB with its cryostat, its HAWAII 2RG detector and its electronics, will be sent from MPIA to Nice in November 2014.

Acknowledgments

MATISSE is defined, funded and built in close collaboration with ESO, by a Consortium composed of French (INSU-CNRS in Paris and OCA in Nice), German (MPIA, MPIfR and University of Kiel), Dutch (NOVA and University of Leiden), and Austrian (University of Vienna) institutes. The Conseil Général des Alpes-Maritimes in France, the Konkoly Observatory and Cologne University have also provided some support to the manufacture of the instrument.

We thank all MATISSE friends for their deep involvement and work and also acknowledge E. Thiebaut, K. Demick, Ph. Mathias, A. Niedzeilski, A. Russell, B. Stecklum, J. R. Walsh, A. C. da Fonte Martins, W. Boland, J.-M. Hameury, A. Crida, J. Colin, L. Pasquini, D. Mourard and A. Roussel for their assistance.

Our special thoughts go to Olivier Chesneau and Alan Moorwood, both of whom left us too early.

References

Burtscher, L. et al. 2013, A&A, 558, A149
Burtscher, L. & Tristram, K. R. W. 2013, The Messenger, 154, 62
Crida, A. et al. 2008, A&A, 483, 325
Eisenhauer, F. et al. 2011, The Messenger, 143, 16
Jaffe, W. et al. 2004, Nature, 429, 47
Kishimoto, M. et al. 2011, A&A, 536, 78
Lagarde, S. et al. 2012, SPIE, 8445-91
Lopez, B. et al. 2013, MATISSE Science Analysis Report, Issue 4
Lopez-Gonzaga, N. et al. 2014, A&A, 565, 71
Leinert, C. et al. 2004, A&A, 423, 537
Meisenheimer, K. et al. 2007, A&A, 471, 453
Menu, J. et al. 2014, A&A, 564, A93
Mosoni, L. et al. 2013, A&A, 552, A62
Petrov, R. G. et al. 2012, SPIE, 8445-0W
Richichi, A. et al. (eds.) 2008, *The Power of Optical/IR Interferometry: Recent Scientific Results and 2nd Generation VLTI Instrumentation*, Proc. ESO Workshop, Springer
Schegerer, A. A. et al. 2009, A&A, 502, 367
Thiébaut, E. & Giovannelli, J. F. 2010, IEEE Signal Processing Magazine, 27, 97
Tristram, K. R. W. et al. 2014, A&A, 563, A82
van Boekel, R. et al. 2004, Nature, 432, 479
Weigelt, G. et al. 2011, A&A, 527, A103
Weigelt, G. et al. 2012, A&A, 541, L9
Wolf, S. et al. 2007, MATISSE Phase A Science Cases, Issue 1

Figure 6. Images from the observation of the first fringes in spring 2014 in the laboratory at MPIA are shown in 6a and 6b. The zoom on the computer screen during the first fringe event is shown in 6c. Only three input beams were used for this test. The spatial direction is horizontal and the spectral dispersion vertical. On the left and right of the screen the photometric channels can be seen (c.f. Figure 3).

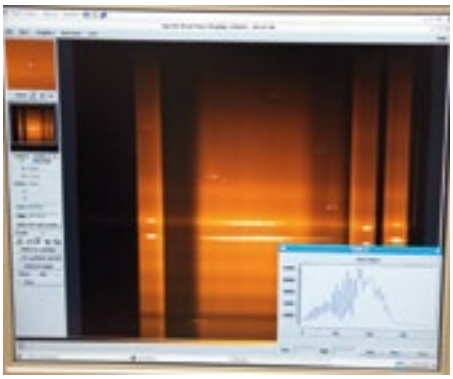

MUSE Commissioning

Roland Bacon[1]
Joel Vernet[2]
Elena Borisiva[3]
Nicolas Bouché[4]
Jarle Brinchmann[5]
Marcella Carollo[3]
David Carton[5]
Joseph Caruana[7]
Susana Cerda[2]
Thierry Contini[4]
Marijn Franx[5]
Marianne Girard[4]
Adrien Guerou[4,2]
Nicolas Haddad[2]
George Hau[2]
Christian Herenz[7]
Juan Carlos Herrera[2]
Bernd Husemann[2]
Tim-Oliver Husser[6]
Aurélien Jarno[1]
Sebastian Kamann[6]
Davor Krajnovic[7]
Simon Lilly[3]
Vincenzo Mainieri[2]
Thomas Martinsson[5]
Ralf Palsa[2]
Vera Patricio[1]
Arlette Pécontal[1]
Roser Pello[4]
Laure Piqueras[1]
Johan Richard[1]
Christer Sandin[7]
Ilane Schroetter[4]
Fernando Selman[2]
Maryam Shirazi[3]
Alain Smette[2]
Kurt Soto[3]
Ole Streicher[7]
Tanya Urrutia[7]
Peter Weilbacher[7]
Lutz Wisotzki[7]
Gerard Zins[8,2]

[1] CRAL, Observatoire de Lyon, Saint-Genis-Laval, France
[2] ESO
[3] Institute of Astronomy, ETH Zentrum, Zurich, Switzerland
[4] IRAP, Observatoire Midi Pyrénées, Toulouse, France
[5] Leiden Observatory, Leiden University, the Netherlands
[6] Institute for Astrophysics Göttingen, Germany
[7] Leibniz Institut für Astrophysik Potsdam, AIP, Germany
[8] IPAG, Observatoire de Grenoble, France

The Multi Unit Spectroscopic Explorer (MUSE) is now in Paranal and was installed on the VLT's Unit Telescope 4 in January 2014. MUSE enters science operations in October. A short summary of the commissioning activities and Science Verification are presented. Some examples of the first results achieved during the two commissioning runs are highlighted.

The Multi Unit Spectroscopic Explorer (MUSE) is a second generation Very Large Telescope (VLT) instrument for integral field spectroscopy in the optical range (460–940 nm). It has two modes with different fields of view: 1 by 1 arcminutes at a spatial sampling of 0.2 arcseconds; and, when coupled to the Adaptive Optics Facility, a laser tomography adaptive optics assisted mode with a field of 7.5 by 7.5 arcseconds (with 25 milliarcsecond pixels). The instrument concept is described in Bacon et al. (2006) and an update on construction is given in Bacon et al. (2012).

After its successful Preliminary Acceptance in Europe in September 2013[1], MUSE was shipped to Paranal. A large set of boxes representing 24 tonnes and 200 cubic metres of material arrived in Paranal in early October and the reintegration process started. From October to December 2013 the consortium engineers, with the support of ESO Paranal and Garching staff, proceeded to the reintegration and final alignment of the instrument in the new Paranal integration hall. Early in January 2014, the instrument, fully aligned, was moved to Unit Telescope 4 (UT4).

Since MUSE was too large to enter through the dome entrance door, it had to be lifted by a dedicated crane to pass through the dome slit — a scary moment! On 19 January 2014, MUSE successfully "landed" on the Nasmyth platform B of UT4. After a few checks, it was connected to the telescope system and some fine-tuning of the alignment was performed. On 31 January 2014, a few minutes after dome opening, MUSE saw its first light: the high proper motion sub-dwarf M star, VZ Pictoris, at a distance of 4 pc, known as Kapteyn's star. The first light target was a symbolic choice because 13 years is not only the time spent by the light to reach MUSE from the star's surface, but it is also the duration of the project, which started in 2001 when the consortium answered the ESO call for ideas for second generation VLT instrumentation.

Commissioning

After some technical half nights to finalise the instrument's alignment on the telescope, the first commissioning period started. During 15 nights, from 7 to 21 February 2014, functional tests and performance assessments were performed. From the first minute, MUSE worked as expected and the whole run went very smoothly, with no down time.

The performance, as anticipated by the laboratory measurements, is excellent and in general, much better than the original specifications. The MUSE image quality is so good that it is limited by the 0.2-arcsecond sampling. Definitive proof of this key performance statistic was obtained in the third commissioning run when an exceptionally good seeing of less than 0.4 arcseconds on a stellar cluster was simultaneously recorded by the telescope guide probe and measured on the final datacube provided by MUSE. The other important performance assessment is the throughput of the instrument, which peaks at 55 % at 700 nm. When including the telescope and atmosphere transmission, this translates to an end-to-end peak efficiency of 35 %, an outstanding achievement for such a complex instrument. This makes MUSE the most efficient spectrograph on the VLT in the 500–850 nm wavelength range.

In parallel with the functional tests and the performance assessment, we obtained a series of showcase observations to demonstrate the capabilities of MUSE on a number of different astronomical targets. At the end of this first commissioning run, half a billion spectra had been obtained. This impressive number of spectra was successfully ingested by the Paranal computer infrastructure and successfully reduced on the pipeline and offline workstations. Figure 1 shows just a sample of some of the targets observed during the commissioning from Jupiter, nearby star clusters and nebulae to nearby galaxies and a more distant galaxy cluster.

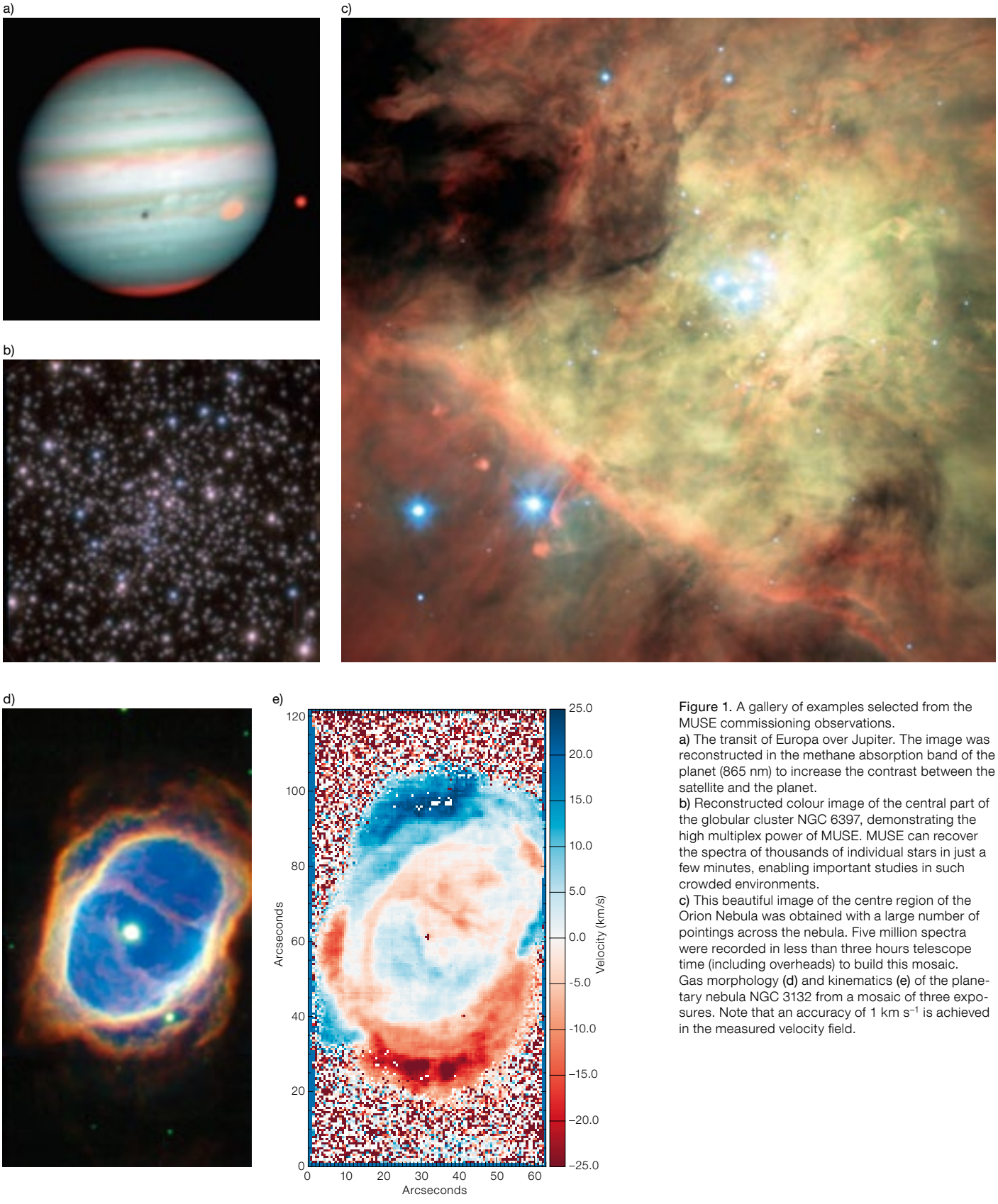

Figure 1. A gallery of examples selected from the MUSE commissioning observations.
a) The transit of Europa over Jupiter. The image was reconstructed in the methane absorption band of the planet (865 nm) to increase the contrast between the satellite and the planet.
b) Reconstructed colour image of the central part of the globular cluster NGC 6397, demonstrating the high multiplex power of MUSE. MUSE can recover the spectra of thousands of individual stars in just a few minutes, enabling important studies in such crowded environments.
c) This beautiful image of the centre region of the Orion Nebula was obtained with a large number of pointings across the nebula. Five million spectra were recorded in less than three hours telescope time (including overheads) to build this mosaic.
Gas morphology **(d)** and kinematics **(e)** of the planetary nebula NGC 3132 from a mosaic of three exposures. Note that an accuracy of 1 km s^{-1} is achieved in the measured velocity field.

f)

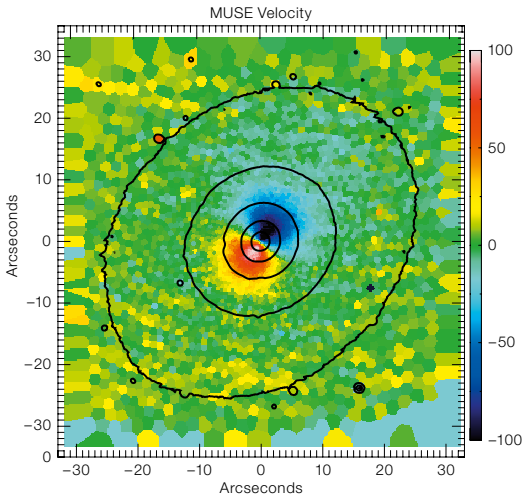

g)

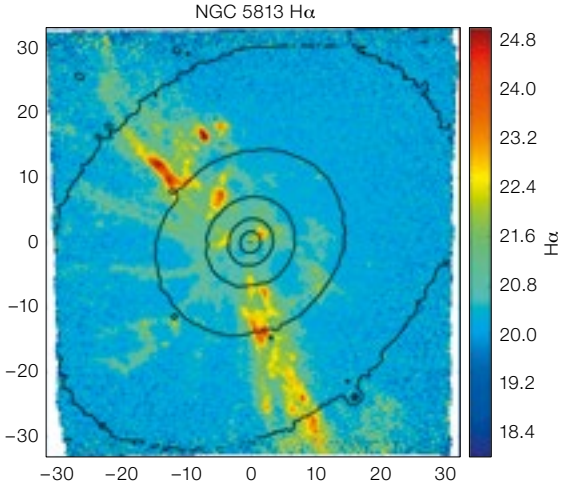

h)

i)

j)

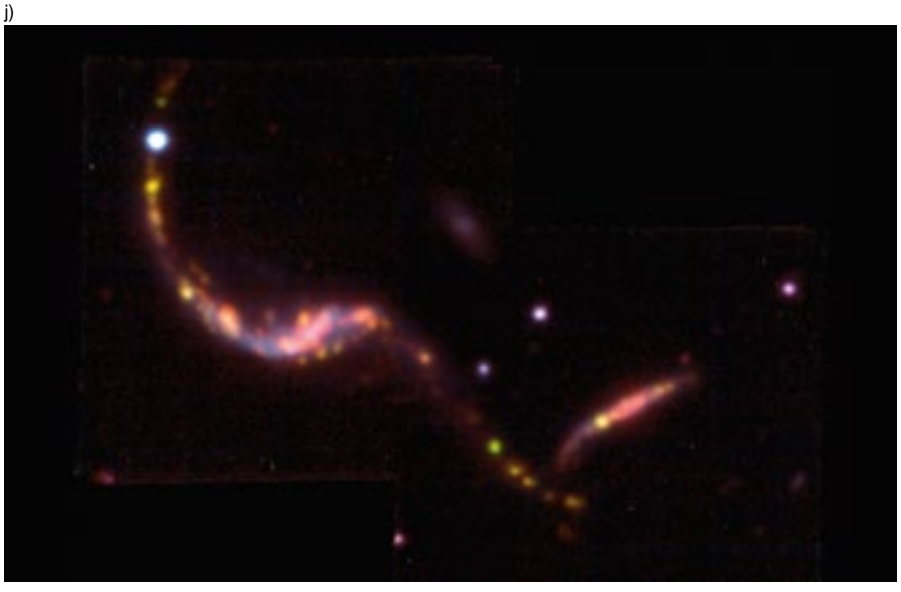

f) The high spatial resolution of MUSE is well demonstrated in the stellar velocity field of the central part of the elliptical galaxy NGC 5813 which exhibits a well-known kinematically decoupled core.
g) The same exposure shows the spectacular Hα emission morphology of the galaxy.
h) Motion and morphology of the gas in the NGC 4650A ring galaxy is represented in this colour picture (relative gas velocities are colour coded in green–red).
i) More distant objects have also been observed, such as the lensing massive cluster of galaxies SMACSJ2031.8-4036. The colour picture is a zoom of five highly magnified images (in blue) of the known $z = 3.5$ Lyman-α emission galaxy located in the background of the cluster.
j) Another example of interaction processes in galaxies is shown in this reconstructed image of AM353-272, alias the Dentist's Chair. MUSE will be an ideal tool to study the complex kinematics and physical conditions in these types of galaxies.

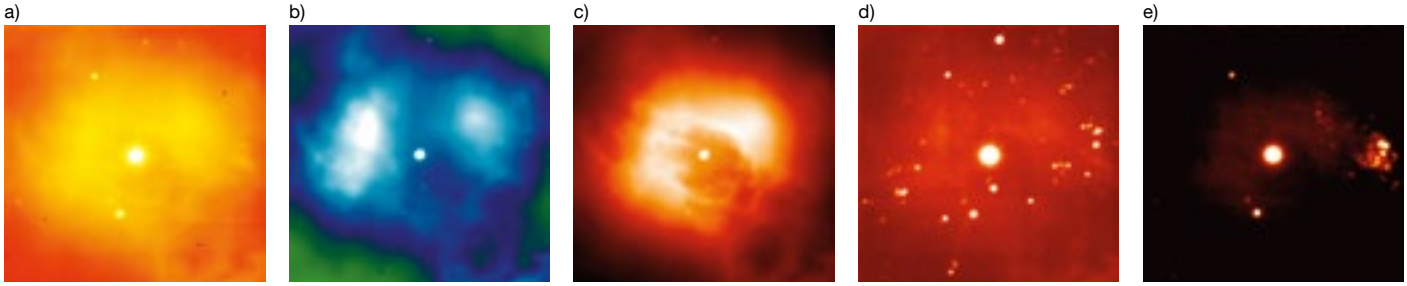

Figure 2. A series of images of the planetary nebula NGC 4361, observed to test the impact of the dithering strategy on the line spread function, illustrate the discovery potential of MUSE. The reconstructed images of the nebula in white light (**a**) and different emission lines ([O III] in (**b**), Hα in (**c**), [N II] in (**d**) display various morphologies which are indicative of the physical conditions (ionisation, density and temperature, as well as reddening) of the gas. While further exploring the datacube at the telescope around Hα, the puzzling image shown in (**e**) was revealed to be the Hα image of a background galaxy at $z = 0.02$. Given that this galaxy is just located behind the nebula and that its Hα emission is two orders of magnitude fainter than the planetary nebula Hα emission at this location, any imager, including the Hubble Space Telescope, would not be able to separate the galaxy emission, while MUSE uncovered the galaxy in just a few minutes of integration.

The quality of the datacubes produced, as demonstrated by the examples in Figure 1, is also a good demonstration of the instrument quality and the maturity of the data reduction system. The hard work of all the consortium and ESO staff along all these years has clearly paid off and MUSE started producing science data quality products after just a few nights of commissioning. This figure also demonstrates that MUSE should be able to provide new insights into a large variety of astronomical objects, from the surfaces of Solar System bodies to the most distant galaxies.

The second commissioning period was split into two runs, the first around the new Moon in early May and the second, also in dark time, from late July to early August 2104. These runs were used to improve the observing strategy, the reduction pipeline and the instrument control software. An example of the improvement achieved is the Slow Guiding System (SGS), which is used to maintain the alignment of MUSE with respect to the telescope by guiding on stars located at the edge of the science field of view. The SGS can now guide on stars of V magnitude 21.5, or even on faint galaxies, and it monitors in real time the achieved image quality and the photometry. All this useful information is saved with the raw data and can be used later for comparison within of a set of exposures.

During this second commissioning, we also performed other science case observations, some on deep sky objects to measure the performance of MUSE for this type of science. MUSE also has a high discovery potential as demonstrated in Figure 2. This figure shows a set of images of the planetary nebula NGC 4361 taken from a MUSE cube. This large Galactic planetary nebula was observed to test the effect of the dithering strategy on the spectral line spread function. The cube turned up a surprise in the form of a background dwarf galaxy, projected on the nebula (see Figure 2e).

All the commissioning data are publicly available[2]. The commissioning activities have also been documented in the MUSE blog[3].

Science Verification

As usual for new VLT instruments, a public call for Science Verification (SV) time was made and for MUSE more than 85 proposals were received; 49 were scheduled for observation. The science topics covered are extremely wide and include studies such as the thickness and composition of clouds in the atmospheres of brown dwarfs; constraining the multiple stellar populations in globular clusters; star formation history in circumnuclear rings of spiral galaxies; the interstellar medium in galaxies affected by ram-pressure stripping; dynamical constraints on intermediate-mass black holes; and studies of lensed quasars and high-redshift proto-clusters.

The MUSE SV consisted of two observing runs: 20–29 June and 18–24 August 2014. Thanks to the high efficiency and reliability of the instrument, all but two programmes were fully completed. All data are publicly available from the MUSE SV webpage[4].

The MUSE wide field mode (1 by 1 arcminute) in natural seeing is now being offered to the community starting in October this year (Period 94). The wide-field mode with adaptive optics and the narrow-field mode will come later when the Adaptive Optics Facility (AOF; Arsenault et al., 2012) and GALACSI are deployed on VLT.

References

Arsenault, R. et al. 2006, The Messenger, 123, 6
Arsenault, R. et al. 2010, The Messenger, 142, 12
Bacon, R. 2006, The Messenger, 124, 5
Bacon, R. 2012, The Messenger, 147, 4

Links

[1] MUSE Preliminary Acceptance Europe: http://www.eso.org/public/announcements/ann13071/
[2] Access to commissioning data: http://www.eso.org/sci/activities/vltcomm/muse.html
[3] MUSE blog: http://muse-vlt.eu/blog
[4] Access to MUSE SV data: http://www.eso.org/sci/activities/vltsv/musesv.html

Ensuring the Reliability and Performance of Instrumentation at the Paranal Observatory

Frederic Gonté[1]
Alain Smette[1]
Sergio Abadie[1]
José Luis Alvarez[1]
Pedro Baksai[1]
Juan Beltran[1]
Henri Boffin[1]
Pierre Bourget[1]
Giovanni Carraro[1]
Roberto Castillo[1]
Willem-Jan de Wit[1]
Alvaro Diaz[1]
Dimitri Gadotti[1]
Julien Girard[1]
Nicolas Haddad[1]
George Hau[1]
Valentin Ivanov[1]
Jean-Louis Lizon[1]
Pedro Mardones[1]
Antoine Mérand[1]
Steffen Mieske[1]
Lorenzo Monaco[1]
Jared O'Neal[1]
Laurent Pallanca[1]
Emanuela Pompei[1]
Andrés Ramirez[1]
Miguel Riquelme[1]
Chester Rojas[1]
Linda Schmitobreick[1]
Ricardo Schmutzer[1]
Jonathan Smoker[1]
José Javier Valenzuela[1]
Gerard Zins[1]

[1] ESO

Instrumentation at the Paranal Observatory is currently composed of 18 scientific instruments (operational, in commissioning or on standby) and nine technical instruments (test camera, fringe trackers, adaptive optics modules, laser guide star facility, tip-tilt sensor). Over the 15 years since their first implementation and operation, enough information on their typical behaviour has been gathered to define a global plan for preventive maintenance and/or general refurbishment for each instrument in order to retain their reliability and performance. Several examples of monitoring of instrument performance are presented and reasons for failure are listed. We describe the range of activities undertaken to ensure efficient and reliable Paranal instrumentation.

Introduction

Since the installation of the first test camera on the Very Large Telescope (VLT) Unit Telescope 1 (UT1) in 1998 at the Paranal Observatory, a full set of instruments has been installed and is in operation. A list of references for Paranal instrumentation is available[1]. Very few have been decommissioned (e.g., FORS [Rupprecht et al., 2010] and ISAAC [Spyromilio et al., 2014]). The instrumentation at the Paranal Observatory employs virtually all the possible technologies developed for the ground-based astronomical community over the last 20 years. Spanning a wavelength range from 0.315 µm to more than 20 µm, it includes adaptive optics (AO) and interferometric systems for high spatial resolution imaging and spectroscopy, large field of view imagers, multi-object spectrometers, integral field units (IFUs), high resolution spectrometers, etc.

Table 1. Scientific and technical instruments on the UTs.

Instrument name	First light	Current telescope	Status	Purpose
Test Cameras 1 & 2	1998		TC1 decommissioned; TC2 standby	Visible imaging for VLT integration, commissioning and Science Verification and later for various tests and commissioning
FORS 1	1998		Decommissioned in 2009	Ultraviolet–visible imaging and low/medium resolution spectroscopy; multi-object spectroscopy; imaging and spectropolarimetry
ISAAC	1998		Decommissioned in 2013	1–5 µm imaging; low- and medium-resolution spectroscopy; polarimetry; high time-resolution imaging
FORS 2	1999	UT1 Cassegrain	In operation	Ultraviolet–visible imaging and low/medium resolution spectroscopy with two exchangeable CCDs (blue and red sensitive); high time-resolution imaging and spectroscopy; multi-object spectroscopy; imaging and spectro-polarimetry
UVES	1999	UT2 Nasmyth	In operation	Ultraviolet and visible visible high-resolution spectroscopy
NACO	2001	UT1 Nasmyth	In operation	Near-infrared high spatial resolution imaging and low resolution spectroscopy with AO; polarimetry
FLAMES	2002	UT2 Nasmyth	In operation	15-arm IFU and fibre-fed multi-object visible medium- and high-resolution spectroscopy
VISIR	2002	UT3 Cassegrain	Upgrade ongoing; to be re-commissioned end 2014 and early 2015	Mid-infrared imaging and spectroscopy
VIMOS	2002	UT3 Nasmyth	In operation	Visible imaging; multi-object spectroscopy; IFUs
SINFONI	2004	UT4 Cassegrain	In operation	Near-infrared IFU spectroscopy with AO
CRIRES	2006		Taken out of operation in July 2014 for upgrade	1–5 µm long-slit high-resolution spectroscopy
LGSF	2006	UT4 M2	In operation	Laser guide star for SINFONI
HAWK-I	2007	UT4 Nasmyth	In operation	Near-infrared wide-field imaging
X-shooter	2008	UT2 Cassegrain	In operation	Ultraviolet to near-infrared medium-resolution spectroscopy
KMOS	2012	UT1 Nasmyth	In operation	24-arm near-infrared IFU spectroscopy
MUSE	2014	UT4 Nasmyth	In operation	24 IFU visible medium-resolution spectroscopy with Adaptive Optics Facility (AOF)
SPHERE	2014	UT3 Nasmyth	Commissioning	Near-infrared classical and coronagraphic imaging, polarimetry, low-resolution spectroscopy and IFU with extreme AO

Each instrument can be considered as a separate entity, but the instrumentation can also be viewed as a global system, implemented over a period of time. We present an overview of this global system of Paranal instrumentation.

The instruments

VLT instruments

Each of the four UTs hosts up to three scientific instruments. In addition UT4 hosts the laser guide star facility (LGSF). The location of an instrument has sometimes changed from one focus to another in order to optimise the observing time on sky for each telescope. Table 1 presents an overview of all the scientific instruments operated at the UTs. Figure 1 shows the current view of the UTs and their instrumentation, together with the two survey telescopes.

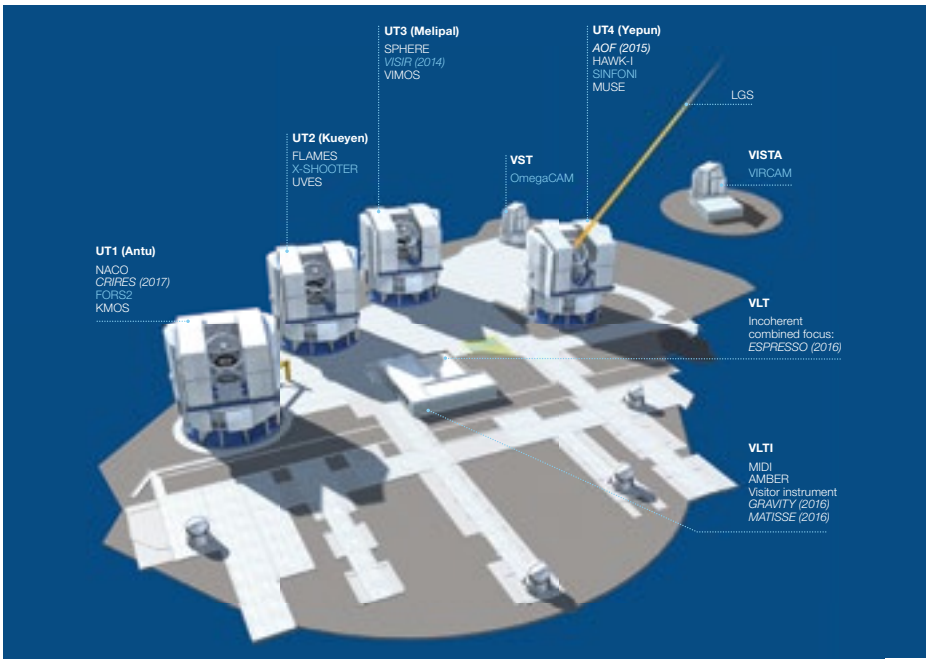

Figure 1. Paranal Observatory and its instrumentation. Instruments listed in blue are at the Cassegrain foci of the telescopes. Instruments listed in italics are not yet installed.

VLTI instruments

All the Very Large Telescope Interferometer (VLTI) scientific instruments are hosted in the VLTI underground laboratory on the VLT platform. Technical instrument systems (field stabiliser, fringe tracker and Multi-Application Curvature Adaptive Optics [MACAO] modules) are located in the VLTI lab or in the coudé path of the UTs. The instruments are fed by the UTs or by the Auxiliary Telescopes (ATs). Table 2 is an overview of all VLTI scientific and technical instruments operated at Paranal.

Survey instruments

Table 3 presents a summary of the Cassegrain cameras on the two survey telescopes, the VLT Infrared Survey Telescope for Astronomy (VISTA) and the VLT Survey Telescope (VST).

Average age of instrumentation

The first scientific instruments (FORS 1 and ISAAC) were integrated in 1998 at Paranal on UT1. In the whole history of Paranal, only VINCI (2004), FORS1 (2009) and ISAAC (2013) have been decommissioned, while PRIMA (2014) has been cancelled. CRIRES was taken out of operation in July 2014 for an upgrade to transform it to a cross-dispersed spectrograph (see Dorn et al., 2104; Follert et al., 2014). Thus a total of 21 scientific and ten technical instruments have already been installed, not including the visitor instruments or experiments, such as UltraCam, DAZLE (Dark Age *z* (redshift) Lyman-α Explorer), Multi-conjugate Adaptive optics Demonstrator (MAD), the Active Phasing Experiment (APE), etc. Figure 2 shows the growth in number of instruments and their average age by year.

The average age of the instrumentation in operation is currently 8.4 years. It will reach more than ten years by 2018, even

Instrument name	First light	Location	Status	Purpose
VINCI	2001	VLTI lab	Decommissioned in 2004	*K*-band VLTI commissioning instrument
MIDI	2002	VLTI lab	In operation	Mid-infrared two-beam combiner and spectrometer
MACAO-VLTI	2003–2005	UTs at coudé	In operation	Four AO modules for VLTI
AMBER	2004	VLTI lab	In operation	Near-infrared three-beam combiner and spectrometer
FINITO	2005	VLTI lab	In operation	Fringe tracker for AMBER and MIDI
IRIS	2005	VLTI lab	In operation	Four-beam tip-tilt monitor
PRIMA	2008		Cancelled in 2014	Phased referenced imager
FSU-A	2008	VLTI lab	In operation	*K*-band fringe tracker for MIDI, initially part of PRIMA
PIONIER	2010	VLTI lab	In operation	Near-infrared four-beam combiner (visitor instrument until P94)

Table 2. Scientific and technical instruments dedicated to interferometry.

Instrument name	First light	Telescope	Status	Purpose
VIRCAM	2009	VISTA	In operation	Wide-field infrared survey imager
OMEGACAM	2011	VST	In operation	Wide-field visible survey imager

Table 3. Survey instruments on the two survey telescopes.

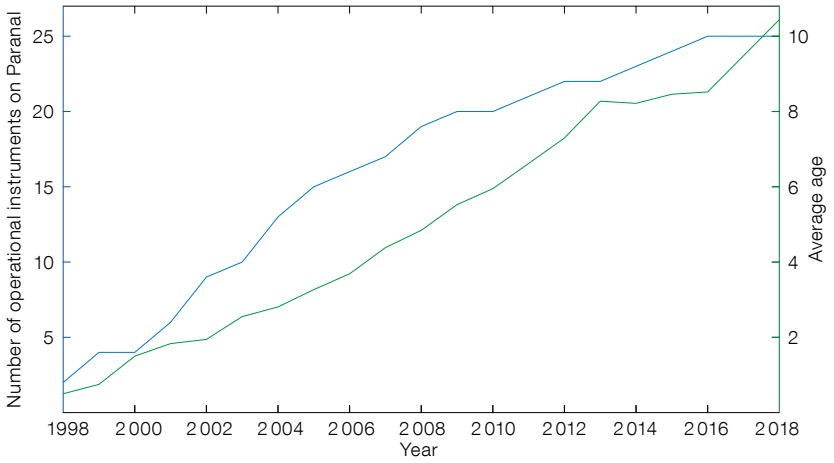

Figure 2. The number of operational instruments (in blue) and their average age (in green) are shown since the start of operation of the Paranal Observatory.

though the last of the second generation instruments will be installed over the next three years (Adaptive Optics Facility [AOF], ESPRESSO, GRAVITY and MATISSE; see Pasquini et al. [2013]). The number of instruments and their ages (Figure 2) allow us to deduce general statistics on their lifetime behaviour. It should be recalled that the lifetime defined at contract level is ten years for VLT instruments.

Monitoring of performance

An Instrument Operations Team (IOT) is associated with each scientific instrument. Its mandate and responsibility is to maintain the instrument operational environment to ensure the delivery of optimal quality science and calibration data, and science-grade data products whenever possible. The ultimate goal of its activities is to maximise the quality and quantity of the instrument scientific output.

In practice, a full set of tools has been implemented over the years in order to properly monitor the behaviour of both scientific and technical instruments. Some tools are used more frequently by the operator (astronomer and telescope and instrument operator), while others are used more by the engineer or instrument scientist responsible.

Paranal Problem Reporting System

The Paranal Problem Reporting System (PPRS) is a ticketing system designed to track all problems reported at the Paranal Observatory. Each ticket logs the affected system, type of failure, observing time lost on sky, workload necessary to recover the system and the eventual solution. The reporting system started at the end of June 1999; today nearly 57 000 tickets have been recorded, and of these, 22 000 (38 %) are dedicated to instrumentation. The PPRS allows us to easily track the observing time lost on sky and the number of tickets per instrument over the years, giving a good indication of the reliability of an instrument.

Quality control

A health check web page is associated with each instrument, maintained by the Quality Control Group in Garching[2], where the main performance data are logged every day after the calibration data are processed by their respective pipelines: typical applications include monitoring the zero point for the imagers, bias level, dark count rate, flat-field level, spectral resolution, etc. Plots reporting such quantities are updated with a frequency as high as once every 15 minutes and are publicly available. Flags are automatically raised when a measurement is outside a pre-defined range.

Such quality control plots allow daytime astronomers, operation specialists and quality control scientists to quickly spot problems easily (typically a failing function, such as that seen in plot 2 of Figure 3, which was traced to a failing power supply of a lamp) or to follow slow degradation, such as the decrease of the overall FLAMES–GIRAFFE blue transmission caused by the aging of the silver coating of the high-resolution grating (shown in Figure 11). Occasionally users spot issues with data quality that trigger actions on the Paranal side, e.g., with the UVES radial velocity accuracy or the CRIRES slit width repeatability.

Autrep

Autrep is an interface allowing engineers and astronomers to dive into all the data logged by the Paranal instrument and telescope control software. Graphics showing the evolution of the values of pre-defined or most useful parameters over a configurable period are automatically updated every day; all logged data can be retrieved using scripts and compared with other logged data. It is a powerful tool, as it provides easy access to the full data history.

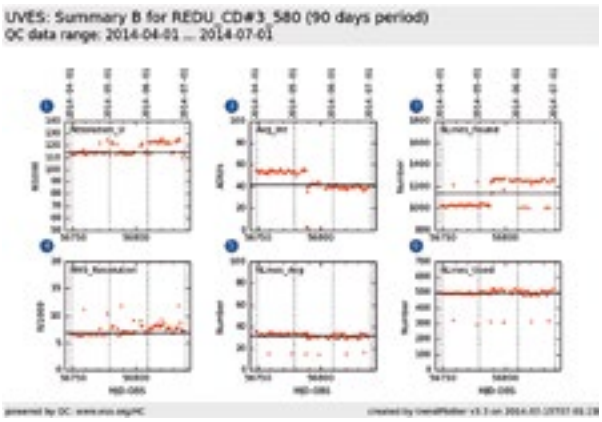

Figure 3. An example of one of the quality control plots obtained daily for UVES, showing the resolution and its root mean square (RMS) obtained on the upper CCD with the cross-disperser #3 for a central wavelength of 580 nm (plots 1 and 4), and associated quantities. Note the drop in the average intensity of the ThAr comparison lines on 10 May shown in plot 2, caused by an instability in the power supply.

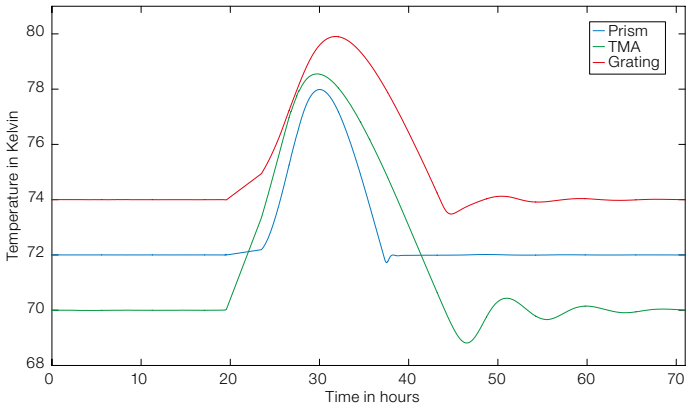

Figure 4. Autrep automatic monitoring of technical data for CRIRES is shown: temperatures for the pre-disperser prism (in black), three-mirror anastigmat (blue) and grating (red).

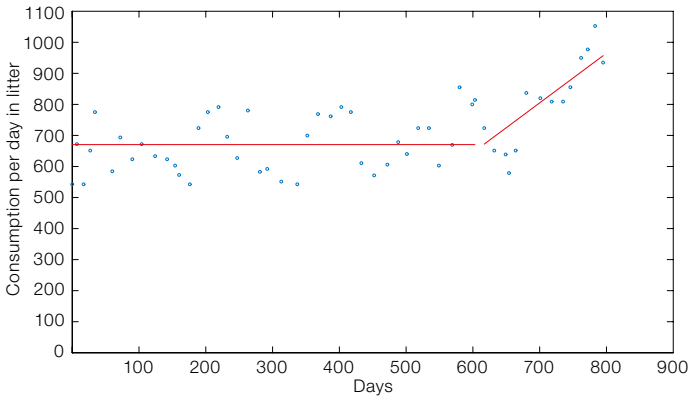

Figure 5. The liquid nitrogen consumption in litres per day on Paranal is illustrated between May 2012 and May 2014. The increase in consumption from late 2013 is due to the installation of KMOS, then MUSE and SPHERE.

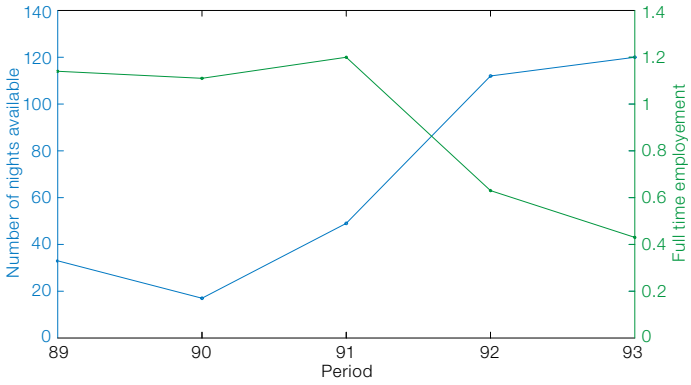

Figure 6. The effect of the LGSF upgrade on nights available (blue) and manpower (green) over the last five periods of observation (Periods 88 to 92). The upgrade from PARLA to PARSEC took place in Period 91.

Figure 4 shows as an example the measurements of the temperature of several components (the prism, three-mirror anastigmat and grating) inside the CRIRES cryostat before, during and after the last power outage on Paranal. Two days were necessary to bring these components back to the temperature stability required for normal operation.

Manual monitoring

Some systems do not have any automatic data logging, but must still be properly monitored. Important parameters are therefore manually logged during daily visual inspections. Figure 5 shows, for example, that the daily liquid nitrogen consumption over the last two years, as measured at the storage tank, has clearly increased significantly since the recent arrival of the three new instruments (KMOS, MUSE and SPHERE). The liquid nitrogen consumption will stabilise at around 1000 litres per day by the end of 2014. It will increase again when ESPRESSO, GRAVITY and MATISSE arrive.

Other analysis tools

Analysis tools can also be dedicated to management. Since 2011, working time in the instrumentation group has been logged: each member of the group reports the type of work (troubleshooting, planned maintenance, project, operation, etc.) spent on each system. From these statistics (e.g., Rabien et al., 2003) it is, for example, possible to extract the impact of the replacement of the dye laser (PARSEC) at the LGSF by a fibre laser PARLA (Lewis et al., 2014), on the manpower required for its maintenance in operational condition. Figure 6 shows the manpower per period of observation (six months) on PARSEC and PARLA. The gain with PARLA was not only a drastic reduction in the manpower needed by this system, but its availability on sky also quadrupled. The manpower saved by this upgrade has been directly re-assigned to implementing the second generation instruments and in making important refurbishments to the aging functions of some first generation instruments.

Monitoring of failures: PPRS and observing time lost on sky

The number of reported problems first increased with the number of instruments in operation, but then started to decrease in 2003 when teething troubles associated with the first instruments settled down. An average of around 70 problems is now reported per instrument per year (Figure 7). In other words, there is one problem every five days per instrument and around five PPRS tickets per day in total. The observing time lost on sky started to decrease later than the number of PPRS tickets, only setting in once the first generation instrumentation was fully implemented. Now, thanks to the presence of several instruments on each UT or at the VLTI, observations can continue with other instruments should one instrument fail. Around 20 hours are lost per instrument per year due to technical problems (Figure 8). This is equivalent to two nights of operation, or around 0.5 % of the available operation time.

The total number of problems and amount of time lost during the lifetime of each instrument are plotted in Figure 8. OmegaCAM should be considered sepa-

Figure 7. The average observing time lost on sky (blue) and the average number of problems reported (green) per year and per instrument from 1999 to 2013.

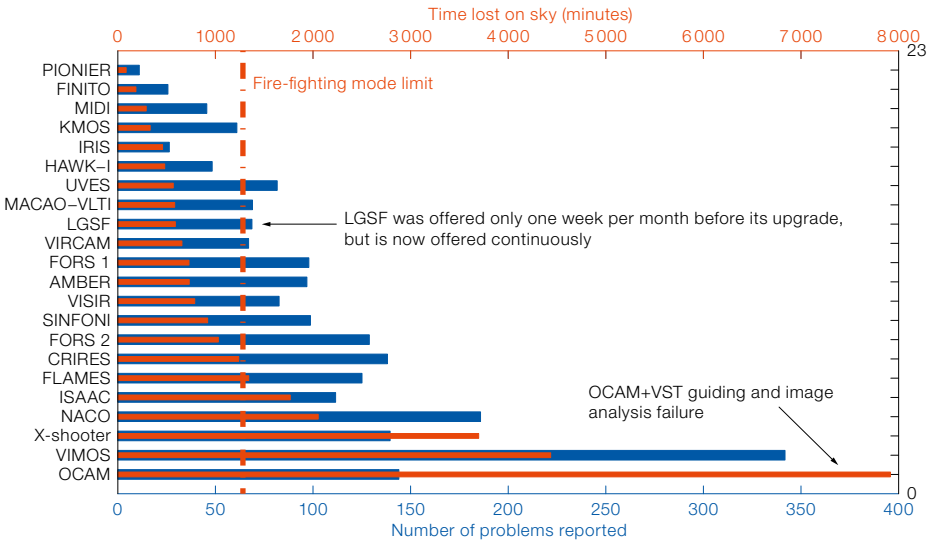

Figure 8. (Above) The observing time lost on sky (red bars) and total number of reported problems (blue bars) are plotted by instrument as an average per year since the start of the instrument operation. The fire-fighting mode limit is a threshold value above which the amount of observing time lost (and then of failures) strongly impacts the operation of the instrument.

rately as it also contains the sensors for guiding and image analysis of the VST; thus all guiding and image analysis problems on the VST are accounted to OmegaCAM. It is also the only instrument on the telescope: hence a failure can impact a large part of the night. Since its commissioning in 2011, significant efforts at the hardware and control software levels have been made to reduce the observing time lost on sky.

The three instruments which have accumulated the largest amount of time lost and the greatest number of problems are VIMOS, X-shooter and NACO. These three instruments have a different history, but essentially their unreliability was due to design flaws.

Instrument lifetime reliability

The average number of problems per year and the average observing time lost on sky as a function of the number of years since the start of operation of the instruments at Paranal are shown in Figure 9. The plots span up to 11 years; since there are only three instruments older than 11 years, a longer time span would not be statistically representative. The lifetime of the instruments is clearly seen to be 11 to 12 years. This matches the expectation of a ten-year lifetime at

Figure 9. (Below) The average number of problems (left) and observing time lost (right) per year is shown during the lifetime of all the instruments.

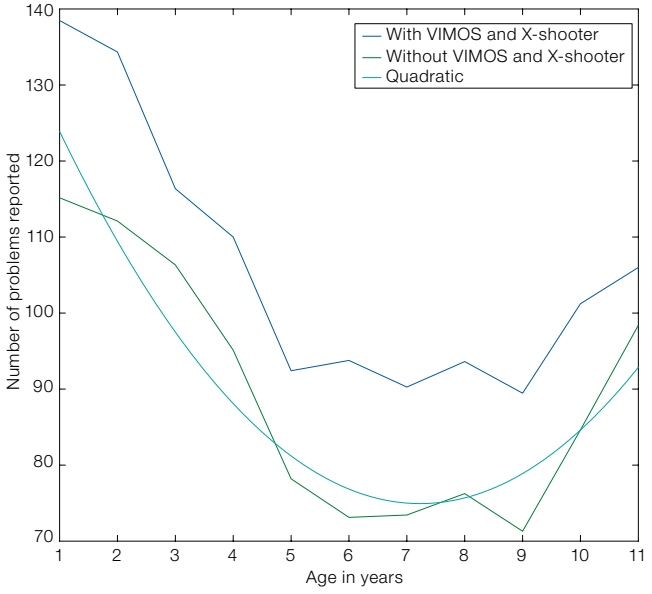

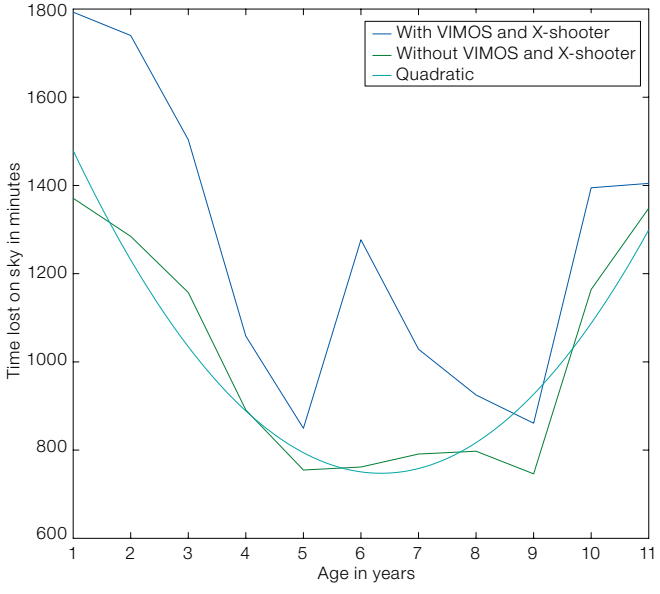

contract level. However a few instruments (VIMOS, CRIRES and X-shooter) have needed a substantial recovery action after just a few years of operation.

The green curves in Figure 9 were calculated excluding X-shooter and VIMOS, whose impact due to design flaws was far larger than the average behaviour. This curve was fitted by a quadratic polynomial. It shows that once initial problems have been solved (after around four years) the instrument is stable for four or five years; afterwards, the number of problems increases again due to aging and hardware parts becoming unavailable and obsolete. The amount of observing time lost due to technical problems affecting instruments follows the same curve. This pattern of behaviour is well known in system engineering.

The quadratic model describes the reliability of Paranal instruments. This is the result of all the work done in Europe, during their development and design, but also at Paranal to maintain them within specifications. One should wonder whether, and how, this curve could be improved, and whether, and how, this lesson could be applied to future instruments, such as for the European Extremely Large Telescope (E-ELT).

The evolution of instrument reliability can be compared to the one expected from the quadratic model by taking the ratio between the statistic for the instrument and the model as a function of time. An example is shown in Figure 10, using the instrument affected by the largest number of problems, VIMOS. The graph clearly shows its recovery towards normal behaviour after an important upgrade on the mask insertion units, detector shutters, flexure compensation system, between its sixth and eighth year of operation. It should be noted that the absolute reliability of the instrument, i.e., the ratio between the observing time lost on sky and the time available for science, is not given explicitly here. Instead, the observing time lost better represents the amount of work to be done, which is why this quantity has been chosen for this article.

Sources of failure

Instrument failures have many different sources. They are linked to different phases of development and operation and can be classified as follows, as can be seen by these few examples:

Top Level Requirements (TLR) and design phases:
- At TLR: The counter-chopping function implemented in NACO could never be used extensively, but it imposed such constraints on the field selector that it was unstable. Recurrent failure of the field selector represents 10 % of the total observing time lost on sky for NACO.
- At design: Examples are the mask exchange unit (MEU) of VIMOS, the atmospheric dispersion corrector (ADC) system of X-shooter and the opto-mechanical stability of AMBER. They all started to fail, or problems became apparent, as soon as the instrument entered into operation, or soon afterwards. The MEU of VIMOS has accumulated more than 300 hours of observing time lost on sky, corresponding to about more than 30 hours per year. Since its upgrade in 2011, the amount of observing time lost has decreased to around 8.3 hours per year. The total observing time lost due to X-shooter's ADCs is about 134 hours. The ADC system was therefore disabled, severely reducing the capability of the instrument; a refurbishment of the ADC system is under discussion. AMBER's warm bench thermal instability caused 16 % of all problems reported. The problem was solved after an upgrade to provide a more stable alignment unit and the implementation of a daily alignment verification procedure.

Manufacturing, integration and commissioning phases:
- At manufacturing: Poorly protected coatings can start to degrade as soon as the components arrive at Paranal; the specification of a component may not be well checked, for example, the transmission or the wavefront error of an optical element; or an element shows a higher failure rate than expected.
- At integration: Cables not well fixed; components not well screwed or glued, such as the filter carriage of OmegaCAM; leak of the cryostat, as on KMOS; software not well finalised and tested; or control loop of a motor not well tuned.
- At commissioning: Set-up not adapted to operational conditions.

Maintenance, operation and aging phases:
- Maintenance: Incomplete refilling with liquid nitrogen causing a cryostat to warm up.

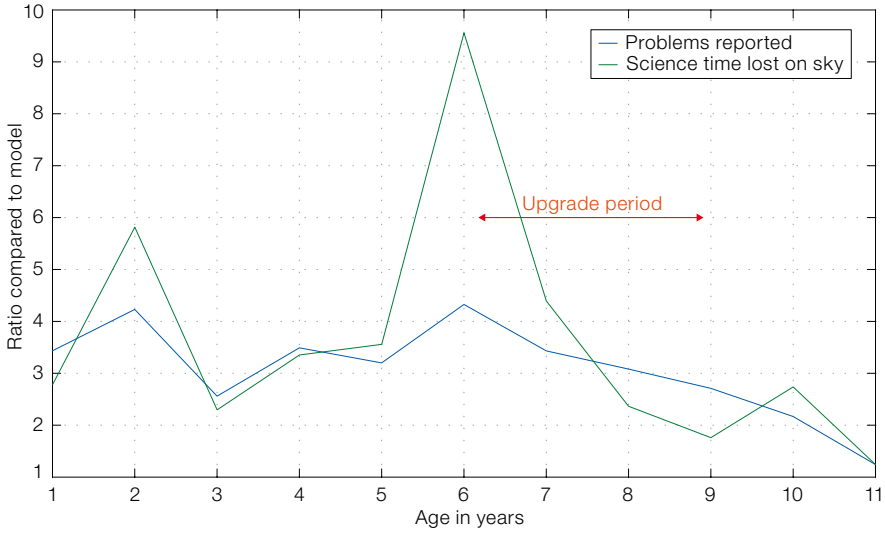

Figure 10. The ratio of the observing time lost (green line) and of the number of problems reported (blue) for VIMOS is compared to the quadratic model defined by the average of all instruments (excluding VIMOS and X-shooter).

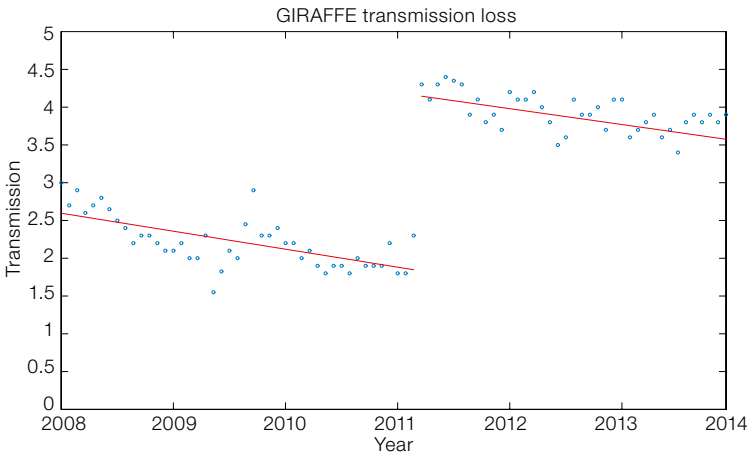

Figure 11. FLAMES-GIRAFFE transmission in the H447.1A setting is plotted before and after cleaning the high-resolution grating in May 2011.

Figure 12. The damaged coating on a SINFONI lens (left) was discovered during inspection after a thermal cycle. The coating was polished away and the lens re-integrated (right).

– Incident: Power blackout resulting in the instrument warming up; earthquake upsetting the alignment.
– Aging: Hard point on rotation or translation stage, degradation of coating (as seen in Figures 11 and 12), burn out of a motor, failure of a drive or leak of a cooling system.

The correction process for problems originating from the TLR or design phases requires a redesign, replacement of the component or a change in the mode of operation. Such problems are the most difficult and expensive sources of failure to solve. They underline why every project should be extremely careful during the definition phase and refrain from shortening this crucial period or minimising its importance.

Problems occurring during manufacturing, integration and commissioning require a replacement, hardware re-integration and/or update and re-implementation (operation or pipeline). This is typically the kind of failure that prevents an instrument from entering operation or limits its capability to be in operation.

The process of correcting problems occurring during maintenance and operation first starts by defining the metrics to be followed. Then the maintenance procedure is corrected and steps taken to ensure adequate training and the availability of spare parts. A refurbishment plan is prepared when the instrument is aging or its components are becoming obsolete. Typical examples of the latter are: non-availability on the market of an electronic board, workstation, detector or version of software or hardware out of production.

Types of activities

Each instrument has been assigned an engineer responsible for its maintenance in operational condition: he/she is in charge of initiating and coordinating all the activities required for this goal, including maintenance. Activities can be divided into four categories: operation-driven, preventive maintenance, condition-based and corrective maintenance. Most of these activities are performed by technicians following a defined procedure established by the engineer responsible for the instrument. Examples of all four categories are presented:

Operation-driven activities

Operation-driven activities are required by the demands of science operations. Examples are:
– daily nitrogen refills for the instruments;
– insertion of mask in FORS or VIMOS;
– exchange of detectors for FORS (from blue to red sensitive CCD, or vice versa);
– development of new observation template software, or modification of existing software, which allows operations at a high level of automation in science service mode, calibration mode and routine tasks, such as daily start-up and shutdown of control software;
– changing the focal station of an instrument in order to optimise the overall science time for the observatory, such as recently carried out for NACO.

Preventive maintenance

Preventive maintenance activities are driven by the lifecycle of a component or by repetitive behaviour, for example:
– Regular software rebuilds are scheduled for each control workstation in order to ensure configuration control, which is the key to maintaining the instrument within operational conditions.
– Since the displacers of the closed cycle coolers have a lifetime of around two years, it has been decided to plan for their replacement after 18 months, i.e., sufficiently before the time of their expected failure, in order to avoid emergency interventions which are disruptive for both science activities and the overall scheduling of time for the observatory personnel.
– KMOS currently suffers from a vacuum loss. After analysis it was decided to pump it on average every week, keeping the instrument in operation, while reducing the impact on the engineers as much as possible. Figure 13 shows the effect of pumping on the KMOS cryostat pressure.

Condition-based activities

Condition-based activities are driven by a change of environmental conditions, such

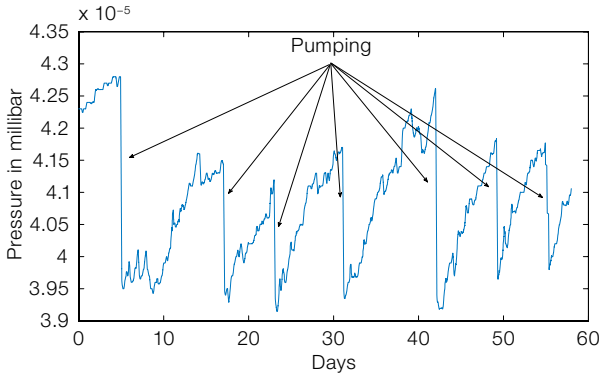

Figure 13. The pressure inside the KMOS cryostat is shown over a period of 60 days from measurements between mid-April and mid-June 2014. The effect of pumping on the cryostat pressure, is evident.

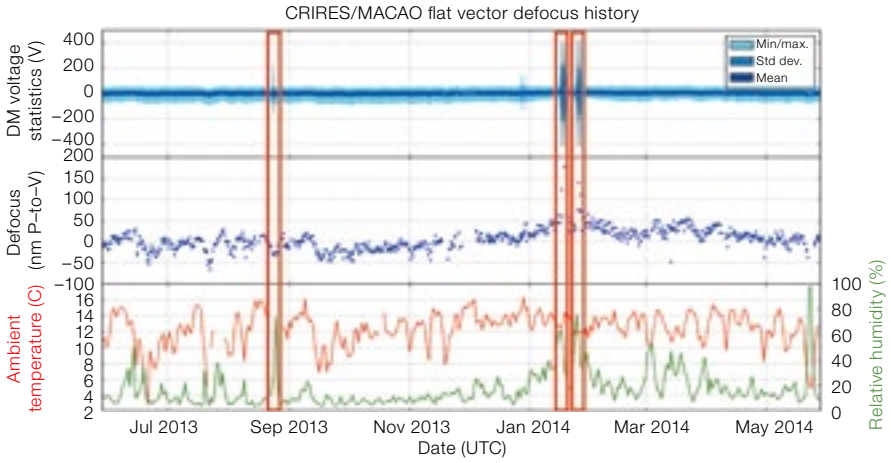

Figure 14. High-humidity events (red boxes) strongly affect the behaviour of the CRIRES MACAO adaptive optics module and prevent its use for operations. After such events, a new calibration and verification process are mandatory.

as the weather. For example, the MACAO systems cannot work properly at high humidity. After each high-humidity event (see Figure 14), a full verification of the performance and calibration of the system is performed.

Corrective maintenance

Corrective maintenance activities are triggered by failures detected during operation (night-time observation or calibration) or during technical verification. Each failure produces a report, which has been used for the statistics given in this article. A few procedures can generally be followed in the case of repetitive failures, like the replacement of a lamp, an avalanche photodiode (APD), a vacuum gauge or the reboot of a local control unit (LCU) or workstation.

Obsolescence and aging

A variety of other actions are required when, for example, an instrument is entering obsolescence, its scientific capability is to be extended or when it is decided that it must be decommissioned.

Refurbishment

Refurbishment of an instrument is necessary when too many functions are jeopardised by aging. Last year, for example, thanks to the help of the Max-Planck-Institut für extraterrestrische Physik, all the motors of SPIFFI (the Spectrometer for Infrared Faint Field Imaging), part of SINFONI, were replaced, as the failure rate was such that only one setting was possible for several weeks. NACO also underwent partial refurbishment, to recover fully the CONICA detector, increase the field selector reliability, replace the closed cycle cooler (CCC), and add a damping system to the CCC.

Upgrade

Reasons for an upgrade differ depending on the instrument. An upgrade is usually proposed when the instrument has completed most of its design science capability, as for VISIR (Kerber et al., 2012), when a real gain in performance is envisaged, such as for VIMOS (Hammersley et al., 2010; 2013) and CRIRES+ (Dorn et al., 2014), or it is becoming more difficult to maintain, as for PARLA (Lewis et al., 2014).

Control software is regularly upgraded following releases of the VLT software core. This activity sometimes includes the replacement of control workstations by more modern and powerful models, such as the current move towards 64-bit architecture.

Decommissioning

Decommissioning an instrument is the ultimate action. Pressure from the scientific community for the continuous use of even a severely aged instrument means that, so far, this situation has only occurred in order to free a focus for a new instrument. The next instrument to be decommissioned will be MIDI to allow for the integration of GRAVITY and MATISSE.

Global approach

The number of instruments for which no refurbishment, upgrade or decommissioning is planned is still large. As a consequence, we will be facing obsolescence and aging problems not only at the level of the electronics (boards, motors) and control software, but also at the level of mechanics (hard point, leaks) and optics (degradation of coatings). ESO is preparing an instrument obsolescence project to face this situation. It focusses on the first generation instruments that are still expected to be operational for at least the next five years, namely: FORS2, NACO, UVES, FLAMES, VIMOS, HAWK-I, OmegaCAM, AMBER and the LGSF.

Conclusions

The reliability and lifetime of the instruments on Paranal correspond on average to those requested at contract level

(ten years, and less than 0.5 % of the scientific time lost). However, the operation and maintenance activities can only be organised with a good understanding of instrument behaviour. This understanding can only be obtained via an accurate and complete monitoring of the system. A methodical approach must then be applied to maintenance, finding the right balance between cost and manpower on the one hand, and the number of problems and amount of observing time lost on sky on the other hand.

Acknowledgements

Ensuring the reliability and performance of the Paranal instrumentation critically relies on the continuous dedication of the Paranal staff, on the support received from Garching engineers and astronomers, in particular from the Quality Control group, and on the continuous follow-up by the various IOTs. We warmly thank them all: this article is an attempt to summarise their respective contributions.

We would also like to thank the instrument consortia for delivering vital support for maintenance and refurbishment of their instruments, in some cases even ten years after delivery.

Petr Kabath helped in the preparation of the LGS statistics.

References

Dorn, R. et al. 2014, The Messenger, 156, 7
Follert, R. et al. 2014, SPIE, 9147-44
Hammersley, P. et al. 2010, The Messenger, 142, 8
Hammersley, P. et al. 2013, The Messenger, 151, 2
Kerber, F. et al. 2012, SPIE, 8446
Lewis, S. et al. 2014, The Messenger, 155, 6
Pasquini, L., Casali, M. & Russell, A. 2013, The Messenger, 154, 2
Rabien, S. et al. 2003, SPIE, 4839, 393
Rupprecht, G. et al. 2010, The Messenger, 140, 2
Spyromilio, J. et al. 2014, The Messenger, 155, 2

Links

[1] Reference list for Paranal instrumentation: http://www.eso.org/sci/facilities/paranal/instruments/InstrumentReferences.html
[2] Instrument quality control information: http://www.eso.org/observing/dfo/quality/

ESO/G. Lombardi

Time-lapse image of the night sky over the Paranal Observatory. See Picture of the Week for 26 May 2014 for more information.

Colour image of the Galactic star-forming region Gum 15 (RCW 32) obtained with the Wide Field Imager on the MPG/ESO 2.2-metre telescope. This small H II region is centred on the bright B-type star HD 74804, a member of the open cluster Collinder 197. The image is a combination of *B*, *R* and Hα filter images. See Release eso1420.

The B Fields in OB Stars (BOB) Survey

Thierry Morel[1]
Norberto Castro[2]
Luca Fossati[2]
Swetlana Hubrig[3]
Norbert Langer[2]
Norbert Przybilla[4]
Markus Schöller[5]
Thorsten Carroll[3]
Ilya Ilyin[3]
Andreas Irrgang[6]
Lidia Oskinova[7]
Fabian R. N. Schneider[2]
Sergio Simon Díaz[8,9]
Maryline Briquet[1]
Jorge Federico González[10]
Nina Kharchenko[11]
Maria-Fernanda Nieva[4,6]
Ralf-Dieter Scholz[3]
Alex de Koter[12,13]
Wolf-Rainer Hamann[7]
Artemio Herrero[8,9]
Jesús Maíz Apellániz[14]
Hugues Sana[15]
Rainer Arlt[3]
Rodolfo Barbá[16]
Philip Dufton[17]
Alexander Kholtygin[18]
Gautier Mathys[5]
Anatoly Piskunov[19]
Andreas Reisenegger[20]
Henk Spruit[21]
Sung-Chui Yoon[22]

[1] Institut d'Astrophysique et de Géophysique, Liège, Belgium
[2] Argelander-Institut für Astronomie, Bonn, Germany
[3] Leibniz-Institut für Astrophysik Potsdam (AIP), Potsdam, Germany
[4] Institute for Astro- and Particle Physics, University of Innsbruck, Austria
[5] ESO
[6] Dr. Remeis Observatory & ECAP, Bamberg, Germany
[7] Institut für Physik und Astronomie der Universität Potsdam, Germany
[8] Instituto de Astrofísica de Canarias, La Laguna, Spain
[9] Universidad de La Laguna, Dpto. de Astrofísica, La Laguna, Spain
[10] Instituto de Ciencias Astronomicas, de la Tierra, y del Espacio (ICATE), San Juan, Argentina
[11] Main Astronomical Observatory, Kiev, Ukraine
[12] Astronomical Institute Anton Pannekoek, Amsterdam, the Netherlands
[13] Instituut voor Sterrenkunde, Universiteit Leuven, Belgium
[14] Instituto de Astrofísica de Andalucía-CSIC, Granada, Spain
[15] ESA/Space Telescope Science Institute, Baltimore, USA
[16] Departamento de Física, La Serena, Chile
[17] Astrophysics Research Centre, Belfast, UK
[18] Chair of Astronomy, Saint-Petersburg State University, Russia
[19] Institute of Astronomy of the Russian Acad. Sci., Moscow, Russia
[20] Pontificia Universidad Católica de Chile, Santiago, Chile
[21] Max-Planck-Institut für Astrophysik, Garching, Germany
[22] Department of Physics and Astronomy, Seoul National University, Republic of Korea

The B fields in OB stars (BOB) survey is an ESO Large Programme collecting spectropolarimetric observations for a large number of early-type stars in order to study the occurrence rate, properties, and ultimately the origin of magnetic fields in massive stars. A total of 98 objects was observed over 20 nights with FORS2 and HARPSpol to July 2014. Preliminary results indicate that the fraction of magnetic OB stars with an organised, detectable field is low. This conclusion, now independently reached by two different surveys, has profound implications for any theoretical model attempting to explain the field formation in these stars. We also discuss some important issues addressed by our observations (e.g., the lower bound of the field strength) and the discovery of some remarkable objects.

Magnetic fields in OB stars

Magnetic fields affect the evolution and properties of massive stars in several ways; from redistributing the angular momentum in the stellar interior to the formation of a circumstellar magnetosphere through the channelling and confinement of their radiatively driven winds. In some cases, magnetic fields may also lead the stars to end their lives as exotic objects, such as magnetars (highly magnetised neutron stars with field strength up to $10^{14–15}$ Gauss) or gamma-ray bursts.

Yet it is only very recently that the number of known magnetic OB stars has reached a level that allows us to evaluate the field incidence, examine the properties of the fields, and critically test the various models proposed for their creation. The picture now emerging is that relatively strong fields (above, say, 100–200 Gauss at the surface) are only found in about 7 % of all massive stars (Wade et al., 2014) and that the field topology is rather simple (dipolar, or, in some rare cases, low-order multipolar). Moreover, the field strength is not directly linked to the stellar parameters (e.g., it does not scale up with rotation rate). While this is in sharp contrast with the situation for Solar-like stars with dynamo-generated fields, these characteristics are similar to those presented by intermediate-mass stars (the chemically peculiar Ap/Bp stars in the mass range 1.5–8 $M_{\odot}$). This similarity suggests a related origin of the field.

Despite these remarkable achievements and the promising progress made over the last few years, the answers to some important questions still elude us. For instance, the effects of magnetic fields on the internal rotational profile and on the transport of chemical species remain largely unknown. Even the mode of creation of the field in the first place is not completely settled. The magnetic field permeating the interstellar medium (ISM) is amplified during star formation and may naturally relax into a large-scale, mostly poloidal field emerging at the surface (e.g., Braithwaite & Spruit, 2004). The similarity between the magnetic properties of OB and Ap/Bp stars suggests that today we observe the remnant of the field frozen in from the ISM. However, recent studies indicate that a very significant fraction of OB stars may suffer a merger or a mass-transfer event during their evolution (Sana et al., 2012) and it cannot be ruled out that fields are created through such processes (e.g., Wickramasinghe et al., 2014). It has also been proposed that dynamo action can operate in either the radiative zone or in subsurface convection layers, and may lead to observable fields (unlike dynamo-generated fields in the convective core that take too long to reach the

photosphere). Such a dynamo would presumably produce short-lived, spatially localised magnetic structures (e.g., Cantiello & Braithwaite, 2011) that are, however, much more challenging to detect.

A better understanding of the effects and origin of magnetic fields in massive stars requires a significant increase in the statistics of known magnetic OB stars (for instance, only in about ten O stars has a field been firmly detected). It is in this context that, building on our previous experience with ESO spectropolarimetric instruments (e.g., Hubrig et al., 2009a), we have launched the B fields in OB stars (BOB) survey[1].

The BOB survey

A total of 35.5 nights of observations were allocated during Period 91 to 96 as part of an ESO Large Programme (191.D-0255; Principal Investigator: Morel). A two-step approach was adopted: about 20 nights were dedicated to obtaining snapshot observations of a large number of OB stars, while the remaining nights are devoted to confirm the field detection for the candidate magnetic stars and to better characterise the field properties for those that are firmly identified as being magnetic. Two different state-of-the-art instruments with circular polarisation capabilities are used (with low and high spectral resolution, respectively): the FOcal Reducer and Spectrograph (FORS2) at the Very Large Telescope (VLT) for the fainter targets and HARPSpol (the polarimetric unit of the HARPS spectrograph) at the 3.6-metre telescope at La Silla for the brighter ones. About two thirds of the total observing time is allocated on HARPSpol (25 nights). As of July 2014, 20 nights of observations (8 with FORS2 and 12 with HARPSpol) have been completed. Only one night (with FORS2) was lost because of bad weather. About 85 % of the remaining 15.5 nights are scheduled on HARPSpol.

Previously known magnetic OB stars appear, on average, to have rotation speeds significantly lower than the rest of the population. We therefore mostly targeted stars with projected equatorial rotational velocities ($v \sin i$) below 60 km s^{-1} to enhance the probability of detecting magnetic fields. Contrary to the Magnetism in Massive Stars survey (MiMeS; Wade et al., 2014), we concentrated on normal, main-sequence OB stars and did not consider, e.g., Be or Wolf–Rayet stars. The sample is composed in roughly equal parts of O (~ 40 %) and B (~ 60 %) stars; the vast majority are late O- and early B-type stars. BOB and MiMeS can be viewed as two complementary surveys in the sense that there are very few targets in common.

One important aspect of our survey is that the data reduction and analysis are carried out entirely independently by two groups (one from the Argelander-Institut für Astronomie in Bonn and the other from the Leibniz-Institut für Astrophysik in Potsdam) to ensure that the results are robust. The two groups process both the FORS2 and HARPSpol data separately, and employ different tools and analysis techniques (for details, see Hubrig et al., 2014).

The occurrence of magnetic fields in massive stars

Previous results (e.g., Wade et al., 2014) indicated that only about 7 % of massive stars host a magnetic field detectable with current instrumentation (> 100 Gauss). We have so far observed 98 OB targets and only unambiguously detected five magnetic stars. For all the stars, the detection is not only confirmed by the two groups (Bonn and Potsdam), but the field measurements also systematically agree within the errors. In addition, the field is detected at a high significance level with both FORS2 and HARPSpol.

Therefore, our results tend to support those independently obtained by MiMeS and confirm that the incidence rate of strong magnetic fields is low in massive stars and is similar to that inferred for intermediate-mass stars. It should be emphasised, however, that a number of candidate magnetic stars are still being followed up and that the preliminary incidence rate that we obtain (~ 5 %) may eventually be revised upwards.

Regardless of the exact figures, the scarcity of strongly magnetic OB stars has far-reaching implications, from the interpretation of the statistical properties of stellar populations (e.g., X-ray characteristics and impact of magnetic braking on the rotational velocities) to their fate as degenerate objects following the supernova explosion (e.g., as magnetars).

The first magnetic stars discovered by BOB

A magnetic field in a multiple system in the Trifid Nebula

One of the aims of our survey is to uncover magnetic stars with specific and unusual characteristics that would allow us to discriminate between the various channels that could lead to field formation as outlined previously.

An interesting discovery in this context is the detection of a magnetic field in a multiple system in NGC 6514, the Trifid Nebula (Hubrig et al., 2014), which is a very young and active site of star formation. We first observed the three brightest components identified in the central part of the nebula (A, C and D; Kohoutek et al., 1999) with FORS2 and, as shown in Figure 1, clearly detected a circularly polarised signal in component C (HD 164492C). In contrast, no such features were visible for the two other components (an early O star and a Herbig Be star).

Further observations on two consecutive nights with HARPSpol confirmed the existence of a field with a longitudinal strength ranging from 400 to 700 Gauss (the strength of the disc-averaged, line-of-sight component of the surface magnetic field). These high-resolution observations reveal complex and variable line profiles pointing towards a multiple system (made up of at least two early B-type stars). The situation is complicated further by the possible existence of chemical patches on the surface of some components. We will continue to monitor this system with both FORS2 and HARPSpol in order to establish whether only one or more components are magnetic. Observing time has also been granted on UVES to determine the orbital parameters of this system and the properties of the individual components. A complete characterisation of this peculiar system may provide valuable information about the

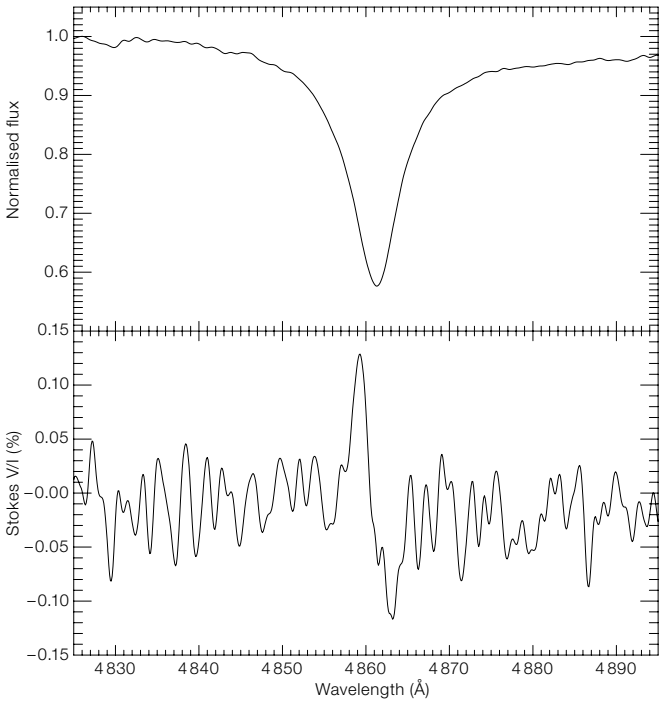

Figure 1. Stokes I (upper) and V/I (lower) FORS2 spectra of HD 164492C in the vicinity of the Hβ line (from Hubrig et al. 2014).

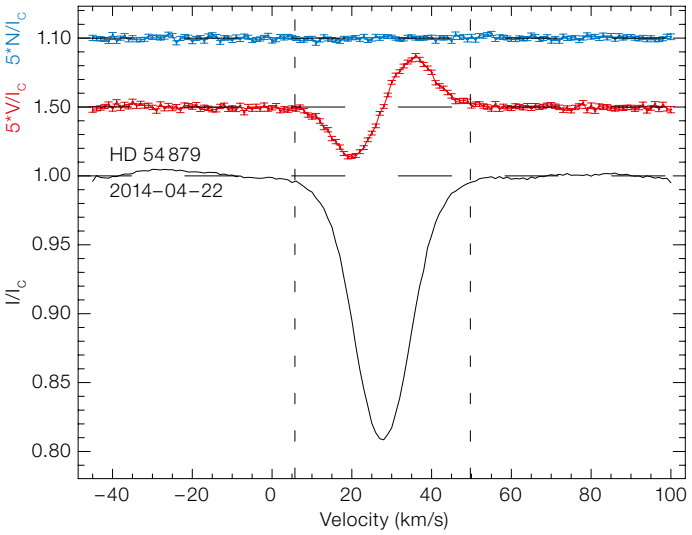

Figure 2. Stokes I (black), Stokes V (red) and diagnostic null N (blue) profiles of HD 54879 obtained through least squares deconvolution (LSD) techniques with HARPSpol (from Castro et al., 2014).

interplay between binarity and magnetic fields in massive stars (e.g., through a mass-transfer episode).

A new magnetic, He-rich star with a tight age constraint

The rare magnetic, helium-rich stars (some 30 are known) are the most massive chemically peculiar stars. These main sequence stars of spectral type ~ B2 display spectral, brightness and magnetic variability that can be accommodated by models where the dipolar field is tilted with respect to the rotational axis. Their photospheric abundance anomalies are believed to arise from the competition between radiative levitation and gravitational settling in the presence of a stellar wind.

While the surface abundance inhomogeneities give rise to the observed variability in some stars of this kind, a rigidly co-rotating circumstellar magnetosphere can result in variability in other cases, like in the prototype He-rich star σ Ori E. These objects have traditionally been used to study the interaction of the stellar wind with the (strong) magnetic field. Some stars have been shown to undergo rapid rotational braking (e.g., Mikulášek et al., 2008), which presents the opportunity to study angular momentum extraction from massive stars virtually in real time. This has stimulated magnetohydrodynamical simulations of angular momentum loss in magnetically channelled line-driven winds, which provided, for instance, first estimates of spin-down times (ud-Doula et al., 2009). Magnetic, He-rich stars can therefore be viewed as extreme laboratories where the still poorly understood effects of magnetic fields on the evolution of massive stars can be studied in detail. Of importance is the understanding of how the properties of He-rich stars develop during their main sequence evolution.

Our spectropolarimetric observations of the B1 star CPD −57° 3509 in the young (~ 10 Myr) open cluster NGC 3293 with FORS2 and HARPSpol reveal a strong and rapidly varying field (by up to 900 Gauss for the longitudinal component between two consecutive nights). The field is found to change polarity, which shows that both magnetic hemispheres are visible as the star rotates. The polar field exceeds 3 kiloGauss assuming a dipole geometry. A preliminary spectral analysis, assuming non-local thermodynamic equilibrium, indicates that CPD −57° 3509 is helium-rich (about three times solar) and has evolved through about one third of its main sequence lifetime (Przybilla et al., 2014). This makes CPD −57° 3509 one of the most evolved He-rich stars with a tight age constraint, promising to provide crucial information on the evolution of stars with magnetically confined stellar winds. Observing time has recently been granted on FORS2 and the Ultraviolet and Visual Echelle Spectrograph (UVES) to study this object in greater detail and to eventually reconstruct the abundance maps at the surface through Doppler imaging.

A non-peculiar magnetic O star

The few magnetic O stars known are very often peculiar. Their strong magnetic fields are believed to give rise to spectral peculiarities and/or to drive periodic line-profile variations (e.g., the Of?p stars or θ^1 Ori C). In contrast, we have discovered a narrow-lined O9.7 V star (HD 54879) hosting a strong field (with a dipole strength above 2 kiloGauss; see Figure 2), yet displaying no evidence, in the few optical spectra taken over five years, of any spectral peculiarity or variability (Castro et al., 2014). Only the broad and emission-like Hα profile is variable. This might be related to the presence of a centrifugal magnetosphere where wind material is trapped in closed magnetic loops and prevented from falling back to the star by centrifugal forces. Further observations

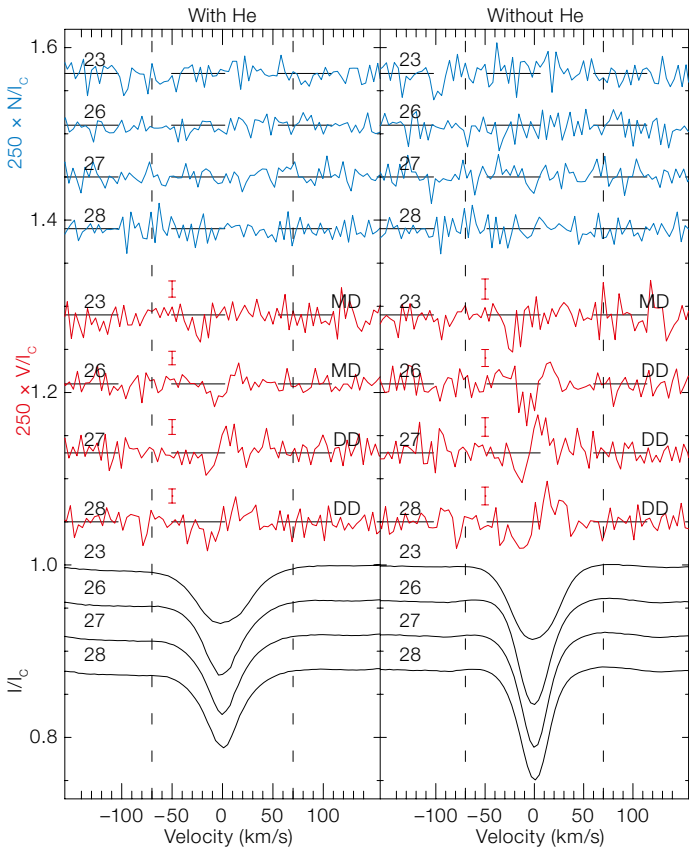

Figure 3. (Left) Stokes I (black), Stokes V (red), and diagnostic null N (blue) profiles of β CMa obtained through least squares deconvolution (LSD) techniques with HARPSpol during the period 23–28 December 2013. The left and right panels show the profiles obtained using a line mask with and without He lines, respectively. MD and DD correspond to a marginal and a definitive detection, respectively (from Fossati et al., 2014).

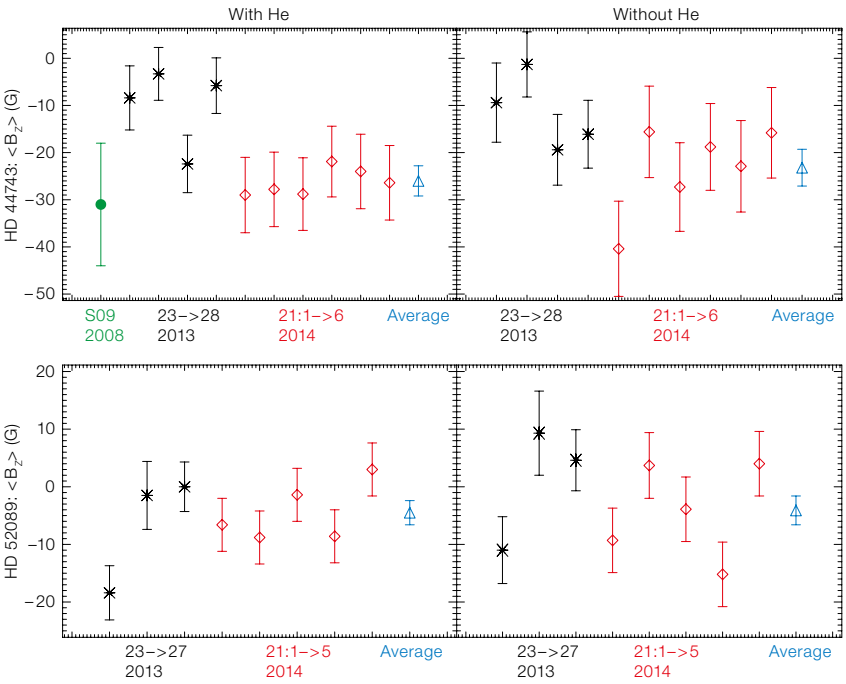

Figure 4. (Below) Time series of the longitudinal field measurements of β CMa (upper panels) and ε CMa (lower panels). The black crosses correspond to the observations carried out on four different nights in December 2013, while the red rhombs show the values obtained from consecutive observations on 21 April 2014 (the blue triangle is the average value obtained on that night). The green circle indicates the ESPaDOnS measurement of β CMa carried out in 2008 by Silvester et al. (2009). From Fossati et al. (2014).

are necessary to confirm the lack of spectral peculiarities and, if so, to understand the distinct behaviour with respect to other strongly magnetised O stars. A parallel investigation of the magnetic variability also needs to be undertaken.

The occurrence of weak fields in OB stars

One of the most intriguing properties of magnetic stars of intermediate mass is the bimodal distribution of fields that are either strong (above 300 Gauss) or extremely weak (< 1 Gauss). The lack of objects with ordered fields of intermediate strength appears not to be an observational bias and therefore to reveal a real dichotomy (e.g., Lignières et al., 2014). Investigating the origin of this "magnetic desert" may prove essential in our quest to understand the origin and evolution of fields in stars that cannot support a dynamo acting in the deep, outer convective envelope.

To examine whether such a magnetic desert also exists for more massive stars (above ~ 8 $M_{\odot}$), we have obtained very high-quality spectropolarimetric observations with HARPSpol of two very bright (V ~ 1.5–2.0 mag) early B-type stars (β CMa and ε CMa). By pushing the signal-to-noise ratio to the limit (up to ~ 700 for the unpolarised Stokes I spectrum) during a run that took place in December 2013, we repeatedly managed to detect a weak Zeeman signature across the line profiles (see Figure 3). Subsequent observations carried out in April 2014 have confirmed the detection. This result is particularly interesting in the case of β CMa, which is a very well-known pulsating star of the β Cephei type, since our identification of the pulsation modes allows us to precisely constrain some important parameters, such as the inclination of the rotation axis with respect to the plane of the sky. It should be noted that the field measurements are not appreciably affected by pulsations.

As discussed by Fossati et al. (2014), the most interesting outcome of the measurements is that the fields appear to be roughly constant and relatively weak in both cases. The longitudinal components are at most 30 Gauss in modulus (Figure 4), which translates into a polar strength of ~ 150 Gauss assuming a dipolar geometry. Although all the available

measurements of β CMa in the literature are entirely consistent with a field of that magnitude, it should be pointed out that there is some indication for a stronger field in ε CMa from FORS1 observations carried out back in 2007 (Hubrig et al., 2009b; Bagnulo et al., 2012). Despite the fact that the case for a weak field is much stronger in β CMa, we will continue to discuss both stars in the following.

Confidently detecting fields of tens of Gauss or less in fainter targets is very challenging, even with modern instrumentation. If our upcoming observations confirm the weakness of the fields in β CMa and ε CMa, then the question arises whether these two bright stars only represent the tip of the iceberg. Is there a large population of stars with weaker fields or that are even truly non-magnetic (see Neiner et al., 2014)? A clear answer to these questions may not be possible until similar detection thresholds can be routinely achieved for fainter stars. However, it seems conceivable that weak fields are considerably more widespread in massive stars than the currently available data would suggest.

It is important to note that the Zeeman signatures observed in β CMa and ε CMa are typical of stars hosting a stable, large-scale field. It is therefore likely that the field is not dynamo-supported. In this picture, the fields in β CMa and ε CMa are not continuously sustained and are prone to decay on evolutionary time-scales. Indeed both stars are close to the terminal age main sequence. It is possible that their advanced evolutionary stage is at the origin of their weak fields (see Landstreet et al. [2008] in the case of the Ap/Bp stars). The possibly different field strength distribution of intermediate- and high-mass stars thus raises the issue of a mass-dependent time-scale for the field decay.

Acknowledgements

Thierry Morel acknowledges financial support from Belspo for contract PRODEX GAIA-DPAC. Luca Fossati acknowledges financial support from the Alexander von Humboldt Foundation. Maryline Briquet is F.R.S.-FNRS Postdoctoral Researcher, Belgium. We would like to thank Claudia McCain for maintaining the project web page.

References

Bagnulo, S. et al. 2012, A&A, 538, A129
Braithwaite, J. & Spruit, H. C. 2004, Nature, 431, 819
Cantiello, M. & Braithwaite, J. 2011, A&A, 534, A140
Castro, N. et al., in preparation
Fossati, L. et al. 2014, to be submitted to A&A
Hubrig, S. et al. 2009a, The Messenger, 135, 21
Hubrig, S. et al. 2009b, AN, 330, 317
Hubrig, S. et al. 2014, A&A, 564, L10
Kohoutek, L. et al. 1999, A&AS, 134, 129
Landstreet, J. D. et al. 2008, A&A, 481, 465
Lignières, F. et al. 2014, in Proc. IAUS, 302, 338
Mikulášek, Z. et al. 2008, A&A, 485, 585
Neiner, C. et al. 2014, A&A, 562, A59
Przybilla, N. et al., in preparation
Sana, H. et al. 2012, Science, 337, 444
Silvester, J. et al. 2009, MNRAS, 398, 1505
ud-Doula, A. et al. 2009, MNRAS, 392, 1022
Wade, G. A. et al. 2013, in Proc. IAUS, 302, 265
Wickramasinghe, D. T. et al. 2014, MNRAS, 437, 675

Links

[1] BOB public web page: http://www.astro.uni-bonn.de/BOB/

Y. Beletsky (LCO)/ESO

Sunset image of La Silla taken in May 2013 when the three planets Jupiter (upper), Venus (lower left) and Mercury (lower right) were visible in near alignment — an example of a syzygy. See Picture of the Week dated 3 June 2013 for more information.

STEP: The VST Survey of the SMC and the Magellanic Bridge

Vincenzo Ripepi[1]
Michele Cignoni[2,3]
Monica Tosi[3]
Marcella Marconi[1]
Ilaria Musella[1]
Aniello Grado[1]
Luca Limatola[1]
Gisella Clementini[3]
Enzo Brocato[4]
Michele Cantiello[5]
Massimo Capaccioli[6]
Enrico Cappellaro[7]
Maria-Rosa L. Cioni[8,9]
Felice Cusano[3]
Massimo Dall'Ora[1]
Jay S. Gallagher[10]
Eva K. Grebel[11]
Antonella Nota[2,12]
Francesco Palla[13]
Donatella Romano[3]
Gabriella Raimondo[5]
Elena Sabbi[2]
Fedor Getman[1]
Nicola R. Napolitano[1]
Pietro Schipani[1]
Simone Zaggia[7]

[1] INAF-Osservatorio Astronomico di Capodimonte, Naples, Italy
[2] Space Telescope Science Institute, Baltimore, USA
[3] INAF-Osservatorio Astronomico di Bologna, Italy
[4] INAF-Osservatorio Astronomico di Roma, Italy
[5] INAF-Osservatorio Astronomico di Teramo, Italy
[6] Università Federico II, Naples, Italy
[7] INAF-Osservatorio Astronomico di Padova, Italy
[8] University of Hertfordshire, Hatfield, United Kingdom
[9] Leibnitz-Institut für Astrophysik Potsdam, Germany
[10] University of Wisconsin-Madison, USA
[11] Astronomisches Rechen-Institut, Zentrum für Astronomie der Universität Heidelberg, Germany
[12] European Space Agency, Space Telescope Science Institute, Baltimore, USA
[13] INAF-Osservatorio Astrofisico di Arcetri, Firenze, Italy

STEP (Small Magellanic Cloud in Time: Evolution of a Prototype interacting late-type dwarf galaxy) is a Guaranteed Time Observation survey being carried out at the VLT Survey Telescope. STEP will obtain homogeneous photometry in the *g*-, *r*-, *i*- and Hα-bands over an area of 74 square degrees covering the main body of the Small Magellanic Cloud (42 square degrees), the Bridge that connects it to the Large Magellanic Cloud (30 square degrees) and a small part of the Magellanic Stream (2 square degrees). Our photometry will allow us to detect and measure the magnitudes of individual stars well below the main sequence turnoff of the oldest populations. Here we describe the observing strategy, the photometric techniques, and the upcoming data products of the STEP survey. Preliminary results for the first two fields for which data acquisition is complete are also presented.

Introduction

The Local Group dwarf galaxies provide an ideal laboratory for studying and testing galaxy formation theories and cosmology. Their close proximity allows individual stars to be resolved, with accurate photometry and spectroscopy. (see e.g., Tolstoy et al., 2009). Their stellar populations can be characterised in detail and their star formation histories (SFHs) derived. The Small Magellanic Cloud (SMC) is the closest dwarf galaxy of late morphological type; hence the best location for detailed studies of the properties of this the most common class of galaxies. Its low chemical abundance (Z = 0.004) makes the SMC the best local counterpart to the large majority of dwarf irregulars and blue compact galaxies, whose metallicity distribution is peaked at this mean value. The SMC is also a member of the nearest group of interacting galaxies. In fact, it is tidally interacting with its neighbours, the Large Magellanic Cloud (LMC) and the Milky Way. Investigating the signatures of these interactions (the Bridge towards the LMC and the Magellanic Stream) will allow us to constrain models of galaxy interaction. Hence the SMC is an ideal benchmark in the study of the effects of tidal interactions on galaxy evolution.

We are carrying out the first deep and homogeneous photometric survey of the entire SMC body and of the Bridge by exploiting the large field of view (FoV) and the high resolution of the OmegaCAM instrument on the VLT Survey Telescope (VST); see Ripepi et al. (2014) for a detailed presentation of the survey. The STEP survey is the optical complement to the VISTA Magellanic Cloud (VMC[1]) ESO Public Survey (Principal Investigator [PI] M.-R. Cioni), which is collecting *Y*, *J* and *Ks* near-infrared photometry over an area of about 184 square degrees covering the LMC, SMC and Bridge. STEP is part of a large international effort aimed at studying in detail stellar populations, structure and evolution of the SMC, and based on photometric and spectroscopic data acquired at the major international facilities (e.g., Hubble Space Telescope [HST] and Very Large Telescope [VLT]).

The colour–magnitude diagram (CMD), containing stars born over the whole lifetime of the galaxy, is a fossil record of its SFH. Since the lookback time that can be safely be investigated is of the order of the evolutionary time of the least massive main sequence (MS) star that can be resolved, deep CMDs are crucial to detect Solar-like MS stars (corresponding to the oldest MS turn-off with evolutionary times comparable with an entire Hubble time). Although this is usually the realm of HST (see e.g., Cignoni et al., 2012; 2013), HST's small FoV does not allow a systematic study of the whole SMC.

With STEP we aim to investigate the stellar populations of the SMC with CMDs up to 1–2 magnitudes fainter than the turn-off (TO) of the oldest population (with sufficient photometric quality to reach a 2 Gyr resolution for stars born 10 Gyr ago), for a huge area including the entire SMC and the Bridge as well. We also intend to use classical variable stars (e.g., RR Lyrae and Cepheid stars), as population tracers in the relatively unexplored region of the Bridge, and a spatially complete census (up to ~ 1 $M_{\odot}$) of pre-main sequence (PMS) objects to investigate the first stages of star formation.

With these broad capabilities, the STEP survey will allow us to answer the following open questions: 1) What is the global SFH and age–metallicity relation (AMR) of the SMC?; 2) Do field and star cluster components share the same

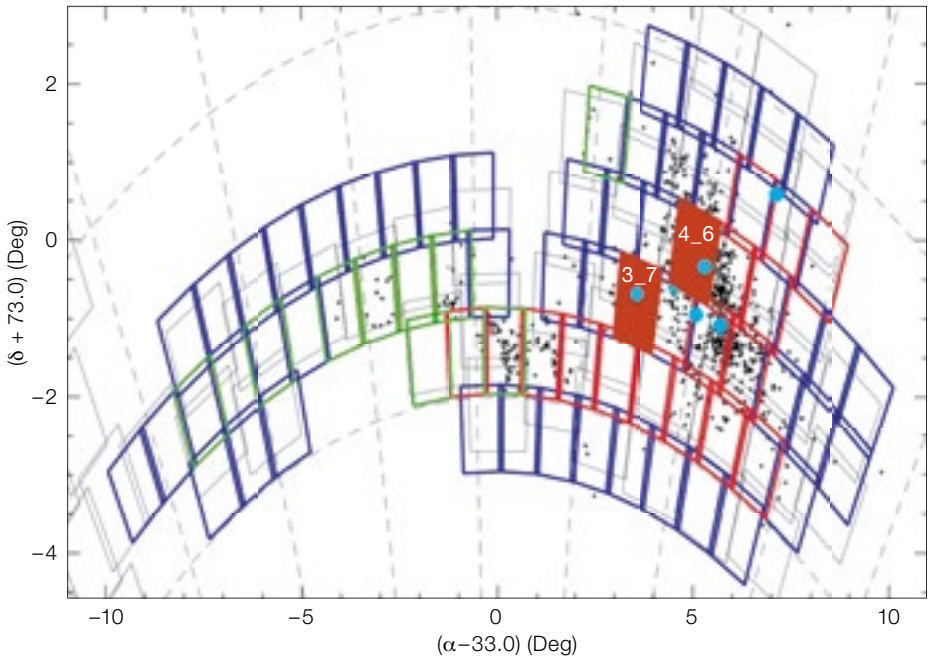

Figure 1. Map of STEP tiles (the two tiles centred in the direction of the Magellanic Stream are outside of the figure). To highlight the location of the SMC body and of part of the Bridge, black dots indicate the position of known star clusters and associations (according to Bica et al. [2008]). The thick boxes correspond to the 1 square degree FoV of the VST tiles. Red boxes represent tiles whose observations are completed, green boxes those with completed time series photometry and blue boxes the remaining ones. For comparison, thin grey boxes show the VMC tiles, whereas the HST fields are the small cyan-filled circles (note that the true size of HST fields is significantly smaller). The two tiles analysed in this work (tiles 3_7 and 4_6) are highlighted with filled red boxes.

SFH and AMR?; 3) Are there trends in SFH connected with the interaction history of the SMC?; 4) How did the stellar component of the Bridge form and what is its SFH?; 5) What is the impact of metallicity on PMS accretion and on the global properties of star formation?

STEP observing strategy

In order to address the questions listed above, we proposed, and have obtained, part of the VST Guaranteed Time Observation (GTO) allocation by ESO to the Italian Istituto Nazionale di Astrofisica (INAF) in return for the procurement of the telescope. With STEP we aim at acquiring *g*, *r*, *i* and Hα photometry for 72 square degrees covering the whole SMC body, the Bridge and 2 square degrees of the Magellanic Stream down to a limiting magnitude (on the AB system) of $g \sim 24$ mag with signal-to-noise (S/N) of 10 and Hα photometry to ~ 22.5 mag with S/N of 5.

The survey is organised into tiles of one square degree each, partially overlapping with each other to allow a homogeneous calibration (see Figure 1). In addition, we acquired 24-epoch time series photometry of 8 square degrees on the Bridge down to $g \sim 19.5$ mag (i.e., reaching fainter than the mean magnitude of the RR Lyrae stars), with S/N of 100. When summed, these images will allow us to reach $g \sim 24$ mag with S/N of 10. Originally, we planned to image the whole Bridge with time series. However, the overheads proved to be too high and we decided to cover the remaining Bridge fields without time series. STEP tiles are placed so as to maximise the overlap with the VMC survey (Cioni et al., 2011).

The STEP observing strategy is reported in Table 1, whereas Table 2 shows the constraints for our observations. For each tile and for each filter in the SMC body we obtain a couple of mosaics created by merging five dithered sub-images. We acquire a mosaic of short- and long-exposure times in order to reach faint magnitudes, avoiding saturation for any star. The time series images, on the contrary, consist of just one shot for each filter. For each tile we also obtain pairs of *g*, *i* (*r*, Hα) images during a photometric night, in order to build up lists of secondary standards for the final photometric calibration (usually the scientific images are taken in non-photometric conditions, to increase the probability of execution — see Table 2).

Table 1. Observing strategy of the STEP survey (e.g., 5 × 25 s means five dithered exposures of 25 s each).

Period	T_{exp}(g)	T_{exp}(i)
88–90	5 × 25 s; 5 × 520 s	5 × 25 s; 5 × 520 s
91–93	5 × 25 s; 10 × 300 s	5 × 25 s; 10 × 300 s
	Photometric calibration	
88–93	1 × 45 s	1 × 45 s
	Time series	
88–91	1 × 25 s; 1 × 120s	1x25 s; 1 × 180 s

Observations and data reduction

The VST (built by the INAF–Osservatorio Astronomico di Capodimonte, Naples, Italy) is a 2.6-metre-wide field optical survey telescope (Capaccioli & Schipani, 2011) sited on Paranal. The telescope is equipped with OmegaCAM, a 1-square-degree camera built by a consortium of European institutes (Kuijken, 2011). The camera is a 32 CCD, 16 k × 16 k detector mosaic with 0.214 arcseconds per pixel scale.

STEP observations started in late 2011 during ESO Period 88 and are currently continuing. Usually, the observations are carried out in service mode. The different colours of the tiles shown in

Field	Seeing (arcseconds)	Moon	Airmass	Weather
SMC	1.0–1.1	0.5	1.8	Clear
Bridge	1.1	0.5	1.8	Clear
Bridge (TS)	1.4	0.8	1.8	Thin cirrus
Phot. Cal.	1.5	0.8	1.8	Photometric

Table 2. Observing constraints. Seeing is to be interpreted as the full width at half maximum measured on the image. TS stands for time series while Phot. Cal. means photometric calibration.

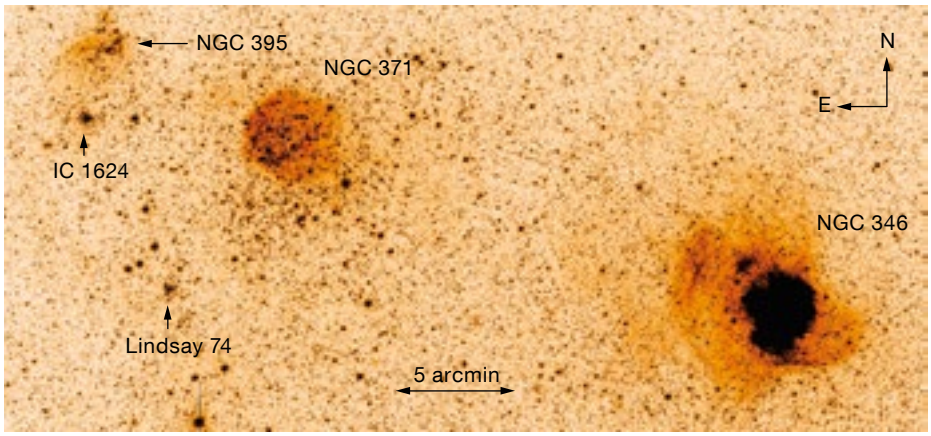

Figure 2. *g*-band VST plate showing the northern part of tile 4_6, including the well-known star-forming region NGC 346 and several other interesting clusters and associations, which are labelled.

Figure 1 illustrate the execution status as of Period 92. The total number of hours of observation allocated up to now to STEP during Periods 88–92 is 182 h; the hours of actual observations in the same period were about 98.7, with an efficiency (hours observed/allocated) of about 50 %. As a consequence of this rather low observing efficiency, the current percentage of completion of the entire survey is about 30 %.

In the following we describe the first two tiles that have been completely reduced and analysed, namely tiles 3_7 and 4_6 (see Figure 1). These tiles are representative of different environmental conditions in the SMC: tile 3_7 is located in the Shapley wing, a substructure whose origin is likely connected to the interaction with the LMC, whereas tile 4_6 is placed in the relatively unperturbed, but mostly active, northern part of the body of the SMC.

The data reduction was carried out by means of the VSTTube package (Grado et al., 2012), which has been specifically developed to handle OmegaCAM data. The pipeline includes the following steps: 1) accurate gain homogenisation (flat-fielding); 2) image concentration correction; 3) preliminary absolute photometric calibration; 4) relative photometry, relative and absolute astrometry by means of SCAMP[2]; and 5) image resampling and co-addition through the SWARP[3] package. A portion of the final mosaic for tile 4_6 is shown in Figure 2, where several star clusters and associations are clearly visible.

The PSF photometry on the final mosaics was carried out with Peter Stetson's DAOPHOT/ALLSTAR package. The catalogues were matched by means of a custom procedure. The final precision of the photometry can be appreciated in Figure 3 (upper panels). It can be seen that our sensitivity requirement is met even in the crowded regions of the SMC body. A detailed estimate of the completeness of our photometry is a fundamental stage in an accurate reconstruction of the SFH. To this aim, we have devised a custom procedure to add several thousands of artificial stars to our images without generating self-crowding. The result of the completeness experiments for both tiles is shown in Figure 3 (lower panels). It can be seen that 50 % completeness is achieved for $g \sim 23.5$ mag in tile 4_6, which is much more crowded than tile 3_7; we reach the same completeness level at $g \sim 24$–24.5 mag in tile 3_7.

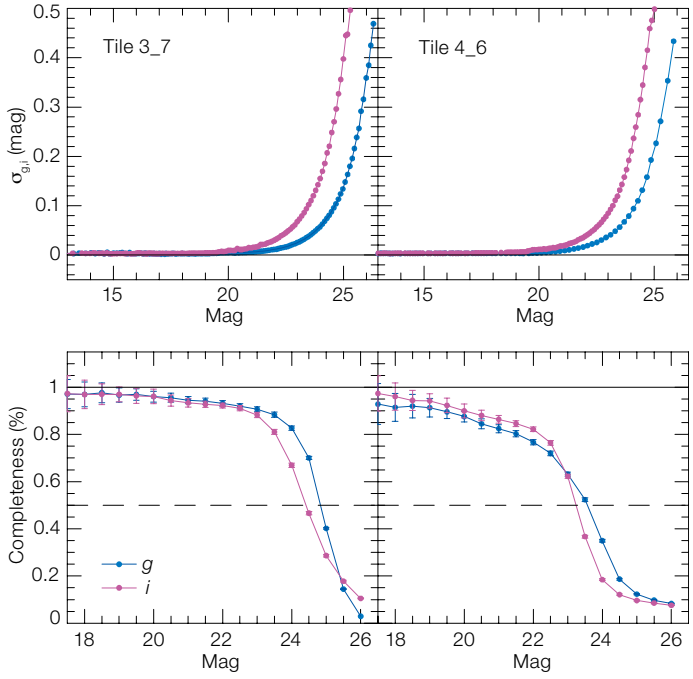

Figure 3. Upper panels: The photometric errors (averaged per bins of magnitude) in *g* (blue) and *i* (magenta) are shown for a sub-frame 20 × 21 arcminutes in size, placed in the middle of tiles 3_7 and 4_6. Lower panels: the completeness in the same regions are shown. The 100 and 50 % levels of completeness are shown with black solid and dashed lines, respectively.

The colour–magnitude diagram

Figure 4 shows the CMDs of the stars measured in tile 3_7 (left panel) and 4_6 (right panel). Since tile 4_6 is located in a populous part of the SMC, the corresponding CMD hosts over four times more stars than tile 3_7, which is placed in the relatively low density and peripheral wing. As a consequence crowding is more severe in tile 4_6 and the corresponding CMD much shallower (but still 1 mag deeper than the oldest MS TO) and sparser. To guide the eye, isochrones of different ages and metallicities (Marigo et al., 2008) are overlaid on the CMDs. The metallicity of the youngest isochrones is assumed to be $Z = 0.004$, which is consistent with spectroscopic derivations from H II regions in the SMC and from stellar abundances in very young stars, while the metallicity of the older isochrones is chosen to best fit the red giant

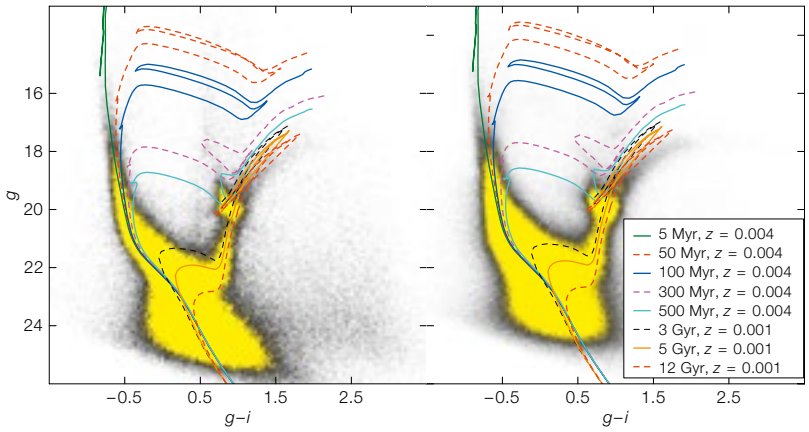

Figure 4. CMD of tile 3_7 (left panel) and 4_6 (right panel) with overlaid stellar isochrones from Marigo et al. (2008): for metal abundance Z = 0.004, ages 5 Myr (green continuous line), 50 Myr (red dashed line), 100 Myr (blue continuous line), 300 Myr (pink dashed line) and 500 Myr (cyan continuous line); for Z = 0.001, ages 3 Gyr (black dashed line), 5 Gyr (orange continuous line) and 12 Gyr (dashed red line). The assumed distance modulus and reddening E(B - V) are 18.9 and 0.08 mag for tile 3_7 (left panel), 18.9 and 0.04 mag for tile 4_6 (right panel) respectively.

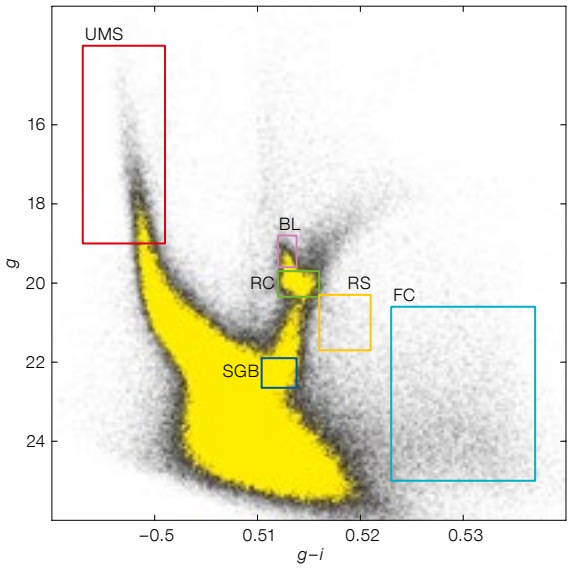

Figure 5. For tile 3_7, the CMD regions used to identify Upper Main Sequence (UMS), Blue Loop (BL), Red Clump (RC), Sub Giant Branch (SGB), reddened RC stars (RS) and Field Contamination (FC) sources are illustrated.

branch (RGB). The assumed distance modulus is $(m - M)_0$ = 18.90 mag, while the assumed reddening values, E(B - V) = 0.08 and 0.04 mag for tiles 3_7 and 4_6, respectively, are chosen to provide the best fit.

In terms of stellar populations, the mere presence in both fields of an extended MS, a well-populated blue loop (BL) and red clump (RC) phase, as well as a wide RGB, is a clear indication of common prolonged activity in the SMC. Indeed, RGB and RC stars are stellar evidence of activity prior to 1 Gyr ago, while BL and bright MS stars are tracers of activity a few hundreds of Myr and a few Myr ago, respectively. However, both CMDs show an apparent lack of horizontal branch (HB) stars, suggesting that both the regions, and presumably the entire SMC, formed a minor fraction of their stars at epochs older than 10 Gyr ago.

There are interesting differences between the CMDs for tiles 3_7 and 4_6. First of all, the morphology of the RC is rather elliptical in tile 4_6 CMD, while it shows a clear protrusion towards brighter magnitudes in tile 3_7. Considering that the RC protrusion is likely populated by objects at the transition between the RC and BL phases, hence stars with ages between 500 Myr and 1 Gyr, our conclusion is that the region of tile 3_7 has been relatively more active than for tile 4_6 at these epochs. If we take into account the fact that tile 3_7 is in the low-density wing, at the frontier of the Bridge connecting the SMC to the LMC, it is tempting to relate the higher activity in tile 3_7 with an SMC/LMC interaction. Moreover, the CMD of tile 4_6 shows a prominent RGB bump (physically caused by the H-burning shell crossing the chemical discontinuity left over by the convective envelope), just above the RC, a feature absent in tile 3_7.

From a theoretical point of view, the evidence of an RGB bump brighter than the RC is a clear indication that intermediate and old star formation took place at relatively low metallicity (Z = 0.001 or less) in tile 4_6. However its apparent lack in tile 3_7 CMD could be just due to the lower number of stars and requires further exploration with a synthetic CMD approach in order to be corroborated. On the other hand, the populous RC protrusion in the CMD of tile 3_7 represents a significant difference from tile 4_6, since the latter is globally much more populated. All these differences have to be investigated taking into proper account the larger crowding of tile 4_6, and the corresponding larger photometric errors and blending effects.

The spatial distribution

The spatial distribution of stars in different evolutionary stages yields important information on the star formation processes over the region. We have counted stars in different age regions of the CMD (see Figure 5), sampling the upper main sequence (UMS; red box), blue loop (BL; pink box), red clump (RC; green box), and sub-giant branch (SGB; blue box). Field contamination (FC; consisting of interlopers from the Milky Way and background galaxies) and highly reddened RC stars (RS) are sampled within the cyan and yellow boxes, respectively. In order to illustrate the power of this approach, Figure 6 shows the spatial distributions of these different groups of stars for tile 4_6.

It is clear that tile 4_6 harbours many clusters and associations, probably because of the generally high activity of this region. The stellar density of older populations (RC and SGB, middle left and bottom left panels, respectively) increases smoothly towards the SMC centre (in this case, the lower-right corner of tile 4_6), while the density of younger populations (UMS and BL, top left and top right panels, respectively) is very irregular and dominated by inhomoge-

neities. Indeed, most UMS stars are found aggregated in clusters/associations (identified clusters are indicated with labels c1 to c18 in the maps in Figure 6), with the most prominent ones corresponding to NGC 346 (c15 in the map) and NGC 371 (c9).

We point out that the distribution of RC stars shows clusters as well (c10, c11, c12), but that none of them turns out to have a counterpart in the UMS map (Figure 6). A simple explanation is that all agglomerates found in the latter are younger than 100 Myr, and hence, too young to host RC stars, while clusters detected only in the RC maps are necessarily too old to still have UMS stars in existence. It is also worth noting that among the clusters visible using RC stars, namely c10, c11 and c12, only c10 and c12 are seen also in the SGB map. Indeed, the c11 cluster, the well-known NGC 419, is about 1 Gyr old, and hence, the transition between the MS and the RGB phase, i.e. the SGB phase, is poorly populated (the Hertzsprung Gap). There is an excellent correspondence between the literature ages and the evolutionary phase adopted to detect the different c1–c18 structures, testifying to the reliability of this approach. Finally, the map of reddened RC stars (middle right panel in Figure 6) suggests a very patchy reddening distribution.

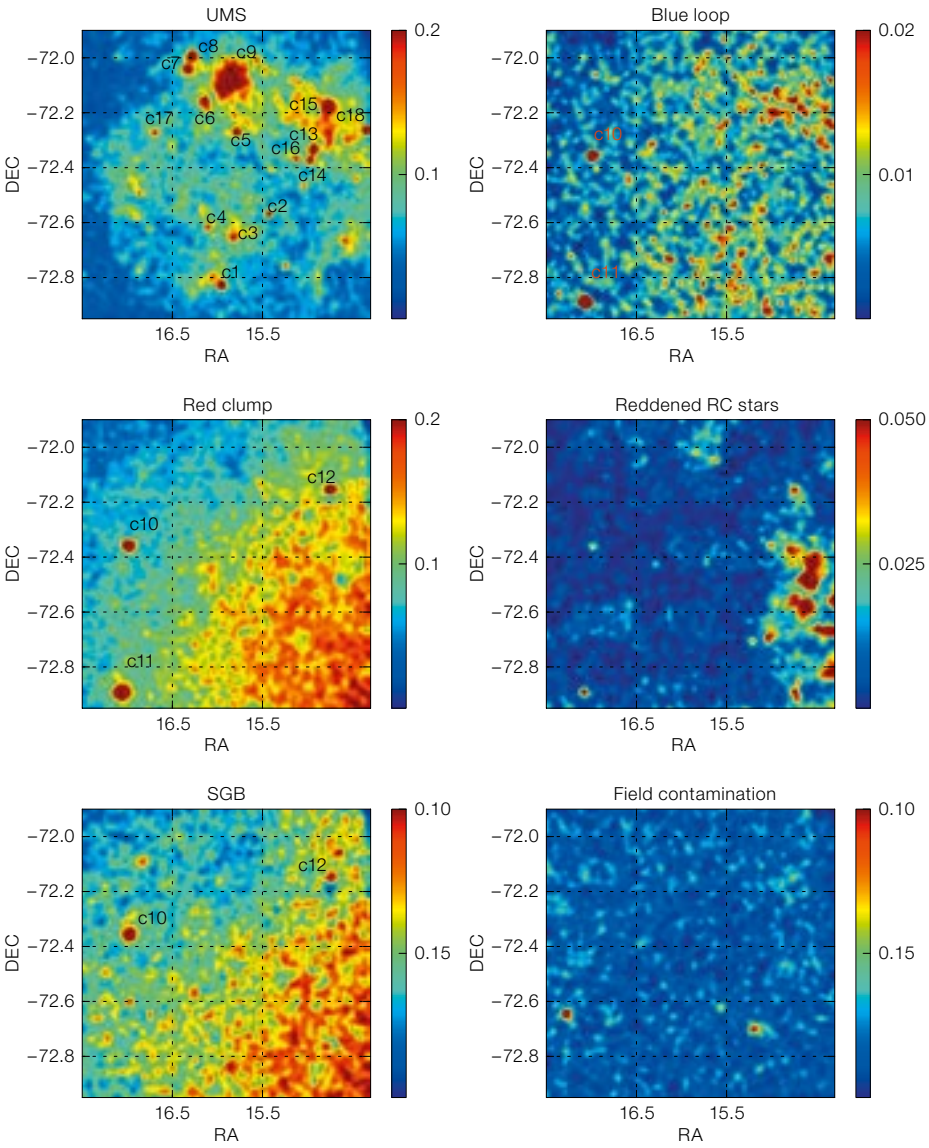

Figure 6. The spatial distributions of the stellar populations selected from the CMD of Figure 5 are shown. The maps are produced by calculating a 2D histogram of stellar positions and then smoothing the result with a Gaussian kernel. Labels c1 to c18 indicate clusters identified by eye.

Star clusters

Stellar clusters and associations are among the main targets of the STEP survey. The known objects will be characterised in detail, and new clusters and associations, possibly missed by previous studies, will be searched for. In the previous section we have shown how several clusters can be detected in tile 4_6 through the analysis of the spatial distribution. However these objects are only a small part of the clusters/associations content of tile 4_6, and the compilation by Bica et al. (2008) lists 114 clusters and associations in tile 4_6 alone.

In order to get an idea of STEP's capabilities for cluster studies, we have analysed in more detail two systems located in tile 4_6: NGC 419 and IC 1624. NGC 419 is a well-known intermediate-age (~ 1 Gyr) cluster, carefully studied on the basis of HST data and showing a dispersion in age of about 0.15 dex (e.g., Glatt et al. 2009). It is extremely crowded and the central regions are almost inaccessible with the VST. IC 1624 is a younger and looser cluster with respect to NGC 419. We characterised the two clusters by measuring the structural parameters through the analysis of their surface brightness profiles and estimating their ages.

The number densities and surface brightness profiles (SBPs) are useful tools to study the properties of star clusters in different galactic environments. These profiles contain information about the cluster's formation and evolution due to internal dynamical processes and the interaction with the galactic environment. The analytical function most suitable to describe the SBPs of young Magellanic Cloud star clusters is that suggested by Elson, Fall & Freeman (1987, EFF). We used these models in our analysis.

The SBPs of NGC 419 and IC 1624 are shown in the upper panels of Figure 7;

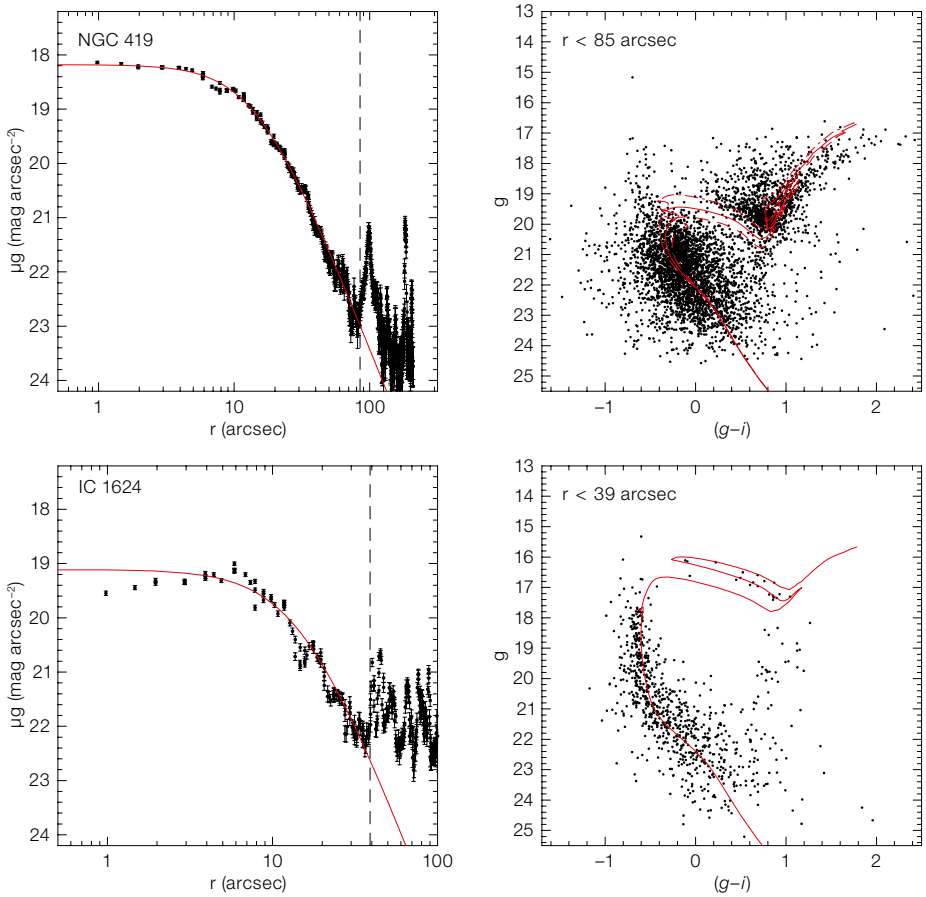

Figure 7. Left panels: Black dots show the observed radial stellar surface brightness profile around the centres of the clusters NGC 419 and IC 1624. The solid red line shows the profile fitting from the EFF law, while the dashed line represents the fitting radius. Right panels: The CMDs of the same clusters within the fitting radius (dots); the red solid and dashed lines in the upper-right panel (NGC 419) show the isochrones for 900, 1000 and 1100 Myr, respectively. The red solid line in the lower-right panel (IC 1624) shows the isochrone for 170 Myr.

in each panel the vertical dashed line indicates the "fitting radius", i.e., the limit within which the fitting procedure is carried out. The profiles in Figure 7 were obtained by: 1) estimating the cluster centre; 2) dividing the profile in annuli of different sizes; 3) averaging the counts in each annulus. Each panel shows the EFF law that best fits the data. We verified that the results for both clusters are in agreement with similar analyses, confirming the reliability of our approach.

To estimate the ages of the two clusters, we first plotted their CMDs within the fitting radius defined above (Figure 7 lower panels). The CMD of NGC 419 is rather scattered, due to the high crowding, which boosts dramatically photometric errors and incompleteness towards the cluster centre. However, the CMD of IC 1624 is rather loose because of the global paucity of stars in this cluster. In terms of age, there is a clear difference between the two clusters, with IC 1624 being much younger than NGC 419.

To be more quantitative, we adopted the isochrones from Marigo et al. (2008) with proper assumptions about reddening and distance modulus to fit the observed CMDs (red solid lines in Figure 7). As a result, for NGC 419, the magnitude difference between RC and bulk of the MS-TO suggests an age between 900 and 1100 Myr, but the large photometric errors prevent any definitive conclusion about a genuine age spread. The situation is completely different in IC 1624. The 170 Myr old isochrone fits all the main evolutionary phases very well, including the MS-TO, the red envelope of the BL and the average luminosity of the loop. The results for the ages of both clusters are, again, in very good agreement with literature results. Similar work will be carried out for all the clusters detected in the context of the STEP survey.

We are looking forward to a timely completion of all the data acquisition in order to exploit STEP at its best and provide the ESO community with the deepest homogeneous survey of the whole SMC ever performed.

References

Bica, E. et al. 2008, MNRAS, 389, 678
Capaccioli, M. & Schipani, P. 2011, The Messenger, 146, 2
Cignoni, M. et al. 2013, ApJ, 775, 83
Cignoni, M. et al. 2012, ApJ, 754, 130
Cioni, M. R. L. et al. 2011, The Messenger, 144, 25
Elson, R. A. W., Fall, S. M. & Freeman, K. C. 1987, ApJ, 323, 54
Glatt, K. et al. 2009, AJ, 138, 1403
Grado, A. et al. 2012, MemSAIT, 19, 362
Marigo, P. et al. 2008, A&A, 482, 883
Kuijken, K. 2011, The Messenger, 146, 8
Ripepi, V. et al. 2014, MNRAS, 442, 1897
Tolstoy, L., Hill, V. & Tosi, M. 2009, ARAA, 47, 371

Links

[1] VMC Survey: http://star.herts.ac.uk/~mcioni/vmc/
[2] SCAMP package: http://www.astromatic.net/software/scamp
[3] SWARP package: http://www.astromatic.net/software/swarp

The KMOS Redshift One Spectroscopic Survey (KROSS)

Richard Bower[1]
Martin Bureau[2]

[1] Institute for Computational Cosmology, University of Durham, United Kingdom
[2] Sub-department of Astrophysics, University of Oxford, United Kingdom

on behalf of the KROSS consortium

A brief overview of the first results from KROSS, a VLT/KMOS guaranteed time programme is presented. KROSS will spatially resolve the dynamics, metallicity and star formation of 1000 mass- and colour-selected galaxies at $z \sim 1$. These data will chart the formation of disc galaxies at the epoch of peak star formation density in the Universe.

At redshift $z \sim 1$, the Universe is roughly half its present age and very different to the present day. In particular, the volume-averaged star formation density of the Universe is an order of magnitude larger than at $z = 0$ (e.g., Lilly et al., 1996). Although recognisable, disc galaxies are just beginning to emerge from the chaos of the first few billion years of the Universe's history, their star formation rates, gas masses and (possibly) interaction rates are far higher than in today's quiescent galaxies.

The second-generation Very Large Telescope (VLT) instrument, the *K*-band Multi-Object Spectrograph (KMOS), is a near-infrared integral field spectrograph with a high multiplexing capability (Sharples et al., 2013). Its 24 integral field units (IFUs) allow maps of key astrophysical quantities to be created faster than ever before, and the near-infrared spectral coverage is particularly powerful to target the well-understood restframe optical wavelength range around $z \sim 1$. The KMOS Redshift One Spectroscopic Survey (KROSS) aims to understand the changes in galaxy properties through a ground-breaking, spatially resolved study of a large and representative sample of galaxies at this key epoch.

Observational challenges of galaxy surveys

Within the past decade, there has been incredible progress in the study of galaxies in the redshift range $1 < z < 2$. A variety of techniques has been used to reliably disentangle distant galaxies from faint foreground objects, and the number of spectroscopically confirmed galaxies in this redshift range now numbers well into the tens of thousands. Restframe ultraviolet (UV) and optical colours, wide-area narrowband surveys and mid-infrared/submillimetre detections have all allowed observers to reliably determine galaxy stellar masses and quantify star formation rates. Although these data do not have the statistical power or quality of local surveys, such as the Sloan Digital Sky Survey (SDSS) or 2dF (Two-degree-Field Galaxy Redshift Survey; e.g., Abazajian et al., 2009; Colless et al., 2001), they do allow us to measure the evolution of stellar mass and to track black hole growth (e.g., Alexander & Hickox, 2012).

Recent studies have also made it possible to chart the dispersal of metals (e.g., Maiolino et al., 2008) and to begin to study the morphological and structural properties of galaxies as they settle onto a recognisable Hubble sequence (e.g., Swinbank et al., 2010). All these surveys have confirmed that the early Universe looks drastically different from its current state, and they have allowed us to begin to infer the formation histories of typical galaxies. At the highest redshifts however, massive galaxies are seen to be undergoing rapid star formation and the Hubble sequence is not yet in place.

Advances in observational surveys have been mirrored by progress in numerical simulations. In particular, models have highlighted the importance of high gas accretion at $1 < z < 2$. At these redshifts, even massive galaxies are continuously fed by narrow and cool "cold streams" of gas from the intergalactic medium (Dekel et al., 2009; van der Voort, 2011), promoting rapid but unstable star formation (e.g., Hopkins et al., 2012). As the Universe ages, these inflows become more tenuous and are eventually disrupted by outbursts from the black holes that grow at the centres of the emerging galaxies (e.g., Bower et al., 2006). By the present day, these processes have led to the formation of a recognisable Hubble sequence. In the current generation of simulations, the emergence of the Hubble sequence arises because of the evolution of the fuelling rates of galaxies, and not because of a decline in the rate of galaxy merging (Behroozi et al., 2013).

Simulation results generally agree well with the global properties of the galaxy population, but they are intrinsically statistical in nature. With increasing survey speeds and growth in computational power, it is now possible to study the development of the internal properties of large samples of galaxies across these redshifts. Indeed, to enhance our empirical knowledge and refine theoretical models, the observational challenge must now be to quantitatively measure the internal structures of intermediate- and high-redshift galaxies across a range of masses and star formation rates (SFR). In this way, we will chart the growth of galaxy discs, comparing the growth of rotation speeds, disc stability and gas content against simulated galaxies.

With sufficient angular resolution, we can test whether secular processes in early systems play a significant role in building the majority of the $z = 0$ stellar mass, and we can identify the key physical mechanisms producing the global trends observed at $z = 0$ (e.g., Forster-Schreiber et al., 2009; Swinbank et al., 2012). Equally important, these constraints are vital to determine whether the numerical prescriptions developed to describe star formation in local galaxies can equally be applied to the dense and rapidly evolving interstellar medium of gas-rich, intermediate-redshift galaxies.

KROSS

Some progress has been made in building samples of galaxies at $z = 0.5$–1 using the VLT Spectrograph for INtegral Field Observations in the Near-Infrared (SINFONI) and the OH-Suppressing Infrared Integral Field Spectrograph (OSIRIS) on the Keck Telescope (e.g., Puech et al., 2008), but with its 24 simultaneous IFUs, KMOS is already revolutionising this field and allows us to rapidly build significantly larger and more representative galaxy

samples at these redshifts. Comparing the new data to those of local optical IFU surveys, such as the Sydney Australian Astronomical Observatory Multi-object Integral Field Spectrograph (SAMI) and the Mapping Nearby Galaxies instrument (MANGA), will reveal how the current Hubble sequence has emerged from the chaos of the early Universe. A key goal of our KMOS guaranteed time programme is to establish a large and well-defined statistical sample of galaxies at $z \sim 1$.

KROSS will create a database of 1000 spatially-resolved, mass-selected star-forming galaxies at the critical $z \sim 1$ epoch. The sample size is large enough that the results can be divided into multiple bins of, e.g., stellar mass (ranging from $10^{9.5}$ to $10^{10.7}$ $M_{\odot}$), SFR, rotation speed and environment. Within each bin it will be possible to quantify trends between residuals from galaxy scaling relations, and to correlate deviations in SFR with velocity asymmetry and disc warping, thus quantifying the response of the nascent discs to interactions, gas flows and internal instabilities. Hence we will determine the relative roles of nature and nurture (and their imprecise boundary) in driving the evolution of the cosmic SFR density.

The first pilot observations to test the feasibility of the survey were taken during KMOS Science Verification in July 2013, when we observed 39 galaxies at $z = 0.84$ from the High Redshift (Z) Emission Line Survey (HiZELS) of the SSA22 field (Small Selected Area), for a total of 2 hours per configuration. All observations were taken in the *YJ*-band filter with a spectral resolution of $R = 3500$. We detected 30 of the targeted galaxies and measured their spatially resolved dynamics, metallicity and star formation rate (Sobral et al., 2013; Stott et al., 2014).

In Period 92, KROSS was allocated its first seven guaranteed nights to target the first 240 star-forming galaxies at $z \sim 1$. Target selection for the survey requires careful consideration. Selecting fainter galaxies makes it simple to fill all of the KMOS IFUs, but fainter (or more distant) galaxies are smaller and therefore less well-resolved spatially. While asymptotic rotation curves can be recovered by exposing for longer, this impacts on survey speed. For the target selection, we thus imposed an optimal *K*-band limit of $K_{AB} = 22.5$ mag. Our aim is to obtain a mass-selected survey of the star-forming galaxy population, so we prioritised galaxies with blue colours ($r–z < 1$). This is sufficient to include essentially all galaxies with significant star formation, but galaxies with redder colours are also included with a well-defined sampling rate.

KROSS preliminary results

Each galaxy was observed for a total of 4.5 hours using ABA sequences (where A is on-source and B is sky, with one IFU from each spectrograph permanently dedicated to sky to improve the OH residual subtraction). Data reduction was carried out with SPARK (the Software Package for Astronomical Reductions with KMOS; Davies et al., 2013). As we are primarily interested in emission line properties, we find the instrument has excellent stability, and our observations are limited by sky noise rather than systematic sky residuals. In total, we detected 93 % of the targets (with most non-detections corresponding to faint or passive galaxies), and derived spatially resolved velocity maps for 80 % of the sample.

The main panel of Figure 1 shows a fraction of the data obtained in one observation. The right-hand panel shows the reduced two-dimensional spectra as they appear after correcting for instrumental effects and sky subtraction; the individual spatial slices are clearly visible. Strong emission lines are evident, including Hα, [N II] and the [S II] doublet. Careful examination of the spectra immediately reveals spatial gradients in the line velocities (rotation) and ratios (abundance). Thumbnails on the left-hand side of Figure 1 show the corresponding velocity fields, colour-coded.

The power of KROSS lies in the speed with which it is possible to build up large samples of intermediate-redshift galaxies. In Figure 2, we show the dynamics of the ~ 200 galaxies in our Period 92 sample with spatially resolved emission lines, the location of each postage stamp indicating the stellar mass and SFR of the target galaxy. The location of the "main sequence" of star-forming galaxies at $z \sim 1$ is illustrated by a dashed line (Karim et al., 2011).

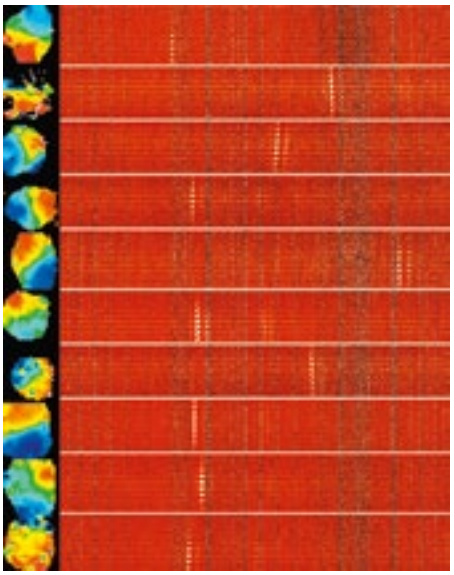

Figure 1. The main panel shows a fraction of the data obtained in a single KMOS observation of a field of $z \sim 1$ galaxies. Strong emission lines are evident, as are the strong velocity and line ratio gradients across the galaxies. The left-hand side thumbnails are the corresponding velocity fields, colour-coded blue (negative velocity) and red (positive velocity) with respect to the galaxy systemic velocity.

Even a cursory examination of Figure 2 shows that the majority of the sample galaxies have disc-like kinematics, and that objects with strongly disturbed velocity fields are rare. However, the median ratio of the ionised gas rotation velocity to velocity dispersion v/σ (where σ is corrected for both instrumental broadening and beam smearing) is $v/\sigma \sim 3$, much lower than in local galaxies with a similar mass (where $v/\sigma \sim 10$). Of course, local galaxies also have much lower specific SFRs, so these initial data already reinforce the idea that higher specific SFRs rates drive greater turbulence (or vice versa). Further analysis will allow us to determine if the change in gas mass agrees with the high fuelling rates of $z \sim 1$ discs predicted in the simulations.

By combining the rotation and velocity dispersion maps, we can measure the fraction of rotationally supported systems in a mass-selected sample of $z \sim 1$ galaxies, and use the Tully–Fisher relation to

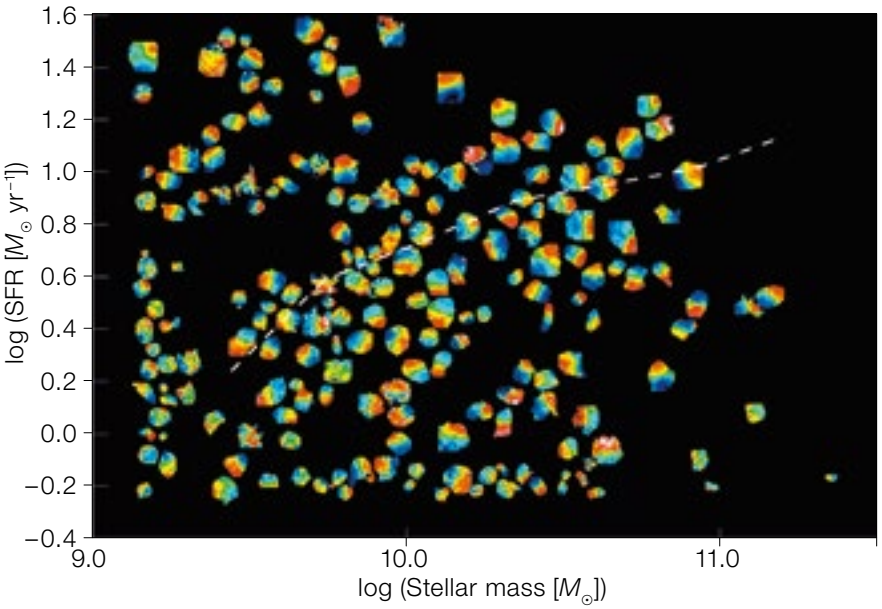

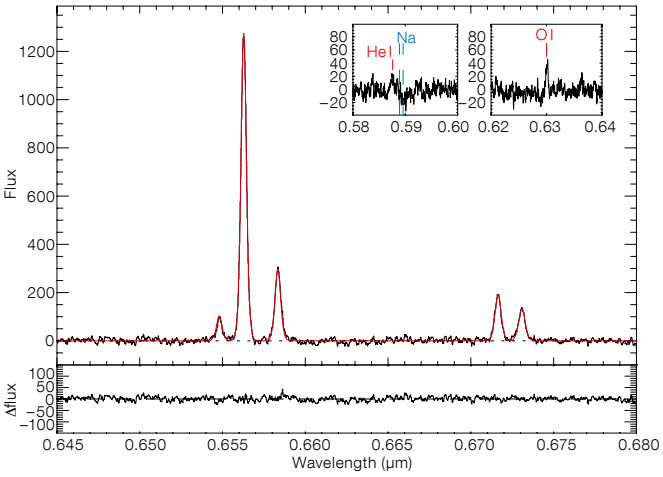

Figure 2. (Above) First results from KROSS, our KMOS guaranteed time survey of 1000 mass- and colour-selected galaxies at $z \sim 1$. The image shows the velocity fields of ~ 200 galaxies with spatially resolved emission lines observed in Period 92, their position on the plot indicating their stellar mass and SFR, with the galaxy velocity fields colour-coded. The dashed line shows the location of the "main sequence" of star-forming galaxies at $z \sim 1$ (Karim et al., 2011). Disc-like kinematics is seen in the majority of the sample.

Figure 3. Stacked spectrum of all KROSS galaxies from Science Verification and Period 92 observations that meet our selection criteria. The continuum was subtracted and the mean velocity of each galaxy spectrum was corrected before constructing the stack, and each spectrum was normalised according to its reddening-corrected SFR before stacking. The insets show zooms around the [O I] 6300 Å emission line and the NaD 5995 Å absorption line. The lower panel shows the residuals from the best-fit model (red).

probe the evolution of the mass-to-light ratio of galaxies with redshift (e.g., Miller et al., 2013). We find that 80 % of our targets rotate regularly, approximately twice the disc fraction at $z \sim 2$ from the SINFONI Integral Field Spectroscopy (SINS) and the Assessing the Mass-Abundances Redshift (Z) Evolution (AMAZE) surveys (Shapiro et al., 2008; Contini et al., 2012). The ratio of stellar to dynamical mass suggests molecular gas fractions of 30–60 %, consistent with the evolution inferred from CO measurements between $z = 0.4$ and 2 (e.g., Tacconi et al., 2013).

The good spectral resolution of KMOS also allows us to infer spatially resolved chemical abundance gradients (via the [N II] / Hα ratio), that can be used to test "inside-out" *vs.* "outside-in" disc formation scenarios (Gilmore et al., 2002).

Finally, we can map the average properties of weaker spectral features by subtracting the local rotation velocities and then binning galaxies both spatially and as a function of stellar mass, SFR, etc. An example of such a stacked spectrum is shown in Figure 3, with the ambitious goal of searching for broad Hα emission arising from outflowing gas ("super-winds"; e.g., Pettini et al., 2002). These features allow us to measure the mass and kinetic energy of the ejecta, presumably associated with star formation and/or active galactic nucleus driven feedback, one of the critical uncertainties in galaxy formation modelling.

KROSS data collection is progressing. By measuring the spatially resolved kinematics of ~ 1000 galaxies at $z \sim 1$, this powerful database will provide deep insight into the different properties of galaxies when the Universe was half its current age, and those of similar mass galaxies today. We will move from asking whether the detailed properties of galaxies at these epochs differ, to understanding the internal mechanics of how and why.

Acknowledgements

The KROSS team would like to acknowledge STFC grants ST/I001573/1 and ST/H002456/1.

References

Abazajian, K. et al. 2009, ApJS, 182, 543
Alexander, D. M. & Hickox, R. C. 2012, NewAR, 56, 93
Colless, M. et al. 2001, MNRAS, 328, 1039
Dekel, A. et al. 2009, Nature, 457, 451
Forster-Schreiber, N. et al. 2009, ApJ, 806, 1364
Bower, R. et al. 2006, MNRAS, 370, 645
Behroozi, P. et al. 2013, ApJ, 762, 31
Contini, T. et al. 2012, A&A, 539, 91
Davies, R. et al. 2013, A&A, 558, 56
Gilmore, G. et al. 2002, ApJ, 574, 39
Karim, A. et al. 2011, ApJ, 730, 61
Lilly, S. et al. 1996, ApJ, 460, 1
Maiolino, R. et al. 2008, A&A, 488, 463
Miller, S. H. et al. 2013, ApJ, 762, 11
Pettini, M. et al. 2002, Ap&SS, 281, 461
Puech, M. et al. 2008, A&A, 484, 173
Shapiro, K. L. et al. 2008, ApJ, 682, 231
Sharples, R. et al. 2013, The Messenger, 151, 21
Sobral, D. et al. 2013, ApJ, 779, 139
Stott, J. et al. 2014, submitted, arXiv1407.1047
Swinbank, M. et al. 2010, MNRAS, 405, 234
Swinbank, M. et al. 2012, MNRAS, 436, 935
Tacconi, L. et al. 2013, ApJ, 768, 74
van de Voort, F. et al. 2011, MNRAS, 414, 2458

ALESS: An ALMA Survey of Submillimetre Galaxies in the Extended Chandra Deep Field South

Ian Smail[1]
Fabian Walter[2]

For the ALESS consortium

[1] Institute of Computational Cosmology, Durham University, United Kingdom
[2] Max-Planck-Institut für Astronomie, Heidelberg, Germany

The ALESS survey is an ALMA Cycle 0 study of ~ 100 luminous high-redshift ultraluminous infrared galaxies in the Extended Chandra Deep Field South (ECDFS), one of the best-studied cosmological deep fields accessible from the southern hemisphere. These galaxies were originally selected based on their bright emission in the submillimetre continuum (so-called submillimetre galaxies, or SMGs) through observations using the APEX bolometer camera LABOCA. Compared to the single-dish LABOCA data, the interferometric ALMA data provide a positional accuracy that is nearly two orders of magnitude higher. The ALMA data thus enable galaxy identifications that were previously impossible, and so remove many of the biases inherent in previous studies of SMGs to give us our first unbiased view of a large sample of this important galaxy population.

The submillimetre is an ideal wavelength regime to search for luminous, but dust-obscured, sources which may represent the most active phase of galaxy formation. Submillimetre surveys most commonly use the atmospheric windows at ~ 870 μm or ~ 1200 μm. These wavebands benefit from the positive *K*-correction produced by the dust spectrum which means that a source with a fixed far-infrared luminosity has an almost constant measured flux density from redshifts $z \sim 1$–8 (i.e., lookback times of ~ 7 to 13 Gyr). Thus a deep submillimetre survey provides an effectively volume-limited sample of the most luminous far-infrared sources out to the highest redshifts.

Over the past ~ 15 years sensitive surveys of the submillimetre sky with bolometer cameras on single-dish telescopes have uncovered an abundant population of ultraluminous infrared sources (with infrared luminosity $L_{IR} > 10^{12}\,L_{\odot}$, corresponding to star formation rates of $> 100\,M_{\odot}\,\mathrm{yr}^{-1}$). These appear to be dusty starburst events occurring in massive galaxies out to the highest redshifts, $z > 5$ (e.g., Walter et al., 2012). Unfortunately, the study of these sources has been hampered by two factors: firstly, the resolution of these single-dish maps is poor, typically ~ 10–30 arcseconds, making it difficult to precisely locate the submillimetre sources; secondly, given their high redshifts and dusty nature, the SMGs are typically very faint in the optical/near-infrared passbands, making it hard to derive their properties (e.g., redshifts, stellar masses, morphologies, etc). In addition, the surface densities of these sources is 1 per 10 square arcminute at a flux density $S_{870\,\mu m} \sim 5$ mJy, so they are too rare to find in large numbers in blank-field searches with submillimetre interferometers, which instead have to rely on targets detected by the single-dish surveys.

Prelude: LESS — The LABOCA ECDFS Submillimetre Survey

In 2004 we began discussing with ESO a proposal to undertake a survey for submillimetre galaxies in the 150 square arcminute GOODS-South field using the planned Large APEX Bolometer Camera (LABOCA) on the new 12-metre Atacama Pathfinder Explorer (APEX) telescope sited at Chajnantor. The main aim of this proposal was to provide a large sample of SMGs in a field ideally placed for study with ESO's facilities, in particular the long-awaited Atacama Large Millimeter/submillimeter Array (ALMA).

By 2007 this proposal had evolved into a public legacy survey of the whole of the 0.5 by 0.5 degree ECDFS. The completed LABOCA ECDFS submillimetre survey (LESS) took 310 hours of observing time to map the full ECDFS to a uniform noise level of $\sigma_{870\,\mu m} \sim 1.2$ mJy beam^{-1} and was published in Weiß et al. (2009). At the time LESS was the largest contiguous deep submillimetre survey undertaken and detected a total of 126 SMGs above a significance level of 3.7σ (with an expectation of no more than five false detections). As discussed above, due to the positive *K*-correction in the submillimetre waveband, the LESS survey should detect all dusty starbursts within the ECDFS with star formation rates of $> 500\,M_{\odot}\,\mathrm{yr}^{-1}$ out to $z \sim 8$.

With ALMA Early Science not yet scheduled in 2009, we used the traditional probabilistic identification techniques (e.g., Ivison et al., 2002) to locate likely counterparts — the individual SMGs — to the LESS submillimetre sources. These approaches rely on proxy tracers, such as radio or mid-infrared brightness, of the luminous submillimetre emission or near/mid-infrared colours, as indicators of extreme dust reddening (Biggs et al., 2011). In this manner we identified probable counterparts to around 60 % of the submillimetre sources (Biggs et al., 2011; Wardlow et al., 2011). With these precisely located counterparts, we could then exploit the wealth of archival multi-wavelength data in the ECDFS to study the active galactic nuclei (AGN) content of SMGs (Lutz et al., 2010), their redshift distribution and stellar masses (Wardlow et al., 2011) and clustering (Hickox et al., 2012), as well as the multiwavelength properties of one of the highest-redshift submillimetre galaxies known (Coppin et al., 2009) and more normal galaxies in the field (Greve et al., 2009). Moreover, combining this submillimetre sample with shorter-wavelength observations from the Balloon-borne Large Aperture Submillimeter Telescope (BLAST) experiment, it was also possible to get a first insight into the restframe far-infrared emission of the SMG population (e.g., Ivison et al., 2010) prior to the launch of Herschel (Magnelli et al., 2011).

MORE from LESS: ALESS — an ALMA study of LESS SMGs

Early Science observations with ALMA (Cycle 0) were advertised in mid-2011 and 5.4 hours were awarded to our consortium to obtain 870 μm continuum maps of all 126 submillimetre sources from LESS (ALMA project #2011.1.00294.S). These short 120 s exposures were intended to yield maps with $\sigma_{870\,\mu m} \sim 0.4$ mJy beam^{-1}, around three times deeper than the LABOCA map, but with a beam of ~ 1.5 arcseconds, compared to ~ 18 arcseconds for APEX, sufficient to unam-

biguously identify the SMGs responsible for the emission detected by LABOCA. Moreover, the ALMA primary beam matches the LABOCA map resolution, ensuring that the SMGs contributing to the emission in the LESS map should fall within the ALMA field of view. Finally, one key feature of the ALMA study was that it would observe the LESS sources in the same waveband as the original LABOCA survey, removing any ambiguity when comparing fluxes between the two studies. As will be seen, this was a critical choice.

The ALMA observations were undertaken in October and November 2011 and released to the consortium in late February 2012. As shared risk observations the data were of variable quality, but after removing maps with noise levels significantly higher than our goal ($\sigma_{870\,\mu m}$ > 0.6 mJy beam^{-1}) or very elliptical beams (axial ratios > 2), we were left with 88 good quality maps from the 122 that were delivered.

Hodge et al. (2013) catalogued the SMGs detected in these maps and presented a MAIN catalogue comprising 99 ALMA-detected SMGs with detection significances of > 3.5σ (with a false detection rate < 1 %) and lying within the primary beam area in our best maps. There are a further 32 SMGs, detected at > 4σ either outside of the ALMA primary beam in the best maps, or within primary beams in the lower quality maps, which we provided in a supplementary catalogue, but do not use in our analysis.

The fundamental characteristics of an unbiased sample of SMGs

One of the first results from ALESS was the incidence of multiple SMGs within a single submillimetre source (Karim et al., 2013; Hodge et al., 2013). This was not entirely unexpected, given earlier known examples (e.g., Smolcic et al., 2012). However, the surprise was that all of the LESS submillimetre sources brighter than ~ 10 mJy broke into several components (see Figure 1 for examples), with the result that there are no individual SMGs brighter than 9 mJy in the ALESS catalogue. Due to the modest depth of the ALESS maps, it is not clear whether this blending bias is limited to the brightest submillimetre sources or occurs at all flux limits.

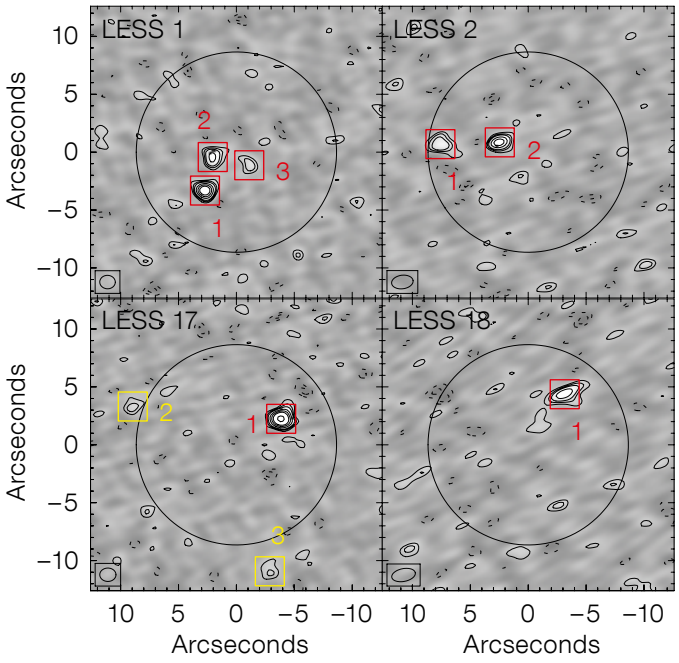

Figure 1. Examples of ALMA 870 μm maps (from Hodge et al., 2013) of submillimetre sources from the LESS survey. Some single-dish sources fragment into several SMGs when observed with ALMA at 1.6-arcsecond resolution. The circle shows the ALMA primary beam (comparable to the LABOCA map resolution) and contours start at ± 2σ, with increments of 1σ. Main and supplementary catalogue sources are indicated by red and yellow boxes respectively, with the ALMA beam at lower left.

However, Hodge et al. (2013) also found a surprisingly high fraction (~ 20%) of good quality ALMA maps which are blank, i.e., maps where LABOCA detected a source but there is nothing above 3.5σ seen by ALMA. As the two datasets were taken in the same waveband, the most likely explanation for this is that multiplicity is also an issue for fainter submillimetre sources as well. This is supported by the detection of these ALMA-blank submillimetre sources in Herschel Spectral and Photometric Imaging Receiver (SPIRE) far-infrared maps (Swinbank et al., 2014), confirming their reality as submillimetre sources, and by the discovery of excess populations of z ~ 2–3 galaxies, observed by the Infrared Array Camera (IRAC) on board the Spitzer Space Telescope, in these maps. These z ~ 2–3 galaxies exhibit enhanced 870 μm emission as shown by stacking analysis (Decarli et al., 2014; Simpson et al., 2014).

ALESS can transform our understanding of the SMG population, providing a unique sample of 99 SMGs with the precise positions necessary to investigate their fundamental properties. Hence in Figure 2 we show the apparent magnitude and flux distributions of the SMGs in the V, K, 3.6 μm and 1.4 GHz bands (Simpson et al., 2014). These distributions demonstrate increasing detection rates from V to K to 3.6 μm, reflecting the typically red colours of the SMGs.

However, Figure 2 also shows that more than half of the SMGs are undetected in the radio waveband above a limit of ~ 20 μJy. This highlights the incompleteness in previous studies which had to rely on radio (or mid-infrared) observations to attempt to statistically associate counterparts with submillimetre sources. These studies typically correctly identified at most half of the SMGs (Hodge et al., 2013). In contrast, our ALMA study allows us to robustly determine the true properties of the SMG population, including the mysterious ~ 10% fraction which are undetected at any wavelength other than the submillimetre (Simpson et al., 2014).

Figure 3 shows the composite restframe spectral energy distribution (SED) of the SMGs in the optical–radio wavebands (Swinbank et al., 2014; see also Simpson et al., 2014). From this plot, we see that a typical ALESS SMG has a far-infrared luminosity of $L_{IR} = 3 \times 10^{12}\,L_{\odot}$, corresponding to a star formation rate (SFR) of 300 $M_{\odot}$ yr^{-1}. As expected this star formation activity is dust-reddened, with an apparent A_V ~ 2 mag for the detectable restframe near-infrared continuum light.

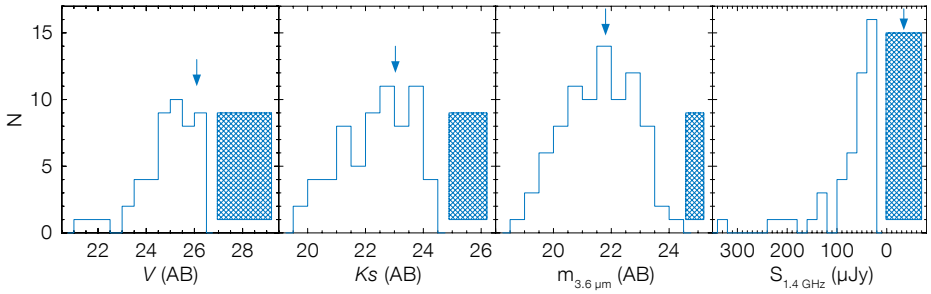

Figure 2. (Above) The *V*, *Ks*, IRAC 3.6 μm and 1.4 GHz brightness distributions for ALESS SMGs from Simpson et al. (2014). The checked region shows the undetected sources and the arrows the medians (including the non-detections): $V = 26.1 \pm 0.2$, $Ks = 23.0 \pm 0.3$ and $m_{3.6\,\mu m} = 21.8 \pm 0.2$ mag. The radio data reaches a 3σ depth of 19.5 μJy, but only detects 45 % of the SMGs, so their median flux must be < 19.5 μJy.

Figure 3. (Below) The composite SED of SMGs from Swinbank et al. (2014). The large red points denote the bootstrap median and the solid curve shows the best-fitting SED, with the 1σ uncertainty indicated by the shaded region, with the residuals shown in the lower panel. The dashed curve shows the composite SED derived for $z \sim 1.5$ U/LIRGs from Lee et al. (2013). The black curves show a three-component grey-body dust SED fit with $T_d \sim 30$, 60 and 120 K components.

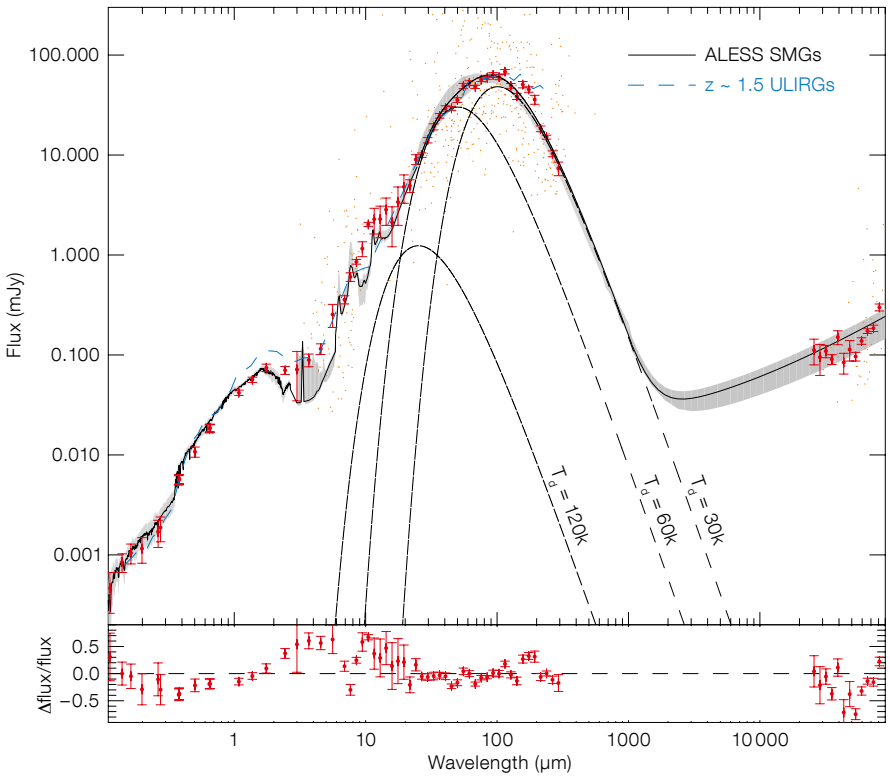

Estimates of the stellar mass from the near-infrared luminosity indicate $M_* \sim 8 \times 10^{10}\ M_\odot$ (Simpson et al., 2014), but with significant systematic uncertainties. Similarly the submillimetre luminosity yields a dust mass of $M_d \sim 4 \times 10^8\ M_\odot$, which implies a typical gas mass of $M_g \sim 4 \times 10^{10}\ M_\odot$. Combining these we obtain a total baryonic mass of an SMG of $M \sim 10^{11}\ M_\odot$ and a gas mass fraction of ~ 40 %, underlining the massive and gas-rich nature of these galaxies (Swinbank et al., 2014).

Starbursts and growing black holes

The precise positions of the SMGs from ALMA also allow us to investigate their AGN content by combining these data with the excellent Chandra X-ray coverage in the ECDFS. In Wang et al. (2013) we estimate that at most 20 % of SMGs are likely to host luminous AGN ($L_X > 8 \times 10^{42}$ erg s^{-1}), with the majority of these showing moderate/high absorption ($N_H > 10^{23}$ cm^{-2}).

This analysis uncovered a submillimetre continuum source lying within 1 arcsecond of a $z = 1.3$ X-ray luminous (but unobscured) quasi-stellar object (QSO; see Figure 4). Submillimetre-bright X-ray QSOs are of particular interest as they may represent a transition phase in galaxy evolution between starburst progenitors and passive descendants. However, in this particular case subsequent spectroscopic follow-up of the ALESS sample (Danielson et al., in prep) has shown that the submillimetre emission is actually from a background SMG at $z = 2.4$, which is being weakly lensed by the foreground QSO host. This system demonstrates the critical importance of precise submillimetre positions for the correct identification of SMGs.

Wang et al. (2013) also exploited the precise ALMA positions, by stacking the X-ray flux at the position of the 49 individually undetected SMGs in the field (Figure 5). These stacks reach an equivalent on-source exposure time of 10 Ms and they detect soft-band X-ray emission at 5.4σ significance. The corresponding average SMG luminosity is $L_X \sim 1 \times 10^{42}$ erg s^{-1}, consistent with the X-ray emission expected from star formation, given the SMG's star formation rates (Wang et al., 2013); as such there is no evidence for luminous activity associated with an active galactic nucleus in the bulk of the SMGs.

The evolution of high-redshift ULIRGs

Simpson et al. (2014) used the extensive archival photometry in the ECDFS (e.g., Figures 2 and 3) to determine photometric redshifts for the ALESS SMGs. Their analysis included a statistical correction for the 20 % of the ALESS sample for which reliable photometric redshifts could not be derived due to the SMG being detected in < 4 photometric bands (most frequently just the IRAC mid-infrared bands, see Figures 1 and 2). These faint SMGs are expected to include the highest-redshift examples of the popula-

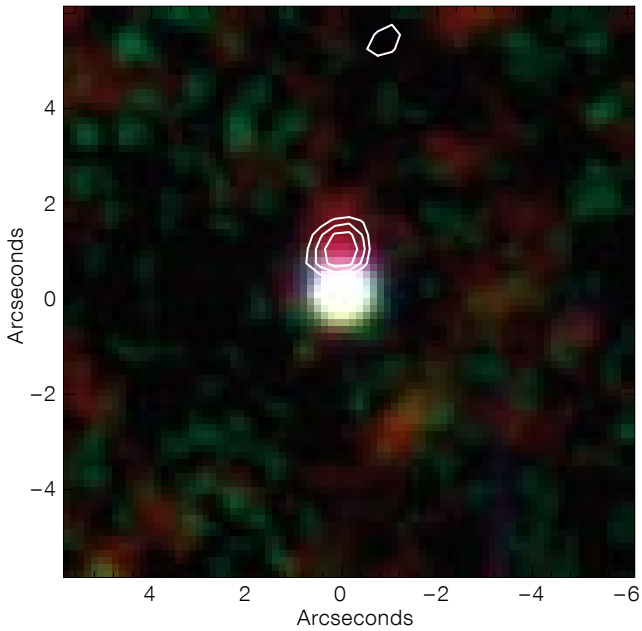

Figure 4. A *VJK* image of ALESS66.1 overlaid with ALMA contours (starting at 3σ in increments of 1σ). The submillimetre position lies within 1 arcsecond from an X-ray detected z = 1.3 QSO which was initially identified as the counterpart (Wang et al., 2013). However the faint red source visible under the ALMA emission is a background z ~ 2.5 SMG, weakly lensed by the foreground QSO (Danielson et al., in prep.).

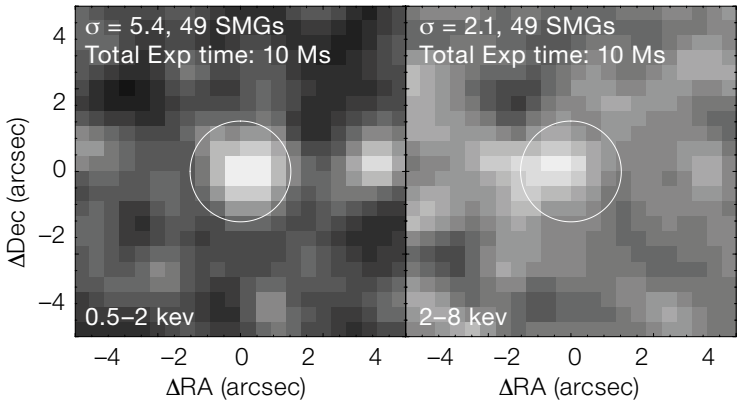

Figure 5. The stacked X-ray emission in the 0.5–2 keV and 2–8 keV bands for the 49 individually X-ray-undetected SMGs from Wang et al. (2013). The stacks have an equivalent cumulative integration of 10 Ms. The measured X-ray luminosities and their X-ray colours are consistent with that expected purely from on going star formation.

tion and Simpson et al. (2014) were able to place a firm limit of ~ 20 % of SMGs at $z > 4$ (see Figure 6).

Simpson et al. (2014) find that the redshift distribution of ALESS SMGs is strongly peaked with a median z ~ 2.3, as seen by previous studies (e.g., Chapman et al., 2005; Wardlow et al., 2011). Plotted as a function of lookback time, the distribution is well described by a Gaussian with peak activity occurring at a lookback time of 11.1 Gyr and a duration of the activity of 1.1 Gyr (full width at half maximum [FWHM]). The ALESS SMGs show a clear and strong peak at z ~ 2, rather than previous claims of a flat redshift distribution for SMGs between z ~ 2–6. This peaked distribution suggests that the evolution of SMGs can be described simply by the combination of the growth of dark matter and the variation in molecular gas mass fraction with time (Hickox et al., 2012).

Next, assuming a simple model with no additional star formation beyond the current burst and no subsequent merging, Simpson et al. (2014) used the redshifts and near-infrared luminosities of the SMGs to predict the properties of their

Figure 6. Left: The redshift distribution of the ALESS SMGs, binned uniformly in time. This is well represented by a log–normal distribution (see Simpson et al., 2014). For comparison we show the redshift distribution from Smolcic et al. (2012) and Weiß et al. (2013), including a correction for lensing probability as a function of redshift from that work. Right: The distribution of ALESS SMGs as a function of time. The distribution is well fit by a Gaussian centred at 11.10 ± 0.05 Gyr (equivalent to z = 2.6 ± 0.1), with a width of 1.07 ± 0.05 Gyr.

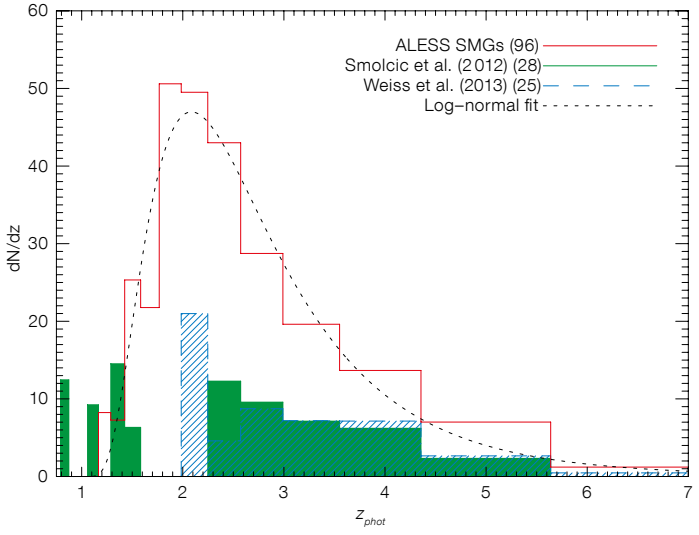

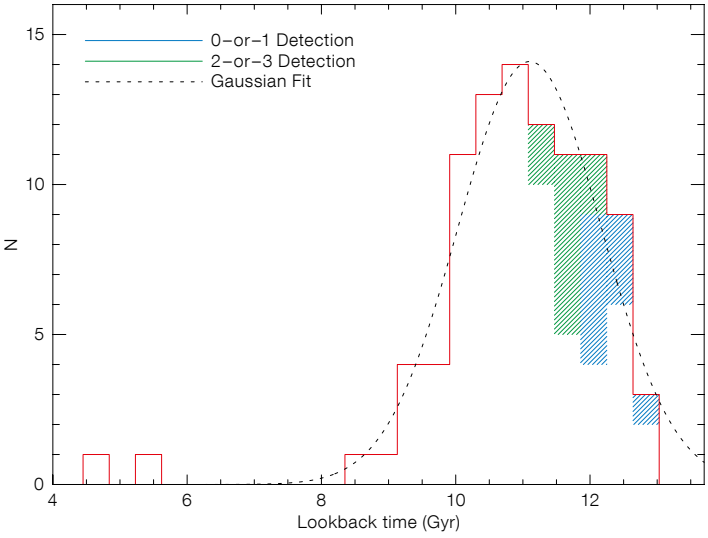

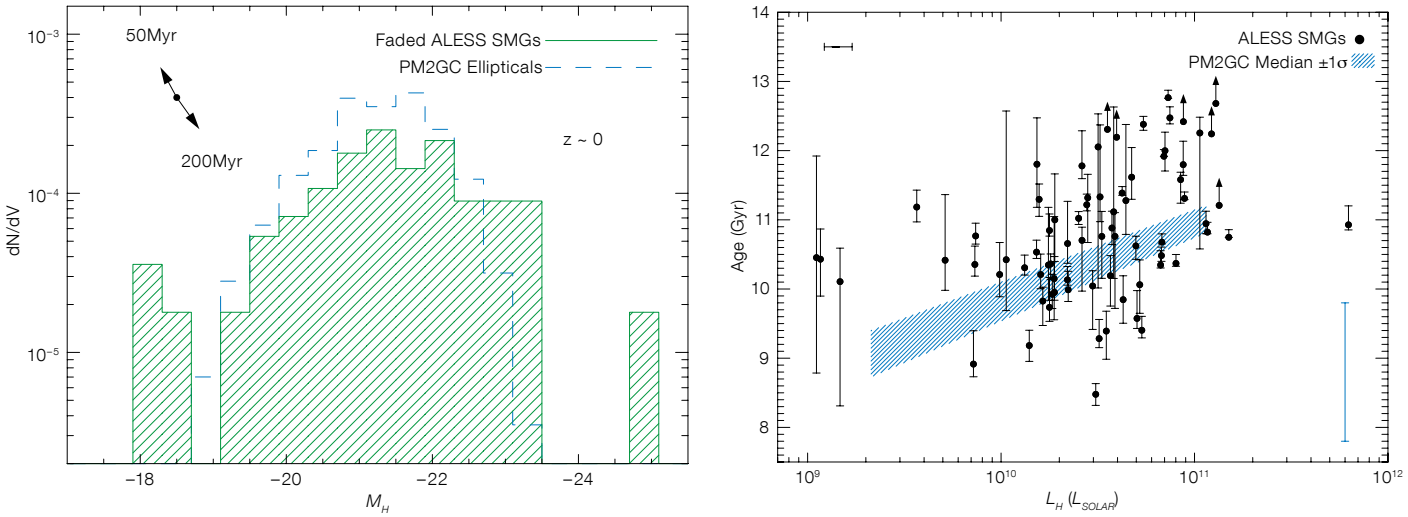

Figure 7. Left: The predicted $z \sim 0$ absolute H-band magnitudes of ALESS SMGs from Simpson et al. (2014), assuming a simple star formation history with a 100 Myr duration burst. The vectors indicate the effect of adopting either a 50 Myr or 200 Myr burst. Right: A comparison of the mass-weighted ages of local elliptical galaxies to the lookback age of the ALESS SMGs (from Simpson et al., 2014). The error bar (bottom right) shows the error in the mass-weighted age from the spectrophotometric modelling.

present-day descendants. Figure 7 (left) compares the faded restframe H-band luminosities of the SMGs (assuming a 100-Myr burst duration) to that of a volume-limited sample of morphologically classified elliptical galaxies at $z \sim 0$ from the Padova Millenium 2 Galaxy and Group Catalogue (PM2GC; Calvi et al., 2013). Simpson et al. found good agreement between the faded SMGs and local ellipticals, in terms of both typical luminosities and space densities. Moreover, by comparing the mass-weighted ages of the $z \sim 0$ ellipticals to the lookback times of the ALESS SMGs, they also found broad agreement in the expected ages (shown in Figure 7, right). Despite the large systematic uncertainty, Simpson et al. were able to conclude that the local ellipticals have ages which are in broad agreement with the ALESS SMGs, consistent with a simple evolutionary model where SMGs are the progenitors of local, giant elliptical galaxies.

Summary

Even during Early Science operations, ALMA has demonstrated its world-leading capabilities for advancing our knowledge of dust-obscured activity in the distant Universe.

The ALESS survey has yielded the first statistically reliable sample of SMGs with robust identifications. The properties of these galaxies are documented in: Hodge et al. (2013), catalogue paper; Karim et al. (2013), number counts; Swinbank et al. (2012), serendipitous [C II] emitters; Wang et al. (2013), X-ray properties; Swinbank et al. (2014), far-infrared properties; Simpson et al. (2014), photometric redshift analysis; Thomson et al. (2014), radio spectral properties; and Decarli et al. (2014), submillimetre stacking of less active populations.

Forthcoming papers will discuss the Hubble Space Telescope morphologies of ALESS SMGs (Chen et al., 2014), an SED analysis using the MAGPHYS code (da Cunha et al.,2014) and the spectroscopic survey of the ALESS SMGs (Danielson et al., in prep.).

More information about the survey, including the full list of ALESS co-investigators, is available[1].

Acknowledgements

Based on data obtained under ESO APEX programmes 078.F-9028(A), 079.F-9500(A), 080.A-3023(A), 081.F-9500(A) and ALMA programme #2011.1.00294.S.

Ian Smail acknowledges support from STFC (ST/L00075X/1), the ERC Advanced Investigator programme DUSTYGAL 321334 and a Royal Society/Wolfson Merit Award. Fabian Walter acknowledges support from the ERC Starting Grant "Cosmic Dawn".

References

Biggs, A. J. et al. 2011, MNRAS, 413, 2314
Calvi, R. et al. 2013, MNRAS, 432, 3141
Chapman, S. C. et al. 2005, ApJ, 622, 772
Chen, C. C. et al. 2014, ApJ, submitted
Coppin, K. E. K. et al. 2009, MNRAS, 395, 1905
da Cunha, E. et al. 2014, ApJ, submitted
Decarli, R. et al. 2014, ApJ, 780, 115
Greve, T. R. et al. 2009, ApJ, 719, 483
Hickox, R. C. et al. 2012, MNRAS, 421, 284
Hodge, J. A. et al. 2013, ApJ, 768, 91
Ivison, R. J. et al. 2002, MNRAS, 337, 1
Ivison, R. J. et al. 2010, MNRAS, 402, 245
Karim, A. et al. 2013, MNRAS, 432, 2
Lee, N. et al. 2013, ApJ, 778, 131
Lutz, D. et al. 2010, ApJ, 712, 1287
Magnelli, B. et al. 2011, A&A, 539, 155
Simpson, J. M. et al. 2014, ApJ, 788, 125
Smolcic, V. et al. 2012, A&A, 548, A4
Swinbank, A. M. et al. 2012, MNRAS, 427, 1066
Swinbank, A. M. et al. 2014, MNRAS, 438, 1267
Thomson, A. P. et al. 2014, MNRAS, in press, arXiv:1404.7128
Walter, F. et al. 2012, Nature, 486, 233
Wang, S. X. et al. 2013, ApJ, 778, 179
Wardlow, J. L. et al. 2011, MNRAS, 415, 1479
Weiß, A. et al. 2009, ApJ, 707, 1201
Weiß, A. et al. 2013, ApJ, 767, 88

Links

[1] ALESS web page: http://www.astro.dur.ac.uk/~irs/LESS

The Deepest VLT/FORS2 Spectrum of a $z \sim 7$ Galaxy: An Easy Target for the E-ELT

Eros Vanzella[1]
Adriano Fontana[2]
Laura Pentericci[2]
Marco Castellano[2]
Andrea Grazian[2]
Mauro Giavalisco[3]
Mario Nonino[4]
Stefano Cristiani[4]
Gianni Zamorani[1]
Cristian Vignali[5]

[1] INAF-Osservatorio Astronomico di Bologna, Italy
[2] INAF-Osservatorio Astronomico di Roma, Monteporzio, Italy
[3] Department of Astronomy, University of Massachusetts, Amherst, USA
[4] INAF-Osservatorio Astronomico di Trieste, Italy
[5] Dipartimento di Fisica e Astronomia, Università degli Studi di Bologna, Italy

GDS_1408, a relatively bright (F125W ~ 26 mag), solid $z \sim 7$ galaxy candidate in the Hubble Ultra Deep Field, has been the target of 52 hours of spectroscopic observations with FORS2 at the VLT. This is the deepest spectrum ever obtained for a galaxy at the epoch of reionisation. Neither emission lines nor a continuum were detected up to 10 100 Å, to a limiting equivalent width of 9 Å; a redshift of 6.82 ± 0.1 is determined, combining the superb HST photometry and the deep FORS2 spectrum. This increased redshift accuracy makes ALMA an interesting option for the confirmation of the redshift. The non-detection of Lyman-α in even the best $z \sim 7$ candidate demonstrates the limitations of the current generation of 8–10-metre-class telescopes for these spectroscopic confirmations; future facilities such as JWST and the E-ELT will be necessary to make decisive progress.

The deep panchromatic surveys of the distant Universe with the Hubble Space Telescope (HST), such as the Great Observatories Origins Deep Survey (GOODS), Cosmic Assembly Near-infrared Deep Extragalactic Legacy Survey (CANDELS) and the Hubble Ultra Deep Field (HUDF), have enabled immense progress in identifying candidates for the first galaxies. The redshifts of these targets have been established by photometric redshifts, relying on the cut-off at the Lyman-α break, but spectroscopic confirmation of these redshifts is very challenging. The Lyman-α line is the most prominent emission feature in the optical/near-infrared region (e.g., Vanzella et al., 2011) and is thus seen as a standard for reliable redshift confirmation. Despite immense efforts, only a few objects are spectroscopically confirmed and some of the faint line detections have been proved doubtful when subjected to deeper observations or more elaborate reduction.

However whilst Lyman-α emission is expected in young galaxies, it is a resonant atomic transition which is very sensitive to conditions within the host galaxy, such as the presence of dust and neutral hydrogen, but also to the damping effect of intergalactic neutral H, and particularly the increased neutral H fraction at the end of the reionisation epoch (Miralda-Escudé et al., 2000; Pentericci et al., 2014). For example, Finkelstein et al. (2013) found only one galaxy at $z = 7.51$ out of 43 candidates at $z > 6.5$ with the Keck/MOSFIRE spectrometer and similarly Schenker et al. (2014) found only one possible Lyman-α line at $z = 7.62$ in the their sample of 19 $z \sim 8$ candidates. In addition to the observational difficulties in detecting a faint line in a part of the spectrum strongly affected by spatially and spectrally varying atmospheric transmission, it may be that the emitted Lyman-α is intrinsically weak. Clearly, all these explanations assume that the efficiency of the colour selection based on the Lyman-α break remains extremely high at $z \geq 7$, i.e., that most of current $z \geq 7$ candidates are indeed at their estimated redshifts.

The source HUDF-J033242.56-274656.6 in the HUDF is the brightest (HST F125W = 26.1 ± 0.02 mag) $z \sim 7$ photometric candidate galaxy in this well-studied region. Figure 1 shows the galaxy as it appears in the HST deep optical and near-infrared imaging (HUDF12). The high-redshift nature ($z > 6.5$) is guaranteed by the large observed break between the ultradeep optical and near-infrared bands (Δmag ~ 4 mag) and the well-determined flat behaviour of the spectral energy distribution (SED) in the near-infrared bands, detected with high signal-to-noise ratio (S/N ~ 20–50 with HST's Wide Field Camera 3 [HST-WFC3]). It has been repeatedly selected as a high-redshift candidate from the earliest Near Infrared Camera and Multi-Object Spectrometer (NICMOS) data to the current ultradeep HUDF data over the past ten years (Vanzella et al. [2014a] and references therein), including extensive Very Large Telescope (VLT) spectroscopy with the Focal Reducer/low dispersion Spectrograph (FORS). All these spectra have now been collected and assessed, combining them into an ultradeep spectrum and compared with multi-band photometry (Guo et al., 2013) to derive new insights into the nature of this pivotal target.

FORS2 observations

HUDF-J033242.56-274656.6 galaxy (G2_1408 in Castellano et al. [2010]) has been observed in four different FORS programmes over the period 2009–2012 and data were combined for 084.A0951(A) (Principal Investigator [PI]: A. Fontana), 086.A-0968(A) – 088.A-1013(A) (PI: A. Bunker) and 088.A-1008(A) (PI: R. Bouwens) with exposure times of 18 (Fontana, F18), 27 (Bunker, B27) and 7 (Bouwens, B7) hours on target, for a total usable exposure time of 52 hours. The F18 data were presented in Fontana et al. (2010) who reported a tentative detection of a Lyman-α line at $z = 6.972$. The B27 programme has also been presented in Caruana et al. (2014). Full details of the observations and reduction of the combined observations are given in Vanzella et al. (2014a). The three individual spectra (F18, B27 and B7) and the 52-hour combined one are shown in Figure 2 as S/N images. The combined spectrum is the deepest one of a galaxy at $z \sim 7$ to date.

No Lyman-α emission detected

The available photometry of GDS_1408 already constrains the redshift to be $6.5 < z < 7.0$, thus Lyman-α should occur between observed wavelengths of 9120 and 9730 Å, where FORS2 is an efficient instrument for its detection. Reliable upper limits on the redshift are provided by the clear detections in the z850 band ($z < 7.3$) and the narrowband filter, NB973 ($z < 7$). The FORS2 600z grism

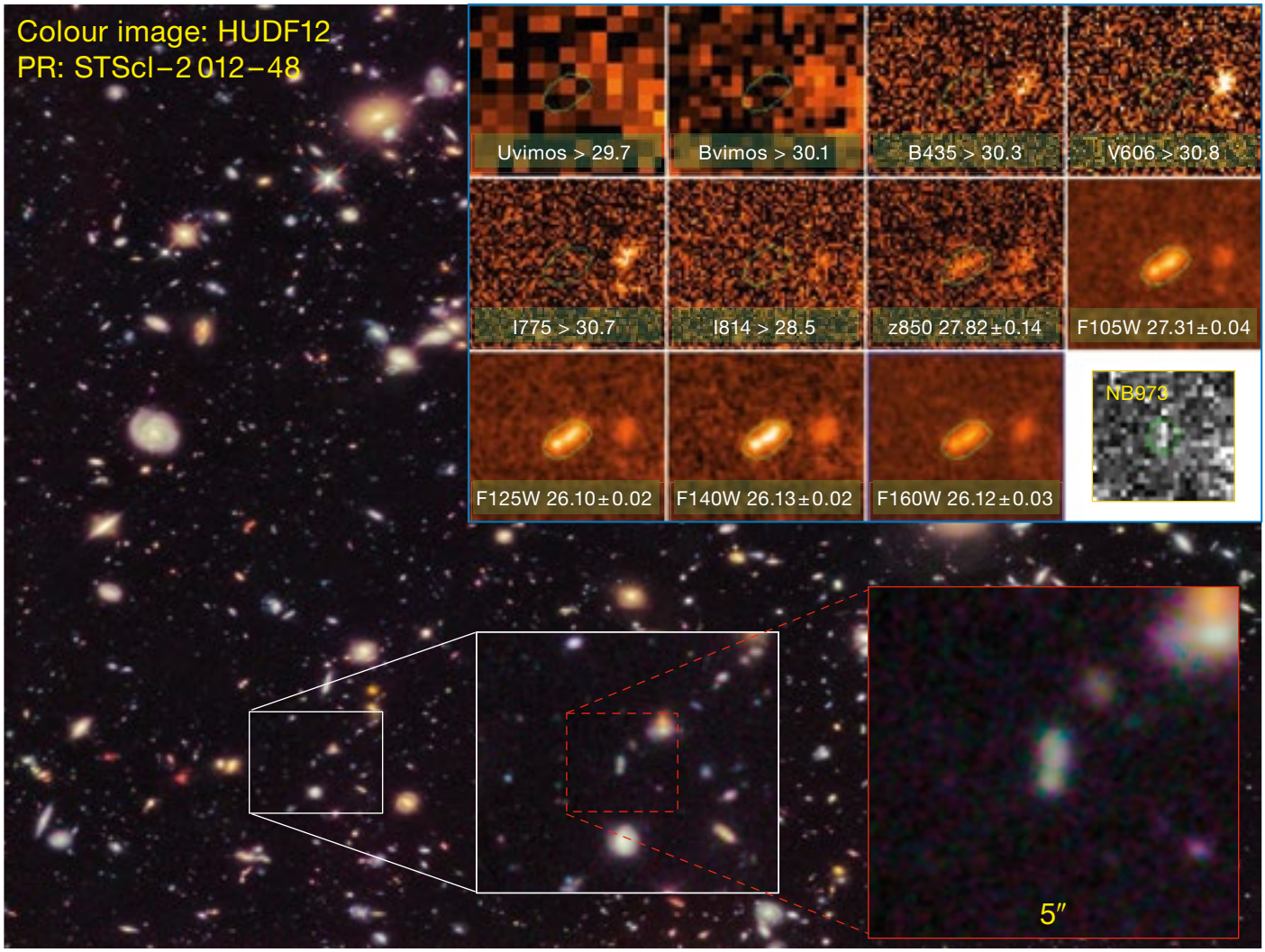

configuration provides a safe constraint on the Lyman-α line flux over the expected range of observed wavelengths. Figure 2 shows that there are no obvious spectral features in the three S/N spectra (F18, B27 and B7) at the position of GDS_1408 (marked by arrows) over the expected wavelength range, indicated by the horizontal dotted line. Most crucially, their combination, shown at the top of Figure 2 shows no emission feature within the expected range, nor a detectable continuum.

The statistical significance of the 52-hour Lyman-α non-detection was estimated by simulations and an upper limit to the Lyman-α flux of 3×10^{-18} erg cm^{-2} s^{-1} at 3–9σ (depending on the exact wavelength position) and its equivalent width (EW) of < 9 Å was determined (see Vanzella et al. [2014a] for details). This represents the faintest limit on the Lyman-α flux ever derived at $z > 6.5$ at such a signal to noise limit.

The depth and photometric quality of data available for this galaxy, and the upper limits derived on the Lyman-α flux and EW, enable the redshift value to be refined by fitting the spectral energy distribution (SED) with young galaxy template spectra and including different equivalent widths for Lyman-α (0–200 Å restframe), focussing on the break between the optical and near-infrared bands. Once the Lyman-α constraints from the spectrum non-detection are included, the redshift of GDS_1408 is constrained between 6.7 and 6.95 at 1σ and 6.6 and 7.1 at 2σ, and produces a refined photometric redshift of 6.82, that is also supported by the broadband

Figure 1. Montage of images of the Hubble Ultra Deep Field focussing on GDS_1408. The background image is from the HST HUDF12 release of Wide Field Camera 3 (WFC3) near-infrared imaging (from STScI Release 2012-48), with enlarged views of GDS_1408 at the bottom. The upper right array of multi-band images (each 3 by 3 arcseconds) shows the appearance of GDS_1408, marked with a green colour, from *U*-band to *H*-band: VIMOS images in *U* and *B*; ACS images in *B*, *V*, *i*, *I* and *z*; WFC3 images in near-infrared bands (filters F105W, F125W [*J*-band], F140W and F160W [*H*-band]); and the detection in the narrowband filter at 973 nm. See Vanzella et al. (2014) for details.

Spitzer Infrared Array Camera [IRAC] fluxes (Smit et al. in preparation). The SED fitting has been performed including the full treatment of the nebular emission (both in lines and continuum) and the estimate of the stellar mass is $5^{+3}_{-2} \times 10^9\ M_\odot$, with a dust attenuation E(B - V) ~ 0.1 mag and a dust-corrected star formation rate of $21^{+20}_{-10}\ M_\odot$ yr^{-1} (Vanzella et al. 2014a).

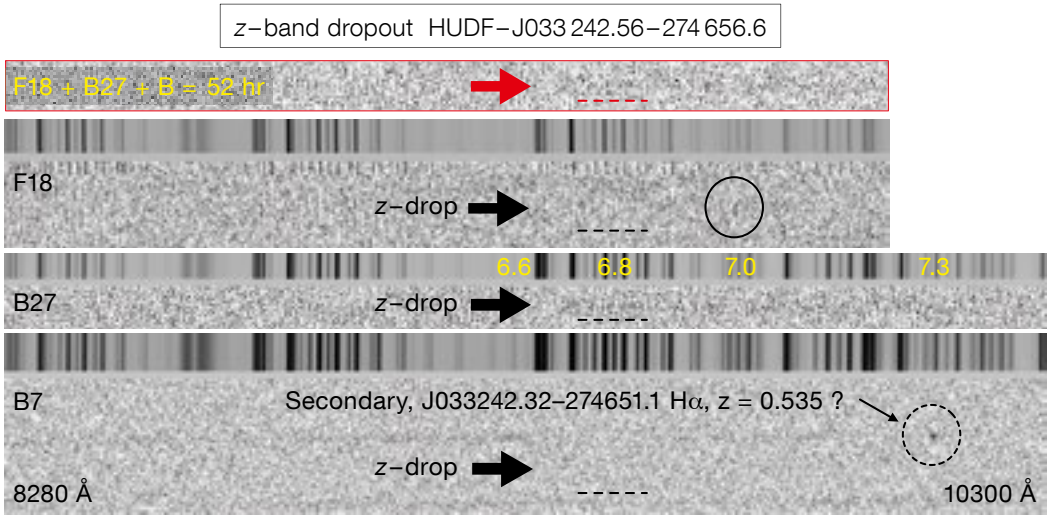

Figure 2. Two-dimensional signal-to-noise spectra and sky spectra of the stacked 52-hour spectrum of the *z*-band dropout GDS_1408 are shown, with the individual spectra of F18, B27 and B7. The expected position of the Lyman-α continuum break is marked with dotted horizontal lines (see text). In the B27 spectrum the redshift values are reported above the sky as a reference. In the F18 spectrum the dotted circle marks the feature discussed in Fontana et al. (2010). The B7 spectrum shows also the Hα emission from the secondary object J033242.32-274651.1 at $z = 0.535$, useful here as an example of FORS+600z sensitivity beyond 1 μm. From Vanzella et al. (2014b).

Why no Lyman-α is detected

The combination of excellent photometry and ultradeep spectroscopy point to the conclusion that the extreme weakness of the Ly-α emission is a real feature of GDS_1408. Both the transport of photons out of the galaxy's interstellar medium and the further damping by the intergalactic medium (IGM) can produce a low-surface-brightness Lyman-α glow around galaxies. The escape of Lyman-α photons from a galaxy is a complex process depending on many factors, such as dust and neutral gas, metallicity, gas geometry, etc. (Verhamme et al., 2006). The escaping Lyman-α can be much smaller than the intrinsic Lyman-α luminosity expected from a star formation rate of $\sim 20\ M_{\odot}\ \mathrm{yr}^{-1}$. The neutral H in the IGM will further dampen the Lyman-α emission through scattering. Based on star formation models, an intrinsic flux of the Lyman-α can be derived, implying an upper limit for the effective escape fraction of < 8 % for GDS_1408.

GDS_1408 is one of the more extended sources among the $z \sim 7$ candidates, with a half-light radius of 0.26 arcseconds, i.e., 1.4 proper kpc (Grazian et al., 2011), and an elongated morphology of 4.8 × 2.5 proper kpc (see Figure 1). It has been shown that the Lyman-α equivalent width and the size observed at 1500 Å in the restframe stellar continuum anti-correlate, such that on average the emitters appear more compact and nucleated than the non-emitters with mean half-light radius of 1 kpc (Law et al., 2007; Vanzella et al., 2009).

Future prospects

The ultradeep FORS2 spectrum demonstrates the current limits of 8–10-metre-class telescopes in the spectroscopic characterisation and redshift measurement of weak Lyman-α emitters at $6.6 < z < 7.3$ with 50 hours of on-target exposure. If $z \sim 7$ is a critical value above which the visibility of Lyman-α lines decreases drastically, then future facilities are necessary to record the spectrum of the ultraviolet (UV) continuum-break and the UV absorption lines and/or optical nebular emission lines from galaxies at $7 < z < 10$. The James Webb Space Telescope near-infrared spectrometer (JWST-NIRSPEC) will probe the optical nebular lines ([O II], [O III], [N II] and Balmer series) and the extremely large telescopes (ELT, 30–40-metre diameter) will allow the detection of UV continuum, and absorption lines, down to $J \sim 27$ mag and the restframe near-infrared emission can be studied by mid-infrared (8–14 μm) instruments, such as the mid-infrared imager-spectrograph (METIS) on the European Extremely Large Telescope (E-ELT).

Before the advent of these facilities, access to $z > 6$ non-Lyman-α emitters like GDS_1408 or very faint sources (more than ten times fainter than GDS_1408) is feasible only in tiny regions of the sky by relying on the strong gravitational lensing effect provided by galaxy clusters.

Spectroscopic observations of feeble galaxies with an intrinsic ultraviolet magnitude as faint as m (1500 Å) ~ 29 have confirmed their ages within the first Gyr after the Big Bang, as recently reported in, e.g., Vanzella et al. (2014b).

Another promising facility that could determine the spectroscopic redshift of GDS_1408, and higher redshift and fainter analogues, is the Atacama Large Millimeter/submillimeter Array (ALMA; e.g., Inoue et al., 2014). The range of probable redshifts for GDS_1408 could be probed by the [C II] 158 μm line, which is observed by ALMA in high-redshift starburst galaxies (e.g., de Breuck et al., 2014). At $z > 6.5$ the rotational transitions of CO J = 7-6 and J = 6-5 are also observable with ALMA.

References

de Breuck, C. et al. 2014, The Messenger, 156, 38
Caruana, J. et al. 2014, MNRAS, in press, arXiv/1311.0057
Castellano, M. et al. 2010, A&A, 511, 20
Fontana, A. et al. 2010, ApJ, 725, L205
Finkelstein, S. L. et al. 2013, Nature, 502, 524
Grazian, A. et al. 2011, A&A, 532, 33G
Guo, Y. et al. 2013, ApJ, 207, 24
Inoue, A. et al. 2014, ApJ, 780, 18
Law, D. R. et al. 2007, ApJ, 656, 1
Miralda-Escudé, J., Haehnelt, M. & Rees, M. J. 2000, ApJ, 530, 1
Pentericci, L. et al. 2014, arXiv:1403.5466
Schenker, M. A. et al. 2014, arXiv:1404.4632
Vanzella, E. et al. 2009, ApJ, 695, 1163
Vanzella, E. et al. 2011, ApJ, 730, 35
Vanzella, E. et al. 2014a, ApJ, 783, 12
Vanzella, E. et al. 2014b, A&A, in press
Verhamme, A. et al. 2008, A&A, 491, 89

ESO/S. R. Aguila

Aerial view of the progress of construction of the road, platform, and service trench at Cerro Armazones, site of the future European Extremely Large Telescope (E-ELT). This image was taken a week before the groundbreaking ceremony (see article on p.2).

Aerial photograph of the now-completed and occupied extension building to ESO Headquarters in Garching. See Picture of the Week 7 July 2014 for more details.

E. Graf (graf-flugplatz.de)/ESO

Report on the Workshop

Herbig Ae/Be Stars: The Missing Link in Star Formation

held at ESO Vitacura, Santiago, Chile, 7–11 April 2014

Willem-Jan de Wit[1]
Rene D. Oudmaijer[2]
Mario E. van den Ancker[1]
Nuria Calvet[3]

[1] ESO
[2] School of Physics & Astronomy, University of Leeds, UK
[3] Department of Astronomy, University of Michigan, USA

The workshop highlighted the many recent advances within the field of Herbig Ae/Be stars and the close links to star and planet formation. Topics such as magnetospheric accretion and the evolution of dust in discs, the structure of circumstellar discs and the role of walls and gaps and their links to planet formation from many observational aspects were covered. The workshop was dedicated to the life and works of George H. Herbig, who sadly passed away at the end of last year.

Introduction

One of the main open questions in star formation concerns the distinct mechanisms by which low- and high-mass stars form. While it is well established that low-mass stars grow in mass by magnetically controlled accretion, the non-magnetic, high-mass stars must grow by another mechanism, as yet unclear. In some critical mass interval, the growth mechanism changes, corresponding to the masses of A- and B-type stars.

Ever since the identification of the Herbig Ae/Be stars (HAeBes; Herbig, 1960) as a class of early-type pre-main sequence objects (Strom et al., 1972), these stars have taken centre-stage in star and planet formation studies. They have masses which place them in the transitional regime between Solar-type stars and high-mass stars. In detail, the change in star formation character between the high- and low-mass stars is the dichotomy between clustered and isolated formation, between boundary layer accretion and magnetospheric accretion, radiative and convective stellar interiors and between fast and slow rotation. Moreover, the discs around Herbig stars are in general brighter than around their low-mass counterparts, the T-Tauri stars. Therefore HAeBes are prime laboratories in which to study the evolution from actively accreting discs towards debris discs and mature planetary systems.

Importantly, the relative proximity of HAeBes in local young star-forming regions allows a detailed view of their evolving environment. As such, they are pivotal for understanding both the formation of stars and of planets. Nonetheless, the last large meeting purely dedicated to Herbig Ae/Be stars took place some 20 years ago and a review on the state of this particular field was overdue. With this scientific motivation in place, and guided by ESO's innovative edge in infrared instrumentation, our proposal to organise an ESO Workshop on Herbig Ae/Be stars was approved. Shortly after approval, the sorrowful news arrived that the founding father of this field, George Herbig, had passed away at the age of 93. George Herbig pioneered the field of star formation, and especially that of young stars and their nebulous surroundings. His legacy includes the identification and first description of Herbig Ae/Be stars. In consultation with the director of his home institute in Hawaii, it was decided to dedicate the ESO Workshop to the life and works of George H. Herbig.

The workshop took place at the ESO/ALMA Vitacura campus with close to one hundred registered participants (see Figure 1). In the spotlight were the results obtained with instruments like the CRyogenic high-resolution InfraRed Echelle Spectrograph (CRIRES) and X-shooter, and the Very Large Telescope Interferometer (VLTI) spatial imaging capabilities with the MID-infrared Interferometric instrument (MIDI), the Astronomical Multi-BEam combineR (AMBER) and the Precision Integrated Optics Near-infrared. Imaging ExpeRiment (PIONIER). These, and other, instruments have for the first time opened up the milliarcsecond and sub-milliarcsecond spatial scales where the crucial accretion disc physics takes place and planet formation processes occur. In addition, space-based advances by means of the Infrared Space Observatory (ISO), the Spitzer and Herschel satellites have allowed the study of the dust and gas in protoplanetary discs at high sensitivities. The first Atacama Large Millimeter/submillimeter Array (ALMA) observations have recently revealed the ongoing planet formation process in HAeBe discs.

Figure 1. The conference participants in the garden at ESO Vitacura.

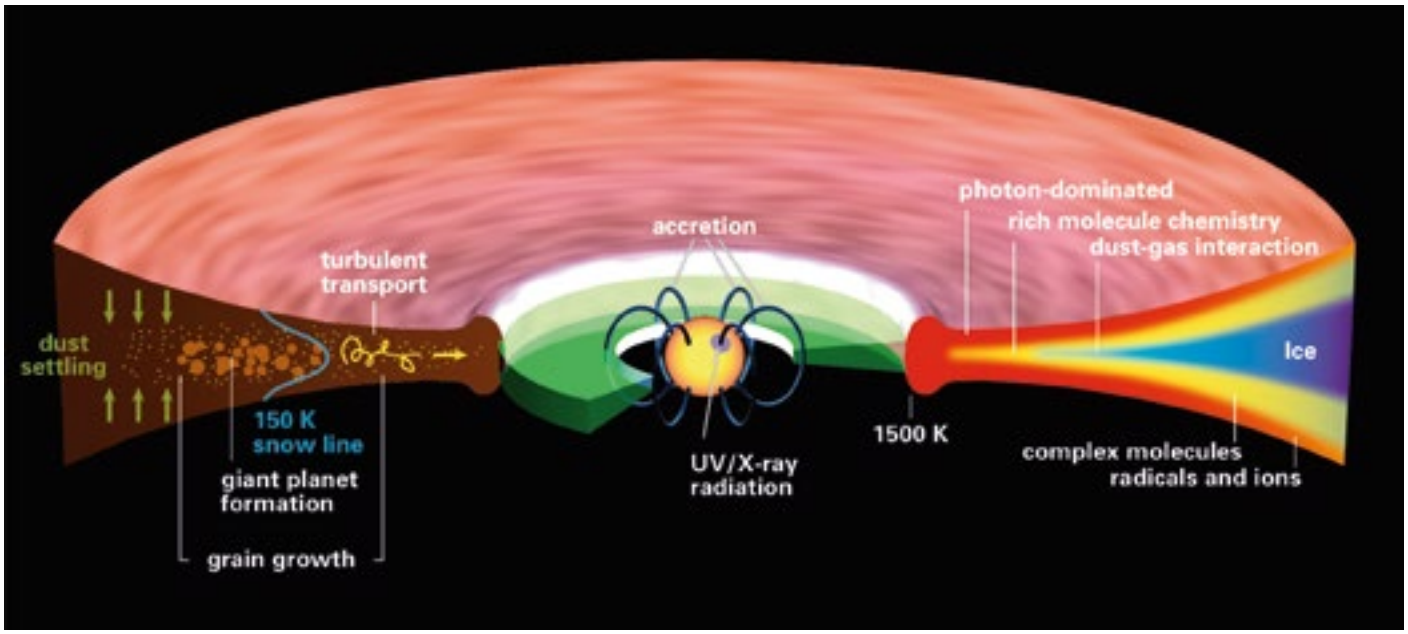

Figure 2. Sketch of the physical and chemical structure of a protoplanetary disc undergoing magnetospheric accretion. From Henning & Semenov (2013).

The scientific programme (available on the workshop webpage[1]) recorded many breakthroughs in the field, established milestones and starting points, and opened new avenues to pushing our understanding of star and planet formation to higher levels. The programme was arranged in sessions according to the physical process, roughly corresponding to increasing length-scale domains. The highest angular resolution traces the inner disc, i.e., the location in the circumstellar environment where there is a strong interaction between the disc material and the star. Longer wavelengths, and lower spatial resolution, preferentially trace the outer parts of the disc, where grain growth, and viscous accretion takes place and giant planets form. In this summary we will reflect on some of the highlights presented at the meeting and work our way from the smallest scales, close to the star, to the physics at larger radii of the HAeBe disc.

Mass accretion at the inner disc

The leading model for accretion onto A- and B-type pre-main sequence stars is magnetospheric accretion. The adoption of this model is partially justified on the grounds that, during the earliest phase of the star formation process, the properties of the intermediate-mass protostars are found to be similar to those of low-mass protostars (contributions by Maite Beltran, Yuefang Wu, Fernando Comerón). In this model, material is guided onto the star via magnetic field lines stretching from the inner disc to one or more regions on the stellar surface. The hot, shocked surface regions generate excess continuum and line emission on top of the star's photospheric spectrum. In this model, the observed excess enables the rate of mass accretion onto the star to be derived. The mass accretion rate is a key physical quantity in star formation as it determines both the timescale and efficiency for star growth, and can be used as a discriminator between different formation models. Figure 2 shows a schematic of a protoplanetary disc.

In a systematic X-shooter study of a large number of systems, the relation between excess emission, line luminosities and mass accretion was investigated across a wide mass range of young objects: from brown dwarfs to classical T-Tauri stars to Herbig Ae stars (talk by Ignacio Mendigutía). Although the magnetospheric accretion model works well for Herbig Ae stars, it is not able to explain the strong observed ultraviolet (UV) excesses in early B-type stars (talk by John Fairlamb). Further support for the magnetospheric accretion model comes from other observed similarities between Herbig Ae stars and classical T-Tauri stars, such as linear polarisation measurements in spectral lines (talk by Jorick Vink), the geometry of the rotating disc and the location of the inner disc radius. Finally, the hydrogen line profiles are also consistent with what is expected for magnetospheric accretion (contributions by Sean Brittain, Alicia Aarnio, Ricardo Ramírez, Monika Petr-Gotzens and Mario van den Ancker).

Despite the success of extending the formation scenario of low-mass stars into the intermediate-mass regime, some fundamental problems are lurking around the corner. One serious problem came to the fore during the meeting. The systematic searches for stellar magnetic fields demonstrate the presence of weak or non-existent magnetic fields in all but a small fraction (~ 6 %) of the HAeBes. For reference, a kiloGauss magnetic field is required in order for the magnetospheric accretion model to work (review talk by Evelyne Alécian). Possibly connected to

the dearth of strong magnetic fields, the closely connected phenomenon of jet formation in Herbig Ae/Be stars appears to be rare (although selection effects cannot yet be excluded). Nonetheless when they are found, their properties are found to be similar to those in low-mass young stars (talk by Catherine Dougados). Soft X-rays emanate from these jets (Christian Schneider) and they can produce (soft) cosmic rays (talk by Tom Ray).

This situation is markedly different for the T-Tauri stars, in which the observed strong fields generated in the outer convective layers are capable of supporting magnetospheric accretion (talk by Gaitee Hussain) and where jet action has a very high incidence. Looking for alternatives to explain the strong UV excess, options were explored in which the excess comes from the gas in the inner disc. However, in the models presented at the meeting, the temperature of this gas seems to be too low to explain the observations (contributions by Stefan Kraus, Catherine Dougados and John Ilee). On the observational side, a hot inner disc seems to be detected in some systems and the CO emission may be explained by UV fluorescence (Sean Brittain, Giuseppe Lodato).

Dust walls and gaps

Cross-fertilisation between long-baseline interferometry and stellar astrophysics has been especially successful for the field of study of the Herbig stars. Probing the bright emission by warm and hot dust particles for nearby stars, milliarcsecond imaging reveals that the HAeBe disc displays a near vertical inner dust wall directly irradiated by the central star. This discovery solved one of the long-standing open questions regarding the hot thermal dust emission in Herbig stars. The dust in the wall is at the sublimation temperature and the observed relation between the star’s luminosity and the distance between star and inner dust wall is consistent with this finding (review by Stefan Kraus).

Recent advances in infrared interferometric instrumentation, like PIONIER, now allow for efficient synthesis imaging at milliarcsecond resolution of the inner dust disc and also provide evidence for a puffed-up inner rim (talks by Jacques Kluska and Wing-Fai Thi). Related to the warm dust component, located further downstream from the inner dust wall, an extensive MIDI dataset provides evidence for flaring and gaps in discs; together with information from the spectral energy distribution, it shows that many discs have asymmetries (talks by Jonathan Menu and Narges Jamialahmadi). In a new development, interferometric data at a range of wavelengths is now combined to probe different regions of the disc. Near-infrared, mid-infrared and millimetre-wave interferometry probe different disc radii, and a variety of spectral tracers are used to characterise both the surface layers and the interior of the disc with the aim of achieving a global, yet detailed, understanding of the disc.

Notable progress was presented regarding the observational diagnostics of the presence of dust-depleted gaps in the radial density distribution of certain discs (the known as transitional discs), a relatively new discipline with repercussions for planet formation. The shape of the spectral energy distribution (displaying an absence of dust within a certain temperature interval) and the absence of the 10 μm silicate feature was addressed in a number of contributions. It appears that all sources with discs, which are strongly flared, also have dust gaps. Nonetheless, some material is still present within these gaps. For example, the infrared spectrum of polycyclic aromatic hydrocarbons (PAHs) may be a good tracer for the material in these gaps. Ionised PAHs appear to be present in low density, optically thin gas flowing through the gap, whereas the PAHs are neutral in the optically thick disc (talks by Carol Grady, Koen Maaskant).

Versatile carbon monoxide

Valuable information on the inner disc (≤ 10 au) can be retrieved by high spectral resolution, in particular in the near- and mid-infrared using the CO to trace the physics. In this way the disc is probed in a region where planet formation is suspected to occur. Observations with CRIRES show that some transitional discs (e.g., around HD 100546) seem to have gaps (≥ 10 au) devoid of CO, which may indicate a disc gap both devoid of gas and dust. Yet, for other HAeBes, the width of the observed CO line profiles seems consistent with formation within ~ 2 au, as in HD 163296, HD 250550 and Hen 2-80 (talks by Sean Brittain, Gerrit van der Plas and Rosina Hein Bertelsen). The CO observations are extremely fertile and versatile and may even provide hints of circumplanetary discs around accreting planets located within the gaps (invited talk by Sean Brittain). What is currently lacking is a systematic CO survey for sources with discs in different evolutionary phases, i.e., primordial, pre-transitional and transitional.

At longer wavelengths, probing the cooler parts of the disc, CO continues to make its mark. Observations with the Photodetector Array Camera & Spectrometer (PACS) and Spectral and Photometric Imaging Receiver (SPIRE) on Herschel have detected the entire CO ladder in many flared gaseous discs and several non-flared systems (talks by Matthijs van der Wiel, Gwendolyn Meeus and Peter Woitke). Detailed modelling demonstrates that the disc scale height at a radius of 100 au needs to be higher for the gas than the dust in order to explain the observed weak CO line emission (talks by Vincent Piétu and Carol Grady). However, it remains difficult to simultaneously explain the bright [O I] emission detected by Herschel (talks by Peter Woitke and Christophe Pinte). Other gas diagnostics which were explored at the meeting include OH, warm H_2O and H_2 (talk by Davide Fedele). NASA’s Stratospheric Observatory for Infrared Astronomy (SOFIA) may add to this inventory of detected lines in the near future (talk by Hans Zinnecker).

Intriguing disc structures from direct imaging

What is revealed indirectly by spectroscopy of the accretion and planet formation processes has found a resounding confirmation arising from advances in direct imaging techniques. Polarimetric differential imaging (PDI), as pioneered by the Strategic Explorations of Exoplanets and discs with Subaru (SEEDS) survey on the Subaru telescope, and systematic

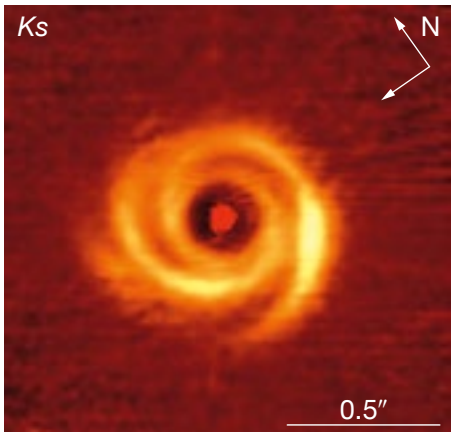

Figure 3. Polarised light emission in *Ks*-band from the disc around the Herbig star HD 135344B. These NACO polarisation differential image data clearly resolve a double spiral arm structure and an inner cavity around the central star (from Garufi et al., 2013).

work done with the NACO camera have shown direct evidence for the existence of gaps, spiral arms and asymmetries in many discs around HAeBes (review talks by Carol Grady and Sascha Quanz; see Figure 3 for an example). Indeed, the diversity in disc substructure, perhaps typified as somewhat overwhelming, was considered as one the milestones presented at the meeting.

The leading contender for the creation of these intriguing disc substructures is ongoing planet formation within the disc. Impressive ALMA Cycle 0 results were presented providing further evidence for disc substructures and ongoing planet formation (talks by François Ménard, Sebastián Pérez, Simon Casassus and Valentin Christiaens). ALMA has also started to provide evidence for the existence of dust traps, caused by a radial pressure bump within the gas once a planet has grown sufficiently massive to open up a gap within the disc (talk by Nienke van der Marel). Transitional discs may be the observational signature of the existence of such dust traps.

The dust in a primordial circumstellar disc which evolves to a planetary system would pass through the following four evolutionary steps: (1) the generation of a dust depletion gap; (2) removal of the millimetre-sized dust; (3) depletion of dust from the inner regions; and (4) concentration of the planetesimals in a ring. The order of these four steps is still unclear (review talk by Mark Wyatt). Infrared spectroscopic and spectro-interferometric studies of dust in these discs show clear differences between pristine and secondary dust and may be able to offer more insights into the order of this evolution (contributions by Thomas Henning, Roy van Boekel, Rodrigo Vieira). For debris discs around A-type stars, the evolutionary successors of the HAeBes like β Pic, the gas appears to be secondary, whereas in the 30-Myr-old system HD 21997 the gas must still be primordial (Mark Wyatt, Agnes Kóspál).

Although disc lifetimes are shorter for intermediate-mass stars than for low-mass stars, no mechanism has yet been identified to explain this mass dependence (contributions by Chikako Yasui, Massanobu Kunimoto). However, the role of binarity on stellar and disc evolution has so far been neglected. Searches for companions around Herbig Ae/Be stars show that single Herbig stars are rare: statistically speaking, for every star there is a companion at some separation (review by Gaspard Duchêne, contributions by Cesar Bricẽno, Gergely Csépány and Bernadette Rodgers). There also appears to be a dependence of metallicity on the accretion rate (Giacomo Beccari). Surveys for new Herbig Ae/Be and intermediate-mass T-Tauri stars are underway in the Magellanic Clouds and in Orion which may enable us to investigate these questions in more detail in the near future (contributions by Blesson Mathew, Jesús Hernández).

Outlook

The workshop in Vitacura highlighted the remarkable progress which has been achieved in the field of Herbig Ae/Be stars in recent years. Imaging at sub-arcsecond down to milliarcsecond scales has given us a new view on the nature of the discs around HAeBes. The sources with flared discs may all have cavities or gaps, and much structure is present in the outer discs. Dust traps may be a signpost of planet formation in these discs. However, so far we have mainly seen snapshots of individual systems. In the coming years, as statistically meaningful samples of Herbig stars will be observed with the new generation of instrumentation, it will be possible to link together the observed disc morphologies in a more systematic way.

An unsolved problem remains whether early Be stars are to be included within the class of Herbig Ae/Be stars. Whereas there is ample evidence that HAes and late-type HBes are indeed young stars in the process of forming planetary systems, the observational evidence for the early-type HBes is still absent. Future facilities, such as the next generation of extremely large telescopes, will offer large gains in spatial resolution which should enable us to tackle this problem for the more distant HBes as well.

The enigmatic issue which came to the fore at the workshop is what drives accretion in the HAeBes. The observed line profiles, spectral excesses and outflows show that HAeBes are accreting, but they appear to have only weak, multipolar magnetic fields. Observational progress in this area may come in the near future from large monitoring programmes on accretion within HAeBes, but further theoretical effort is needed to come up with plausible alternatives to the magnetospheric accretion model.

Acknowledgements

We would like to thank all conference participants, the members of the Scientific Organising Committee and the members of the Local Organising Committee for their contributions in making the Herbig Ae/Be workshop a resounding success. The Royal Astronomical Society is acknowledged for its financial support. Special thanks go out to amateur observatory Roan-Jasé for a fantastic conference dinner under a starry sky.

References

Garufi, A. et al. 2013, A&A, 560, 105
Henning, T. & Semenov, D. 2013, ChRv, 113, 9016
Herbig, G. H. 1960, ApJS, 4, 337
Strom, S. E. et al. 1972, ApJ, 173, 353

Links

[1] Workshop web page: http://www.eso.org/haebe2014.html

Hans-Emil Schuster Celebrates his 80th Birthday

Hans-Emil Schuster was one of the first staff members in Chile; he joined ESO in 1964 and retired in 1991. Hans-Emil was born in Hamburg, Germany and was a student of Otto Heckmann — the first Director General of ESO. He was actively involved in site testing for the ESO observatories of La Silla, and later Paranal, and became acting director of La Silla. He was an active observer, discovering 25 asteroids and two comets, 106P/Schuster and C/1976 D2. He also discovered the Eridanus halo globular cluster (GLC0423-21), with Richard West the Phoenix Dwarf irregular galaxy (ESO 245 -G007) and two planetary nebulae, as well as a supernova in the galaxy NGC 1255. In 2011 Hans-Emil was awarded the rank of Commander of the Order of Bernardo O'Higgins for his services to astronomy in Chile[1].

Hans-Emil Schuster wearing the Order of Bernardo O'Higgins.

Links

[1] Award of Order of Bernardo O'Higgins to Hans-Emil Schuster: http://www.eso.org/public/announcements/ann11075/

Fellows at ESO

Jason Grunhut

I never really considered pursuing a career in astronomy until I started applying for undergraduate programmes. Before that point, all I knew was that I had a passion for science, and that was the direction I was heading. I was certainly intrigued by space sciences, but this had more to do with science fiction than astronomy. In fact, it wasn't until the end of high school that I even settled on physics, in no small part because of a great teacher.

I grew up in Richmond Hill, a large town just north of Toronto, Ontario, in Canada, and attended the University of Toronto (UofT) for my undergraduate degree. It was pretty clear early in my studies that I enjoyed astronomy and wanted to turn this into a career, yet I had no idea what that meant.

Jason Grunhut

Like most students in the astronomy programme at UofT, we were all eager to study galaxies and cosmology. However, that all changed for me after I got my first taste of research. I had the opportunity to work as a research assistant with Charles Thomas Bolton, at the David Dunlap Observatory (DDO). Tom was interested in early-type, higher-mass stars, and, while stellar astronomy is not really perceived as a hot topic anymore, I was (and still am) drawn to it because of the level of detailed physics that can be learned and applied to these objects. It was also during this time that I got to hone my observing skills as a regular observer at the DDO. One of my favourite experiences at the DDO was literally climbing into the 1.8-metre telescope to open the shutters, which were not automated. Of course there were also plenty of not-so-fun experiences, like having to observe from the "warm" room in –25 °C weather, but it certainly makes you appreciate the comfort of modern observatories. It wasn't long after I first started doing research that I finally understood what I could actually expect out of a career in astronomy, and I was hooked!

When it came time to apply for graduate studies, luck was definitely on my side when a former undergraduate student of Tom's — Gregg Wade — was visiting our institution. It was during this visit that Gregg invited me to apply to work with him, and the rest is history. I would go on to do both my MSc and PhD at the Queen's University in Kingston, Ontario, Canada under the supervision of David Hanes (Queen's) and Gregg (who is a professor at the Royal Military College of Canada, also in Kingston). While the focus of my MSc was characterising the stellar properties of young pre-main sequence Herbig Ae/Be stars, this was also the time when I first started working on magnetism in early-type stars, which has now become my dominant interest. It was just before the start of my PhD that Gregg and his collaborators were awarded a significant amount of observing time with the Magnetism in Massive Stars (MiMeS) large programme at the Canada-France-Hawaii Telescope. The bulk of my PhD work involved utilising data from this programme, while I also took up an integral role within the project. I can only imagine that it was because of my involvement in such a successful project that the ESO Garching Fellowship selection committee offered me a position.

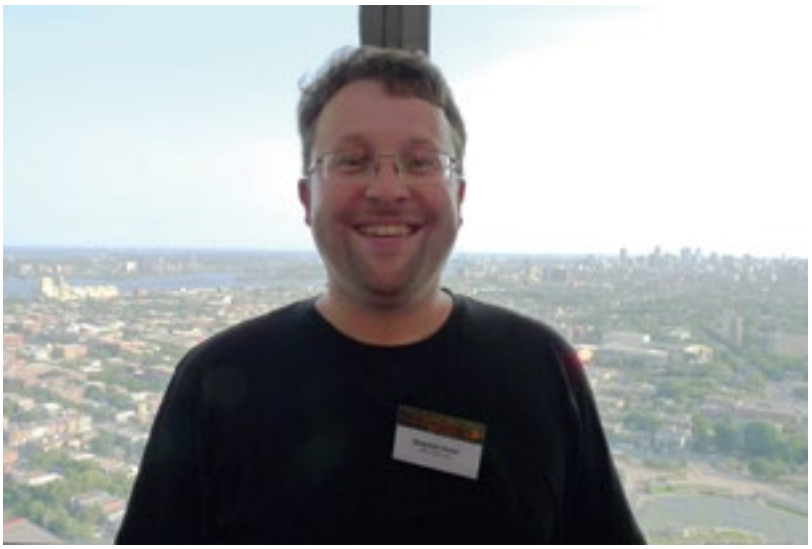

Stephan Geier

I finished my PhD in September 2012 and immediately joined the ESO family, where I have continued to work on several problems related to stellar magnetism in massive stars over the last two years. As part of my duty work, I have been given the great opportunity to assist Dietrich Baade — the Instrument Scientist — and be part of the team in Garching who are overseeing the upgrade to the CRyogenic high-resolution InfraRed Echelle Spectrograph (CRIRES) to CRIRES+. This project has allowed me to interact with many people in other departments within ESO other than just the scientists I would normally interact with. It has been a great learning experience for me, and I've gained a new-found respect for the amount of effort required and challenges faced during instrument development. With only one year left of my Fellowship, I look forward to continuing to work with the CRIRES upgrade project and working with more of the great people here at ESO.

Stephan Geier

Born and raised in a Franconian village, which is located in the northern part of Bavaria, I started studying physics at the University of Erlangen. However, the decision was a close one. From my early childhood on I was interested in all kinds of science-related topics without any special preference. Luckily, I got a scholarship from the Bavarian state, which allowed me to go to university. This is not necessarily a straightforward thing to do for someone coming from the countryside like me. Without any financial obligations to my family, I felt free to choose physics and later on, undecided as I was, started a parallel degree in history and archaeology.

In the old days, before the change to the bachelor and master system in Germany, astronomy courses could only be chosen pretty late. In 2001 I attended the lab course at the Remeis Observatory Bamberg, which hosts the astronomical institute of the University of Erlangen. After a semester abroad at Honolulu, another one of my rather silly ideas with substantial consequences, I finished my diploma thesis about an interesting supernova Ia progenitor binary, supervised by Uli Heber in Bamberg.

My decision to stay in astronomy originated in the transition phase between diploma and PhD thesis, which followed immediately thereafter, again in Bamberg, and again supervised by Uli. I appreciated the freedom I had early on in directing my own research and I received a very warm welcome from the compact

stars community, which provided additional motivation. After graduating in 2009, I started a project to study hot subdwarf binaries that emerged from my PhD thesis and spent another three years in Bamberg as a postdoc. During all those years I had the opportunity to travel quite a lot for observations and to attend conferences all around the world. Furthermore, I could also finish my dissertation in history, which provided a nice contrast to my daily life as astronomer.

The focus of my research lies on spectroscopic analyses of hot subdwarf stars, which we explain as the bare helium cores of red giants, which have lost almost their entire envelope. The mechanisms by which the envelope is lost are still not well understood. Hot subdwarfs are formed only under special, and often extreme, conditions. Interactions with stellar or planetary companions are considered, as well as stellar mergers. As potential supernova Ia progenitors they are relevant for cosmology and as possible remnants of star–planet mergers they might provide insight into the role of planets for stellar evolution. I like the diversity of those objects and their relevance for totally different fields of astronomy.

I appreciated working with very skilled and nice colleagues who shared my enthusiasm for those small stars. What I like most in doing astronomy is the personal freedom to direct my own research. Although times are also changing here, astronomy still remains a field where one guy can sometimes make a difference. Discovering new things and thinking about possible implications is the best part of research for me.

I was very happy when I got the ESO Fellowship, although I didn't really know what to expect. Coming from a small place I was a little bit worried how I would fit into this crowd of pre-selected students and fellows from all around the globe. However, my worries turned out to be totally unjustified and I really like the nice and active people and the open atmosphere at ESO very much. Being an almost local boy is actually quite an exotic thing among the other Fellows. I try to explain and represent my region as well as I can and to educate others about the true quality of beers in Munich.

ESO is like a big window into the great wide world of astronomy, which is especially useful for people coming from smaller institutions. It is also a perfect spot for interactions with other astronomers from the ESO staff, the numerous visitors or through my functional work, which I perform in the Archive Science Group, where I take care of the content validation of the ESO Public Surveys. Another thing I am very thankful for is that ESO gives me the opportunity to fulfill my teaching duties at the University of Erlangen, which are a necessary prerequisite for my Habilitation, which I am planning to conclude next year. While I am already applying for the next jobs, I will definitely enjoy my remaining year as an ESO Fellow.

External Fellows at ESO

In addition to the ESO Fellowships, a number of external fellows are hosted at ESO. A profile of one of the current Marie Curie Fellows is presented.

Izaskun Jiménez-Serra

I must have been around 12 years old when I first told my parents that I wanted to be an astronomer. The idea probably formed in my head during my childhood. I was a privileged child. My father is a teacher of philosophy (his specialty is the philosophy of science) and he encouraged my interest in physics and mathematics. My mother is a researcher in biology so, in a sense, I grew up in an environment where science was present in family life. During the hot summer nights in the countryside of central Spain, my father used to tell us about the theories of the origin of the Universe, which captivated me.

By the time I finished secondary school, I already knew what I wanted to do in life. I chose a physics degree and I specialised in astrophysics at the Spanish Universidad Complutense in Madrid. An opportunity to do a PhD in star formation at the Spanish National Research Council (CSIC is its acronym in Spanish) came up and I did not think twice about accepting. My work was mainly observational in the physical processes and chemistry of supersonic shock waves in star-forming regions. The Atacama Large Millimeter/submillimeter Array (ALMA) was still several years in the future, but my work focussed mostly on the millimetre/submillimetre regime to become a future user of this amazing facility. Those were great years. I not only learned a lot about radio astronomy and star formation, but I also had many enjoyable moments with some of my best friends.

After my PhD, in 2007 I moved to the UK where I took up a postdoctoral position at the University of Leeds. I carried out some theoretical work in the destruction processes of interstellar dust in shock waves to explain some of the observations obtained during my PhD. This position allowed me to learn more about the chemistry in the interstellar medium at

Izaskun Jiménez-Serra

very cold temperatures (and by "very cold" I mean 10 degrees above absolute zero!), which appears in very young solar-type systems. This has become one of my main interests in recent years.

As the next step, I was awarded a Submillimeter Array (SMA) Fellowship to work with the SMA team at the Harvard–Smithsonian Center for Astrophysics (CfA). This position meant I could achieve professional maturity as a researcher. Those were very intense (but exciting!) years where I had the opportunity to operate the SMA, a pioneering instrument for ALMA. This was the first time I was in direct contact with the operational work at a telescope. I had to travel often to Hawaii which was great fun. I will always be very grateful to the SMA and its team who taught me so much!

In early 2013, I came back to Europe, thanks to a Marie Curie Fellowship hosted by ESO (thank you FP7!). This year and a half at ESO has been really exciting. I not only have participated in some of the functional work of the ALMA Regional Centre at ESO, but I have helped in designing science cases for the future development of this extraordinary facility. The atmosphere at ESO is stimulating: there are always many visitors, meetings and conferences around, and its location on the Garching campus allows interactions with researchers from other institutes. At ESO, I have recently started a project to try to detect the building blocks of life, amino acids, in very young solar systems. It may sound like science fiction to many but the truth is that, thanks to ALMA, we are getting close to reach the limits where these complex organics may be detectable!

As for the future, in six months I will be taking a tenure-track fellowship (an Ernest Rutherford Fellowship) at University College London in the UK. This is really exciting since this will allow me to build up my own group and to continue exploring the pre-biotic chemical complexity in young solar systems.

Announcement of the ESO Workshop

ESO in the 2020s

19–23 January 2015, ESO Headquarters, Garching, Germany

This workshop will provide a forum for discussion of the likely astronomical landscape in the 2020s — both core science and burning topics, in so far as these can ever be predicted. Flowing from that, the community is invited to advise the ESO Executive with regard to future facilities, including, but not limited to, those at the optical/infrared observatories at La Silla and Paranal in Chile, at the submillimetre observatories APEX and ALMA on Chajnantor and the European Extremely Large Telescope to be constructed on Armazones.

In addition to high-level summaries there will be ample time for discussion and the presentation of new ideas to shape the future of ESO.

For more information please visit the workshop webpage at:
http://www.eso.org/sci/meetings/2015/eso-2020.html
or contact eso2020@eso.org

Personnel Movements

Arrivals (1 July–30 September 2014)

Europe	
Arab Salmani, Maryam (IR)	Student
Bode, Anita (DE)	Secretary/Admin. Assistant
Guillard, Nicolas (FR)	Student
Hechenblaikner, Gerald (AT)	Deputy Director of Engineering
Kakkad, Darshan (IN)	Student
McClure, Melissa (US)	Fellow
Pellegrin, Federico (IT)	Software Engineer
Pitchford, Lura Katherine (US)	Student
Ruiz Zorrilla, Laura (ES)	Administrative Assistant
Visser, Ruud (NL)	Fellow
Xu, Siyi (CN)	Fellow

Chile	
Asmus, Daniel (DE)	Fellow
Boccas, Maxime (FR)	Head of MSE
Frantz, Michel (FR)	QA&S Team Leader
Gutiérrez Avendaño, Claudia Patricia (CO)	Student
Johnston, Evelyn (GB)	Fellow
Matrà, Luca (IT)	Student
Taylor, Matthew (CA)	Student
Villarroel, Cristian (CL)	Electromechanical Technician
Watson, Linda (US)	Fellow

Departures (1 July–30 September 2014)

Europe	
Davis, Timothy (GB)	Fellow
Galvan-Madrid, Roberto (MX)	Fellow
Gotschewski, Katrin (DE)	Administrative Assistant
Hekman, Pieter (NL)	Electronic Engineer
Krumpe, Mirko (DE)	Fellow
Manara, Carlo Felice Maria (IT)	Student
Neumayer, Nadine (DE)	User Support Astronomer
Pfeffer, Joel Leslie (AU)	Student
Saturni, Francesco Gabriele (IT)	Student
Sbarrato, Tullia (IT)	Student
Tremblay, Grant (US)	Fellow
Wylezalek, Dominika (DE)	Student

Chile	
Al Momany, Yazan (IT)	Operations Staff Astronomer
Bocaz, Paulina (CL)	Executive Officer
Breitfelder, Joanne (FR)	Student
Cardenas, Mauricio (CL)	Software Engineer
Carlier, Arnaud (FR)	Head of MSE
Deschamps, Romain (FR)	Student
Jones, David (GB)	Fellow
Lombardi, Gianluca (IT)	Fellow
Melnick, Jorge (FR)	VLT Programme Scientist
Triat, Albert (CL)	Administrative Assistant
Ureta, Eugenio (CL)	Civil Engineer
Vasquez, Sergio (CL)	Student

Confirmation of the Messenger Subscription

We are currently updating our subscriber database for the printed edition of *The Messenger*. If you wish to continue receiving a hard copy, please read further.

On the label of the envelope in which you received this edition, you will find a unique web link, written in the format http://eso.org/m/MMMM. Please type this link into a browser and tick the box "Subscribe to receive the ESO Messenger" if you wish to continue receiving the printed version. By pressing the "Submit" button, you will then continue to receive the print version of *The Messenger*. If you wish to check your postal address, click on "Update your profile". *The Messenger* is always available on the ESO web[1].

If you have already thrown away the envelope of this edition, you will still have a second chance with the envelope for the next *Messenger* issue (158, December 2014). If you do not confirm your subscription by 31 January 2015, we assume that you no longer wish to receive *The Messenger* in printed form.

In case you do not currently have internet access, please inform us of your desire to continue with the printed subscription, by letter to:
The Editor
The Messenger
European Southern Observatory
Karl Schwarzschild Straße 2
85748 Garching bei München
Germany

Links

[1] The Messenger: http://www.eso.org/sci/publications/messenger/

Colour image of the H II region star-forming complex N59 in the Large Magellanic Cloud. FORS2 images in broadband (*B* and *R*) and narrowband ([O III] 5007 Å and Hα) filters were combined. The large and high-ionisation nebula to the upper right (north west) of the image is N59A and contains NGC 2032 (to the west) and NGC 2035 (centre), which belong to a single H II region. The more symmetric H II region bubbles N59B and N59C are to the east and south respectively. See Release eso1348 for details.

ESO, the European Southern Observatory, is the foremost intergovernmental astronomy organisation in Europe. It is supported by 15 countries: Austria, Belgium, Brazil, the Czech Republic, Denmark, France, Finland, Germany, Italy, the Netherlands, Portugal, Spain, Sweden, Switzerland and the United Kingdom. ESO's programme is focused on the design, construction and operation of powerful ground-based observing facilities. ESO operates three observatories in Chile: at La Silla, at Paranal, site of the Very Large Telescope, and at Llano de Chajnantor. ESO is the European partner in the Atacama Large Millimeter/submillimeter Array (ALMA) under construction at Chajnantor. Currently ESO is engaged in the design of the European Extremely Large Telescope.

The Messenger is published, in hard-copy and electronic form, four times a year: in March, June, September and December. ESO produces and distributes a wide variety of media connected to its activities. For further information, including postal subscription to The Messenger, contact the ESO education and Public Outreach Department at the following address:

ESO Headquarters
Karl-Schwarzschild-Straße 2
85748 Garching bei München
Germany
Phone +49 89 320 06-0
information@eso.org

The Messenger:
Editor: Jeremy R. Walsh;
Design, Production: Jutta Boxheimer;
Layout, Typesetting: Mafalda Martins;
Graphics: Roberto Duque.
www.eso.org/messenger/

Printed by G. Peschke Druckerei GmbH,
Schatzbogen 35,
81829 München, Germany

ISSN 0722-6691

Contents

The Organisation
Groundbreaking for the European Extremely Large Telescope (E-ELT) 2

Telescopes and Instrumentation
Lopez B. et al. – An Overview of the MATISSE Instrument — Science, Concept and Current Status 5
Bacon R. et al. – MUSE Commissioning 13
Gonté F. et al. – Ensuring the Reliability and Performance of Instrumentation at the Paranal Observatory 17

Astronomical Science
Morel T. et al. – The B Fields in OB Stars (BOB) Survey 27
Ripepi V. et al. – STEP: The VST Survey of the SMC and the Magellanic Bridge 32
Bower R., Bureau M. – The KMOS Redshift One Spectroscopic Survey (KROSS) 38
Smail I., Fabian W. – ALESS: An ALMA Survey of Submillimetre Galaxies in the Extended Chandra Deep Field South 41
Vanzella E. et al. – The Deepest VLT/FORS2 Spectrum of a $z \sim 7$ Galaxy: An Easy Target for the E-ELT 46

Astronomical News
de Wit W.-J. et al. – Report on the Workshop "Herbig Ae/Be Stars: The Missing Link in Star Formation" 50
Hans-Emil Schuster Celebrates his 80th Birthday 54
Fellows at ESO – J. Grunhut, S. Geier 54
External Fellows at ESO – I. Jiménez-Serra 56
Announcement of the ESO Workshop "ESO in the 2020s" 57
Personnel Movements 58
Confirmation of the Messenger Subscription 58

Important notice:
Please confirm your subscription!
See page 58

Front cover: VST (VLT Survey Telescope) colour-composite image of the nearby (~ 850 kpc) SA spiral galaxy M33 (NGC 598). On account of its proximity M33 has been well studied at almost all accessible wavelengths. Many H II regions are apparent on this image from their ionised emission and the largest is NGC 604 (north-east of the nucleus), an archetype for the more distant giant extragalactic H II regions. Images with broad *g*- and *r*-band filters and Hα narrowband were combined; the image orientation is north up, east to the left and the image height is 1 degree. See Release eso1424 for details.